G 8279

AN INVESTIGATION ON THE PREPARATION AND PROPERTIES OF SOME TRANSPARENT CONDUCTING OXIDES AND LEAD SELENIDE THIN FILMS

Thesis submitted to
COCHIN UNIVERSITY OF SCIENCE AND TECHNOLOGY
In partial fulfilment of the requirements for the award of the degree of
DOCTOR OF PHILOSOPHY

By

BENOY M. D.

SOLID STATE PHYSICS LABORATORY
DEPARTMENT OF PHYSICS
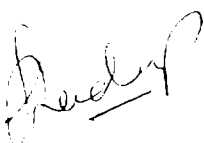COCHIN UNIVERSITY OF SCIENCE AND TECHNOLOGY
KOCHI-682 022
2001

*Dedicated to My Parents
and Brother*

Department of Physics

Cochin University of Science And Technology

Kochi-682 022

India

CERTIFICATE

Certified that the work presented in this thesis entitled "*An investigation on the preparation and properties of some transparent conducting oxides and lead selenide thin films*" is based on the research work carried out by Mr. Benoy M. D, under my guidance in the Department of Physics, Cochin University of Science And Technology and no part of this has been presented by him for the award of any other degree.

Kochi-22

7th May 2001

Dr. B. Pradeep

Reader

(Supervising Guide)

DECLARATION

I hereby declare that the present work entitled "*An investigation on the preparation and properties of some transparent conducting oxides and lead selenide thin films*" is based on the original work done by me under the guidance of Dr. B. Pradeep, Reader, Department of Physics, Cochin University of Science And Technology, and has not been included in any other thesis submitted previously for the award of any degree.

Kochi-22

7thMay2001

Benoy M. D.

Benoy M. D.

CONTENTS

Chapter 3. Experimental Techniques

Chapter 5. Preparation and Characterization of In_2O_3 Thin Films

Chapter 6. Preparation and Characterization of Indium Tin Oxide(ITO) Thin Films

Chapter 7. Preparation and Characterization of

Lead Selenide(PbSe) Thin Films

The investigation of physical properties of matter has progressed so much during the last hundred years. Today physics is divided in to a large distinct group of special branches. These branches are distinguished by the particular area studied, method of investigation and so on. An independent and important branch that has developed is the physics of thin films.

Any object in solid or liquid form with one of its dimensions very much smaller than that of the other two may be called a thin film. It is having only one common property, namely, one of their dimensions is very small, though all their physical properties may be different. Thin layers of oil, floating on the surface of water, with their fascinating colours, have attracted men's curiosity from time immemorial. The earliest application of thin films was the protective coatings in the form of paints. A thin layer of tin has been used from ancient times to protect copper utensils from corrosion. Indium thin films are used in certain applications on account of their good lubricating property. Relay contacts are coated with thin films of rare earth metals in order to prevent burning due to arcing. Hard coatings are also available using diamond like carbon (i-carbon). The basic properties of thin films are of considerable interest because of their potential applications in various fields of science and technology.

Thin films of metals were probably first prepared in a systematic manner by Michael Faraday using electrolysis. The possibility of depositing thin metal films in vacuum by Jule heating of platinum wire was discovered by Nahrwold[1]. Scientific interest in thin films, both fundamental and applied, began with their application first in optics and later in electronics. Optical applications are mainly for the preparation of reflecting coatings on mirrors, decorative coatings on plastics, anti-reflection coating in lenses, interference filters, beam splitters, etc. Electronic applications are mainly in integrated circuits and in the preparation of passive and active components for the micro-miniaturisation of electronic circuits. Thin films are also used in optoelectronic devices such as photoresistors, photovoltaic cells, electro-luminescent displays, etc. In device application, the

optimum material properties cannot be achieved by using single elements. This can be achieved by using compound films or by doping it with suitable dopants.

The properties of thin films are greatly influenced by their methods of preparation and deposition conditions such as deposition rate, type of substrates used, substrate temperature and the background pressure. Specific applications in modern technology demand thin films with very high optical transmission/reflection, hardness, adhesion, non-porosity, high mobility/insulating properties, stability with temperature, stoichiometry and orientation in single crystal film. Therefore a precise control over the preparation parameters is essential for the production of high quality thin films.

There are various methods for the deposition of thin films. Generally it can be classified as physical and chemical methods. In physical method, the particles to be deposited are transferred to vapour phase by a physical process either by a thermal evaporation or by an impact process. In chemical method the thin film is formed by a chemical process in vapour or liquid phase. Out of these vacuum evaporation is the most widely used method. Deposition of compound films by direct evaporation is not possible in many cases, because some compounds decompose on heating resulting in non-stoichiometric or layered films. Gunther's three temperature method [2] overcomes this difficulty and can be used to deposit compound films. The formation of certain compounds is not possible using this method because of the low chemical reactivity of the components. To overcome this difficulty Bunshah [3] introduced the technique of Activated Reactive Evaporation.

Activated reactive evaporation (ARE) is a variant of reactive evaporation. In ARE, the reaction between the evaporated species and the gas is activated by establishing thermionically assisted plasma in the reaction zone. This technique can be used to deposit good quality transparent conducting oxides like In_2O_3, SnO_2, Zinc Oxide, Tin doped Indium Oxide (ITO), and other similar oxides at low substrate temperature.

Studies on transparent conducting films have attracted the interest of many research workers because of their wide applications both in industry and in research. The characteristic properties of such coatings are low electrical

resistivity and high transparency in the visible region. Ever since the first report of a transparent conducting cadmium oxide film prepared by the thermal oxidation of sputtered cadmium by Badeker [4] in 1907, the technological interest in transparent conductors has grown tremendously. Though early works on these films were performed out of purely scientific interest, substantial technological interests in such films were made only after 1940. The technological interest in the study of transparent semiconducting films has been generated mainly because of their potential applications both in industry and in research. Transparent conducting films have demonstrated their utility as transparent electrical heaters for wind screens in aircraft industry. However during the last decade, these semiconducting transparent films have been widely used in a variety of other applications such as gas sensors, solar cells, heat reflectors, protective coatings, transparent electrodes, laser-damage resistant coatings in high power laser technology, antistatic surface layers on temperature control coatings in orbiting satellites and surface layers in electro-luminescent applications. A large number of materials such as In_2O_3, SnO_2, antimony doped tin oxide, fluorine doped tin oxide, tin doped indium oxide, zinc oxide, cadmium oxide and cadmium stannate can be used for semiconducting transparent coatings.

Studies on semiconducting chalcogenide thin films are also of interest, owing to their application in various fields of science and technology, like IR detectors, photoresistors, photodiodes, thin film transistors, etc. It is mainly due to their special electrical and optical properties. These properties mainly depend on the method of preparation, their thickness, structural features and electronic structure. Recently a variety of materials based on Te or Se alloy films with Ge, Sn, Pb, Bi and Sb have been studied for phase change recording media and they are potential candidates for optical data storage applications [5].

This thesis presents a study of the preparation and characterization of In_2O_3, tin doped indium oxide (ITO) and lead selenide (PbSe) thin films. In_2O_3 and ITO films were prepared by activated reactive evaporation. PbSe films were prepared by reactive evaporation.

The first chapter of this thesis contains a resume of the basic principles of semiconductor physics relevant to the work reported here. The second chapter

describes the different methods for the preparation of thin films. Chapter three contains (1) a detailed description of ARE which is used for the preparation of In_2O_3 and ITO films, (2) reactive evaporation (a variant of three temperature method), used for the preparation of PbSe, and (3) details of the electrical and optical characterization techniques. The fourth chapter gives an overview on transparent conducting oxides. The fifth chapter of this thesis contains the preparation and characterization of In_2O_3 thin films prepared by ARE [6]. Preparation and characterization of ITO thin films are given in the sixth chapter. Structural, electrical, optical and thermoelectric properties of ITO thin films prepared on glass substrates kept at room temperature are given in the first part of this chapter. Second part of this chapter contains the structural, electrical and optical properties of ITO thin films prepared at different substrate temperature. The third part of this chapter discusses the variation of electrical and optical properties with thickness of the films prepared on substrates kept at room temperature. Preparation and characterization of PbSe thin films by three-temperature method is given in chapter seven.

Part of the work reported in this thesis has been published in the form of following research papers:

1. Preparation and characterization of In_2O_3 films prepared by activated reactive evaporation.

   M. D. Benoy and B. Pradeep, Bull. Mater. Sci., 20 (1997) 1029

2. Optical properties of In_2O_3 films prepared by activated reactive evaporation

   M. D. Benoy and B, Pradeep, Indian J. Pure & Appl. Phys., 36 (1998) 686

3. Preparation of PbSe films by Reactive evaporation

   M. D. Benoy and B. Pradeep,

   Fifth IUMRS International Conference in Asia, IISc. Bangalore,

   Oct.13-16 (1998)

4. Variation of optical and electrical properties of ITO films with substrate temperature.

   M. D. Benoy and B. Pradeep, National conference on recent advances in materials, Nehru Memorial College, Trichi, Sept. 29-30 (2000)

5. Electrical and optical properties of PbSe thin films

    M. D. Benoy and B. Pradeep, Symposium on fundamentals of

    crystal growth, Crystal growth centre, Anna University,

    Madras, Nov. 6-7 (2000)

6. Electrical properties of indium tin oxide (ITO) thin films

    prepared by activated reactive evaporation.

    M. D. Benoy and B. Pradeep, (Communicated to Thin Solid Films.)

7. Thickness dependence of the properties of indium tin oxide (ITO) thin films

    prepared by activated reactive evaporation.

    M. D. Benoy and B. Pradeep, (Communicated to Applied Physics A.)

REFERENCES:

[1] R. Nahrwold, Ann. Physik, **31** (1887) 417

[2] K.G Gunther, "The Use of Thin Films in Physical Investigation",
(J.C Anderson, Ed.), Academic Press, New York, 1966, **P.213**

[3] R. F. Bunshah and A. C. Raghuram, J. Vac. Sci. Tech. 9 (1972) 1389

[4] K Badeker, Ann. Phys. (Leipzig), **22** (1907) 749

[5] S. Jayakumar, C. Balasubramanian, K. Naryandass, D. Mangalaraj and
C.P.G. Vallabhan, Thin Solid Films **266** (1995) 62

[6] J George, B Pradeep and K. S Joseph,
Rev. Sci. Instrum. **57** (1986) 2355

CHAPTER – 1

SEMICONDUCTOR PHYSICS

1.1 INTRODUCTION

Semiconductors are the most interesting and useful substances among all classes of solids. Although semiconductors have been studied for a long time-since 1920's- they actually came into their own only after Shockly, Bardeen and Brattain invented the transistor in late 1940's. Because of this invention and development of other related devices, semiconductors have become the most actively studied area in solid state physics.

A solid can either be in the state of amorphous, polycrystalline or single crystalline. Each type is characterized by the size of an ordered region within the material. An ordered region is a special volume in which atoms or molecules have a regular geometric arrangement or periodicity. Amorphous materials have order only within a few atomic or molecular dimensions. The polycrystalline materials have a high degree of order over many atomic or molecular dimensions. These ordered regions or single crystal regions, vary in size and orientation with respect to one another. The single-crystal regions are called grains, and are separated from one another by grain boundaries. Single-crystal materials have a high degree of order or regular geometric periodicity throughout the volume of the material. A two dimensional representations of amorphous, polycrystalline and single crystalline materials are shown in figure 1.1.
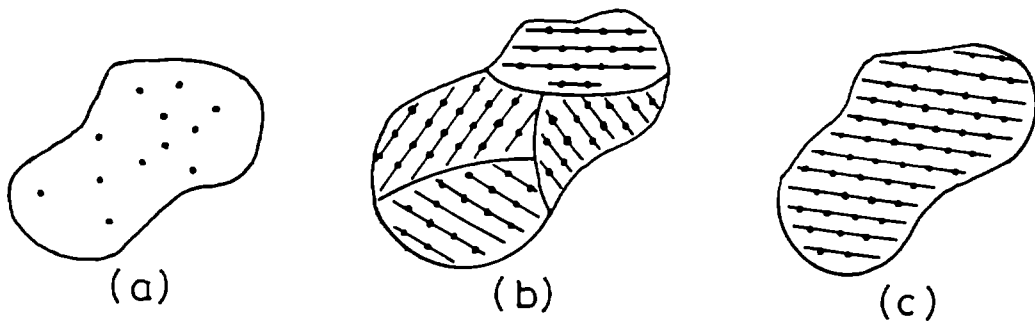
Figure 1.1 Schematics of three general types of crystals: (a) amorphous
(b) polycrystalline (c) single crystal.

1.2 BAND STRUCTURE

The understanding of the behaviour of electrons in solid is most important to explain the various properties of materials. A great deal of experimental work has been carried out on semiconductors, before any satisfactory theory has been put forward to account for their properties. During the past hundred years, three approaches have been developed to explain the electronic properties of materials. First one is the "continuum theory," developed in the last century, considered only the macroscopic properties. Later Paul Drude proposed the "classical free electron theory." This theory has postulated that free electrons in metal drift as a response to an external force and interact with certain lattice atoms. This theory has failed to explain a large number of experimentally observed phenomena. A further refinement in the understanding to the properties of materials was accomplished by the use of quantum theory. The first application of quantum mechanics to the motion of electrons in solids was the treatment of the electrical conduction mechanism in metals by A. Sommerfield. The only essential difference between this and the earlier theories, based on the classical theory of electrons, was that the energy levels, which the various electrons can occupy, are determined by the wave mechanics.

According to Sommerfield's quantum free electron theory, the valence electrons of the constituent atoms are free to move in a field free space, throughout the volume of the specimen, except at the boundary of the solid as shown in figure 1.2a. The potential energy due to the field of all nuclei and all other electrons is assumed to be constant every where inside the metal except at the boundary of the solid. The energy of the free electron as a function of wave vector is given by

$$E = \frac{\hbar^2 k^2}{2m}$$
(1.1)

Where k is the wave vector given by $k = \frac{p}{\hbar} = \frac{2\pi}{\lambda}$. Here λ is the wavelength associated with the free electron and P is the momentum. In this theory, the allowed energy levels for the valence electrons lie very close together and their values extend from nearly the bottom of the potential, trough in which the electrons move to indefinitely high values; that is, the energy spectrum is quasi-continuous and is shown in figure 1.2b.

(a)

(b)
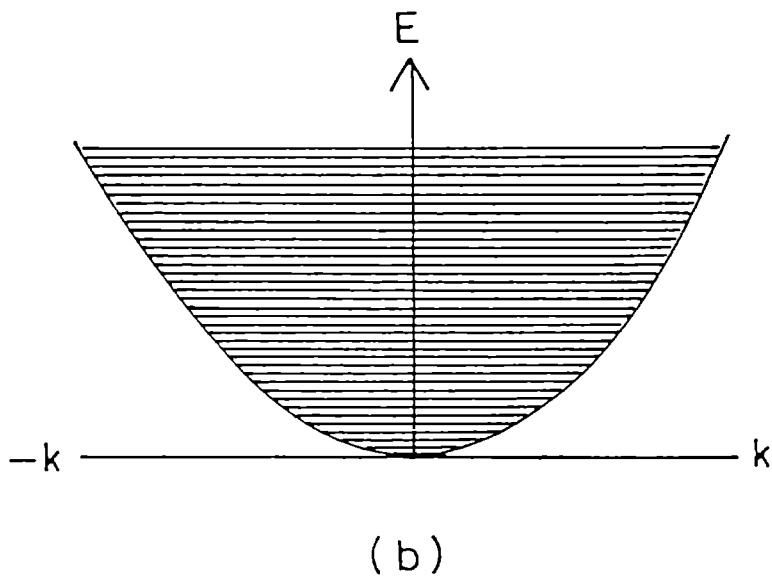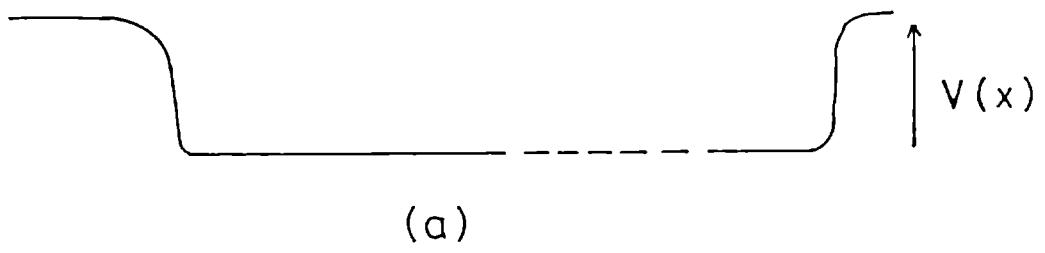
Figure 1.2 (a) Sommerfield model for potential energy V(x) of electrons in a crystalline solid (b) Energy (E) vs. Wave vector (k) for a free electron

The Sommerfield theory explains successfully the phenomena of specific heat, electrical conductivity, thermionic emissions, thermal conductivity and paramagnetism. Yet there are many other physical properties that could not be explained by free electron model. This model fails to explain why some solids are good conductors of electricity, some are semiconductors and others are insulators.

The motion of electrons in crystalline solids is described by a much more refined theory, discussed by F. Bloch, where one does no longer assume that the electrons are free. Here the interaction between the electrons and the atomic nuclei are taken into account. We have then instead of a constant potential in the interior of the solid, a periodic potential with the same period and symmetry as the crystal concerned. It is schematically represented in figure 1.3.

The problem of the motion of electron through periodic potential is solved by reducing the problem to one-body problem by using the following assumptions:

1. The nuclei at the lattice sites are perfectly at rest. Interaction between the electrons and phonons are thus neglected.

2. Interaction between the electrons is ignored. Every electron is in a potential field, which is due to the positive nuclei and an averaged charge distribution of the other electrons. The strong fields of nuclei are thus more or less screened by the electrons.

If we consider the motion of an electron in a periodic potential, we arrive at the following conclusions:

1. The energy spectrum of an electron in a periodic potential consists of a number of allowed energy bands separated by forbidden regions;

2. The energy E is a periodic function in the wave vector k.

These conclusions can be schematically represented by the Figure 1.4.

The discontinuities in the curve occur for $k = \dfrac{n\pi}{a}$, where a is the lattice constant and n = ±1, ± 2, ... Except for these k values, the electrons in a crystal behave like free electrons. These k values define the boundaries of the first, second, etc. Brillouin zones.

According to the band theory of solids, the presence of a forbidden band or energy gap immediately above the occupied allowed states is the principal difference in the electronic structure of conductors, semiconductors and insulators. The

$V(x)$
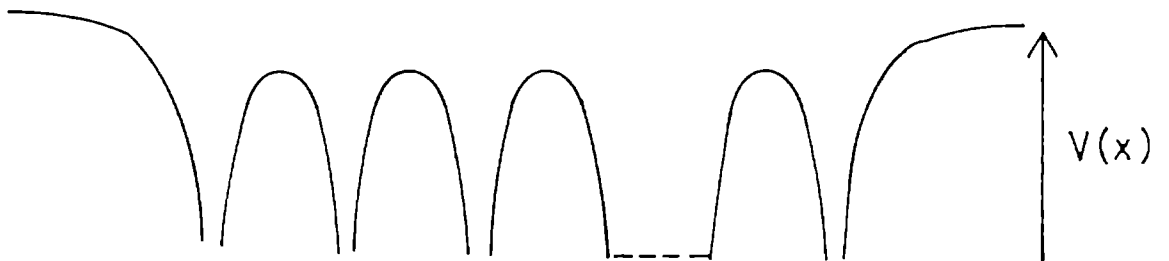
Figure 1.3 Periodic potential due to the atomic core in a crystalline solid.

E

Forbidden
bands

Allowed
bands

$-\dfrac{2\pi}{a}$ $-\dfrac{\pi}{a}$ $\dfrac{\pi}{a}$ $\dfrac{2\pi}{a}$ K
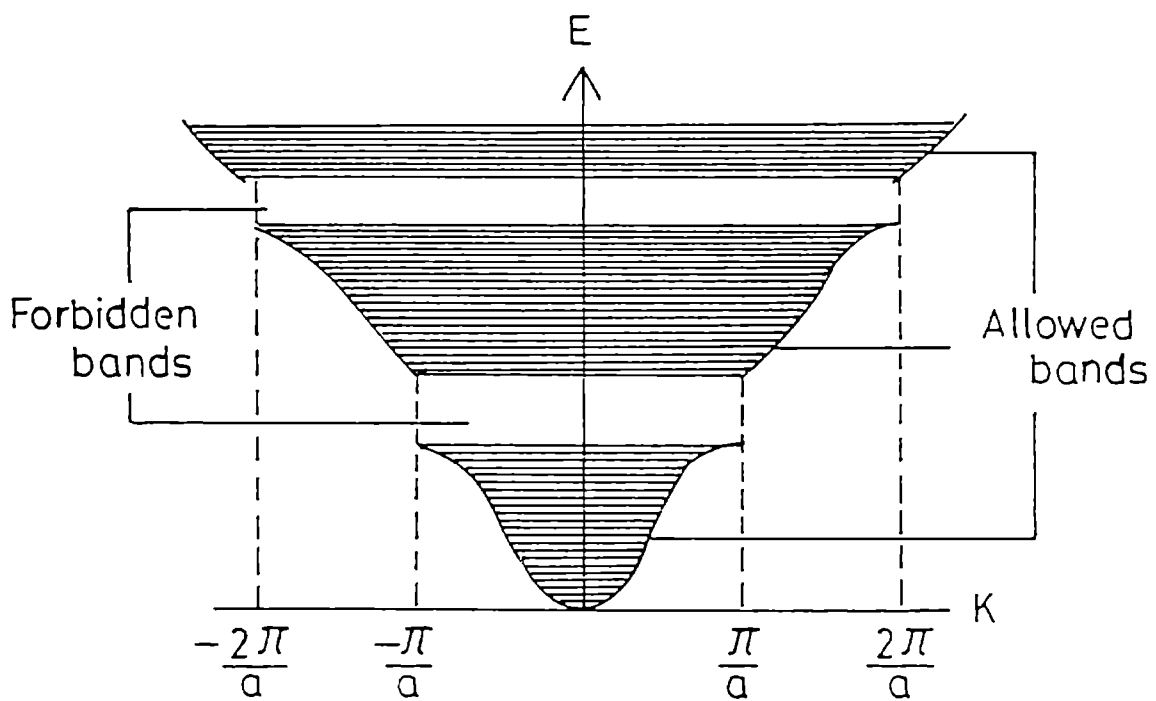
Figure 1.4 Energy (E) vs. wave vector (k) for a periodic lattice of lattice constant, a.

formation of energy bands in a solid from discrete energy levels of individual atoms is shown schematically in figure 1.5. The shorter the distance r (inter nuclear distance), the stronger éfect of neighbouring atoms and the more the levels are smeared. The energy spectrum of the crystal is determined by the smearing of the levels corresponding to the inter atomic distance a_0 typical of given crystal. The energy band formed by the electrons belongs to the first orbit is called the first energy band. Similarly the second orbit electrons form second energy band and so on.

Even though there are a number of energy bands in solids the energy bands of interest are, (a) valence band - the upper most filled band and (b) conduction band - the first empty band above the valence band. The separation between the bottom of the conduction band and top of the valence band is known as "band gap". On the basis of energy bands the solids can be classified as follows:

1. Conductors - here the valence band and conduction band overlap each other. Thus the electrons and vacant energy states intermixed within the bands so that the electrons can move freely within the conduction band under the influence of an electric field. Hence the conductors have a high electrical conductivity
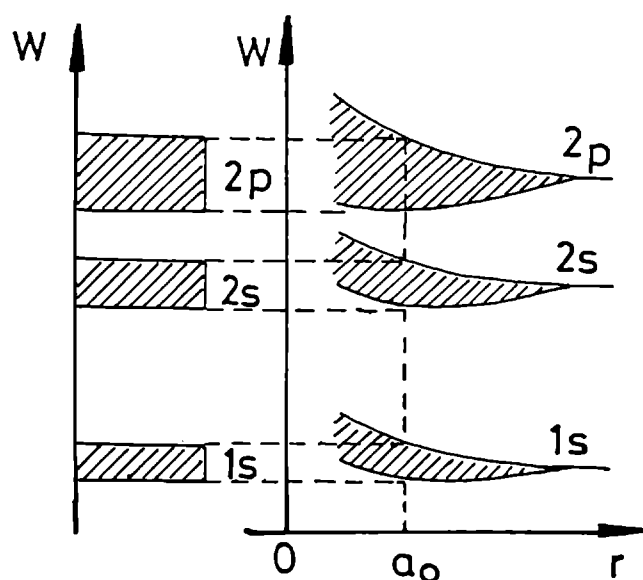
Figure 1.5 Schematic of the formation of energy bands from discrete energy levels.

2. Semiconductors - for which the valence band is full and the conduction band is empty at absolute zero. The energy gap between the valence band and conduction band is very small. Solids with forbidden energy gap less than or of the order of 2eV is generally known as semiconductors. The electrical conductivity of semiconductors lies between 10^{-6} to 10^{3} ohm^{-1}cm^{-1}.

3. Insulators - here the valence band is full while the conduction band is empty at absolute zero. Materials with band gap greater than 3eV are generally known as insulators. They do not allow the passage of electric current through them.

In the case of semiconductors the valence band is completely filled and the conduction band is absolutely empty at absolute zero. So the semiconductors behave as an insulator at a very low temperature. As the temperature is increased the valence electrons crosses over to the conduction band and the conductivity increases. That means the conductors have a negative temperature coefficient of resistance. The energy band diagrams of conductor, semiconductor and insulator are shown in figure 1.6.
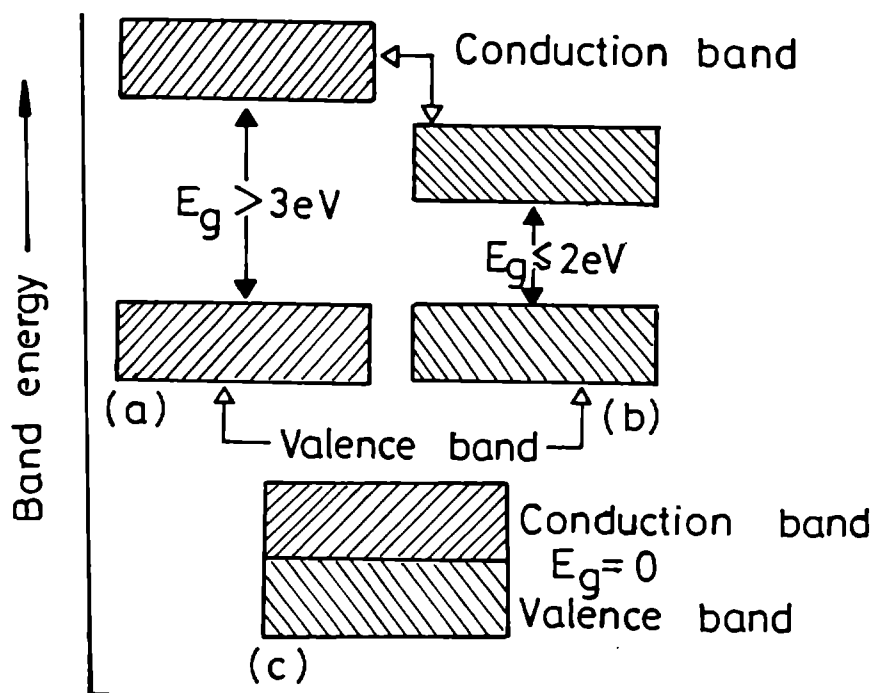
Figure 1.6 Energy band model of (a) insulator, (b) semiconductor and (c) metal.

1.3 INTRINSIC AND EXTRINSIC SEMICONDUCTORS

A semiconductor in which the concentration of charge carrier is a characteristic of the material itself rather than the content of impurities and structural defects of the crystal is called an intrinsic semiconductor. If the crystal lattice is raised to an elevated temperature, thermal excitation will free an electron from the interatomic bonds. This creates a conduction electron and a hole. If a field is applied, it gives rise to an electrical conductivity. Occasionally an electron and hole will meet, and the electron will fall back into the bond. This process is called recombination. We may visualize a continual process of thermal generation and recombination of electrons and holes, so that an equilibrium is established, with an equal number of electrons and holes present to give rise to an electrical conductivity. By raising the solid to a sufficiently high temperate, any insulator can be expected to show this behaviour, which is called "intrinsic semiconduction." The temperature necessary for this is to be determined by the width of the forbidden gap. Figure 1.7a shows the case where there are no free carriers, and figure 1.7b shows an equal number of holes and electrons, as produced either thermally or by absorption of light.
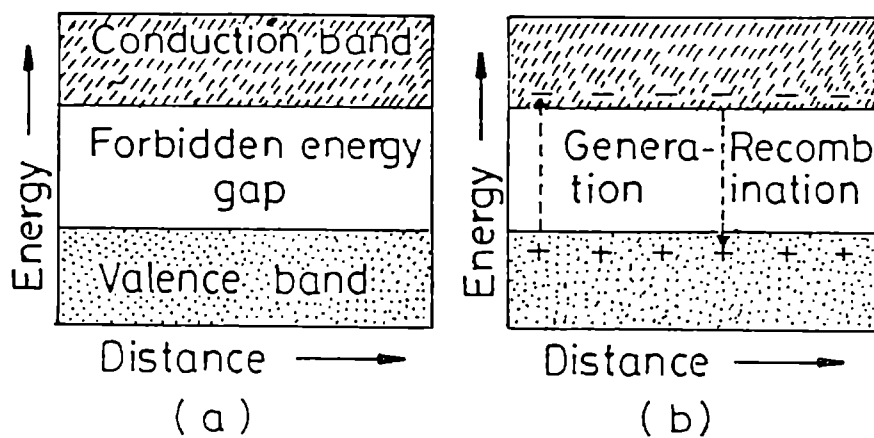
Figure 1.7 Intrensic semiconductor (a) at low temperature,

(b) at elevated temperature, with thermal excitation generating

holes and electrons.

Thus an intrinsic semiconductor has equal number of electrons and holes; that is

$$n = p = n_i$$

where n is the electron concentration, p is the hole concentration and n_i is the intrinsic carrier density and is given by

$$n_i = \frac{2}{h^3}(2\pi kT)^{3/2}(m_e m_p)^{3/4}\exp\left(\frac{-E_g}{2kT}\right) \tag{1.2}$$

where m_e and m_p are the effective mass of the electrons and holes respectively and E_g is the energy gap.

The carrier concentration and hence the conductivity in an intrinsic semiconductor is very sensitive to temperature and depends strongly on the energy gap. The mobility of the current carriers also contributes its share to the conductivity σ. Taking both electrons and holes into consideration we can write

$$\sigma = ne\mu_e + pe\mu_h \tag{1.3}$$

where μ_e and μ_h are the mobilities of electrons and holes respectively. But the temperature dependence of the mobility of electrons and holes is less and hence the conductivity, which is proportional to the density of the carriers, can be expressed as

$$\sigma = \sigma_0 \exp\left(\frac{-E_g}{2kT}\right) \tag{1.4}$$

where σ_0 is a constant

If a semiconductor contains an impurity or impurities, then comes the impurity conduction. The addition of small amount of impurities to the semiconductors is known as doping. Semiconductor with an excess of conduction electrons over holes is normally called "n-type". Those with an excess of holes are called "p-type" as the majority carriers are holes. The carriers are termed as majority carriers and minority carriers depending on the type of carriers, which predominate. The energy level for the donors and acceptors is shown in figure1.8.

When the carrier concentration is predominantly determined by the impurity content, the conduction of the material is said to be extrinsic. Physical defects in the crystal structure may have similar effects as donor or acceptor impurities. They can also give rise to extrinsic conductivity.
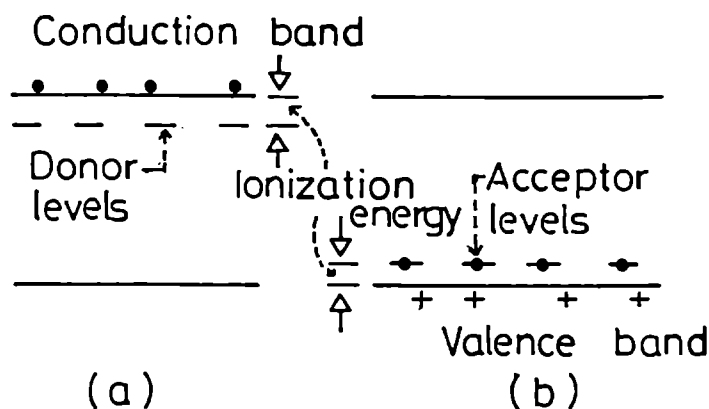
Conduction band

Figure 1.8 Energy levels for (a) donors and (b) acceptors.

The density of free electrons in the conduction band due to the donor levels is given by

$$N = (2n_d)^{1/2} \left[\frac{2\pi m_e kT}{h^2} \right]^{3/4} \exp\left[\frac{-E_d}{2kT} \right] \qquad (1.5)$$

where n_d is the donor density and E_d is the donor activation energy.

This shows that N is proportional to the square root of the donor density. A similar expression holds for the case of acceptors also.

1.4. DEGENERATE AND NONDEGENERATE SEMICONDUCTORS

The doping of a semiconductor with donor impurity or acceptor impurity is in such a way that the concentration of dopant atoms is very small compared to the density of host or semiconductor atom. The impurity atoms are spread far enough so that there is no interaction between donor electrons, in an n-type material. Thus the impurities introduce discrete, noninteracting donor energy states in the n-type semiconductor and discrete, noninteracting acceptor states in the p-type semiconductor. These types of semiconductors are referred to as nondegenerate semiconductors.

If the impurity concentration increases, the distance between the impurity atoms decreases and a point will be reached when donor electrons, for example, will begin to interact with each other. When this occurs, the single discrete donor energy level will split into a band of energies. As the donor concentration further increases

the band of donor states widens and may overlap the bottom of the conduction band. This overlap occurs when the donor concentration becomes comparable with the effective density of states. When the concentration of electrons in the conduction band exceeds the density of states, the Fermi energy lies within the conduction band. This type of a semiconductor is called a degenerate n-type semiconductor.

A schematic model of the energy-band diagrams for degenerate n-type and degenerate p-type semiconductors are shown in Figure 1.9. In the degenerate n-type semiconductors, the states between E_F and E_c are mostly filled with electrons, thus the electron concentration in the conduction band is very large. Similarly in the degenerate p-type semiconductor, the energy states between E_v and E_F are mostly empty; thus the hole concentration in the valence band is very large.
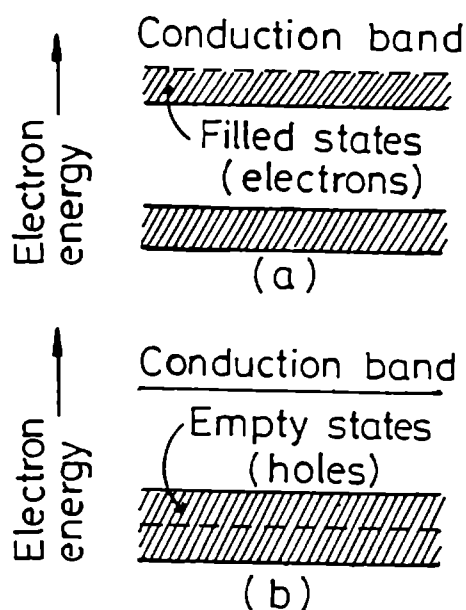
Figure 1.9 Energy band diagram for degenerate (a) n-type and

(b) p-type semiconductors

1.5. HALL EFFECT

A phenomenon observed by E.H. Hall in 1879, turned out to be one of the most important tool in the electrical characterization of materials. When a magnetic field is applied normal to the direction of current through a conductor, a voltage develops normal to the direction of current and magnetic filed. This phenomenon is called Hall effect and the voltage developed is called Hall voltage.

Suppose an electric current J_x flows through a wire in the positive x-direction and the magnetic field B_z is applied normal to the wire in the z-direction. This leads

to an electric field normal to both J_x and B_z. In the absence of the magnetic field, the conduction electrons are drifting with a velocity v in the negative x-direction. When the magnetic filed is introduced, the electrons experiences a force called Lorentz force F_L = e (v×B), which causes the electrons to bend downward as shown in figure1.10. As a result the electrons accumulate on the lower surface, producing a net negative charge there. Simultaneously a net positive charge appears on the upper surface, because of the deficiency of electrons there. This combination of positive and negative surface charges creates a downward electric field called the Hall field.

The field produced by the surface charges causes a force, which opposes the Lorentz force. The accumulation of the charges continues until the Hall force completely cancels the Lorentz force. This is the steady state, and is given by,

$$F_L = F_H \tag{1.6}$$

i.e. $-e\,v_x B_z = -eE_H$

OR

$$E_H = v_x B_z \tag{1.7}$$

where E_H is the Hall field.
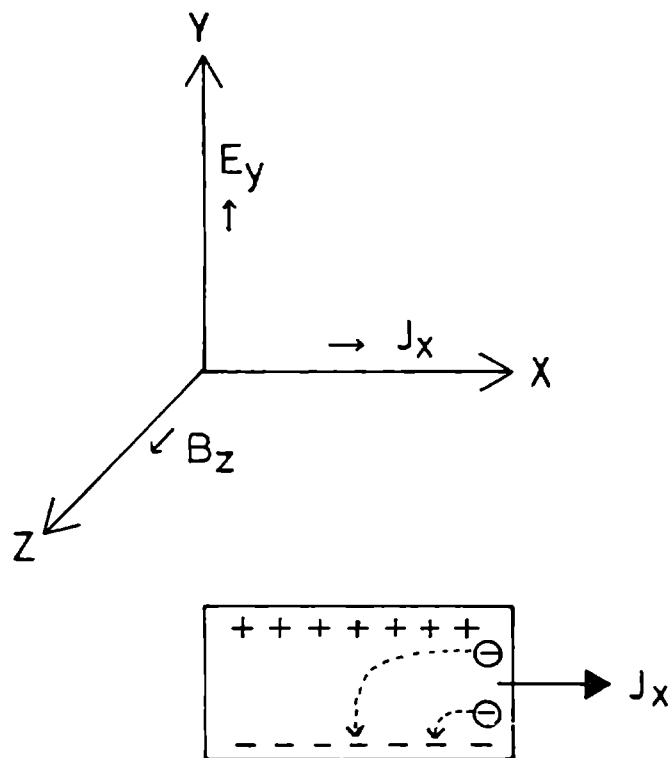
Figure 1.10 Schematic representation of Hall effect.

The current density $J_x = n$ (-e) v_x, where n is the carrier density, e is the electronic charge and v_x is the drift velocity. This leads to

$$E_H = -\frac{1}{ne}J_xB_z \qquad (1.8)$$

From equation (1.8) it can be seen that the Hall filed E_H is proportional to the current density and to the magnetic field. The proportionality constant that is $E_H/(J_xB_z)$ is known as the Hall coefficient, and is usually denoted by R_H. Therefore,

$$R_H = -\frac{1}{ne} \qquad (1.9)$$

The useful features of the Hall coefficient (R_H) are:

(1) The sign of the Hall coefficient depends on the sign of the charge of the current carriers. Thus for n-type semiconductors R_H is negative and for p-type semiconductors R_H is positive.

(2) The carrier concentration can be directly calculated

(3) Since $\sigma = ne\mu$, by measuring the conductivity of the sample, along with the Hall coefficient, we can determine μ, the mobility of the carriers.

1.6 THERMOELECTRIC EFFECTS

Thermoelectric power or Seebeck effect is another important method for studying semiconductors. A temperature difference ΔT between the ends of a specimen gives rise to an emf of $Q\Delta T$ millivolts. Q defines the thermoelectric power in milivolts/degree. Therefore

$$Q = \frac{\Delta V}{\Delta T} \qquad (1.10)$$

When one end of the sample is heated, the mobile charge carriers tend to diffuse from the hot end to the cold end so that the cold end acquires a potential of the same sign as the carriers. This produces a disturbance in the equilibrium distribution of the carriers and sets up an electric field, which opposes the flow of carriers. This electric filed will be positive with respect to the cold end if the carriers are electrons and negative if the carriers are holes.

An expression for the thermoelectric power in terms of the carrier concentration is given by

$$Q = \pm \frac{k}{e}\left[\left(\frac{5}{2} - S\right) - \ln\left(\frac{nh^3}{2(2\pi m^* kT)^{3/2}}\right)\right] \qquad (1.11)$$

where S is a constant depending on the relaxation time of the process, m^* is the effective mass of the carrier and k the Boltzmann's constant. Here (+) refers to p-type and (−) to n-type semiconductors. Thus it is often used to determine the conductivity type in semiconductors.

There are two main components contribute to the thermoelectric power of metals and semiconductors. They are the electron-diffusion component and the phonon-drag component. When a small temperature difference Δt is established across a conductor, heat is carried from its hot end to the cold end by the flow of both electrons and phonons. In a metal the conduction electrons are those having energies near the Fermi energy. The energy distribution of these electrons varies with the temperature of the metal. When it is at a high temperature, the metal has more high-energy electrons. When a temperature gradient is established along the sample, the hot end will have more high-energy electrons than the cold end. The high-energy electrons will then diffuse out of the hot end faster than the slower neighbours. This produces a disturbance in the equilibrium distribution of charge carriers and a net electron current will result. This current will cause electrons to pile up at one end of the metal and thereby produce an emf that opposes the further flow of electrons. This explains the thermoelectric power by electron diffusion.

As the phonons move down the sample, they interact with the electrons and drag them along. This produces an additional contribution to the thermo emf - the phonon-drag component. However at higher temperature the phonons begin to scatter more frequently from each other rather than from electrons or impurities. Phonon-phonon scattering eventually become dominant, the electrons are no longer dragged along, and the magnitude of the phonon drag component falls off at higher temperature.

1.7 OPTICAL PROPERTIES: ABSORPTION PROCESSES

These properties span a wide range of phenomena, and aid us greatly in understanding the basic physical properties of semiconductors. These phenomena are also used in the development of optical devices widely used in research and industry. The absorption is measured in terms of the absorption coefficient, defined as the rate of attenuation of electromagnetic radiations per unit length, as it passes through a specimen.

The optical properties can be divided into electronic and lattice properties. The electronic properties, as the name implies, concern processes involving the electronic states of a solid, while the lattice properties involve the vibration of the lattice. Lattice properties are of considerable interest, but electronic properties receive most attention in semiconductors, particularly so far as practical applications are concerned. In semiconductors, a number of distinct optical properties take place independently.

1.7.1 Fundamental Absorption Process

It is the most important absorption process, and it involves the transition of electrons from the valence band to the conduction band. Because of its importance, the process is referred to as fundamental absorption.

In fundamental absorption, an electron absorbs a photon (from the incident beam), and jumps from the valence band into the conduction band. The photon energy must be equal to the energy gap, or larger. The frequency must therefore be

$$\nu \geq (E_g/h) \qquad (1.12)$$

The frequency $\nu_0 = E_g/h$ is referred to as the absorption edge.

In the transition process (photon absorption), the total energy and momentum of the electron-photon system must be conserved. Therefore,

$$E_f = E_i + h\nu \quad \text{and}$$

$$k_f = k_i + q \qquad (1.13)$$

where E_i and E_f are the initial and final energy of the electron in the valence and conduction bands, respectively, and k_i and k_f are the corresponding electron momenta. The vector q is the wave vector for the absorbed photon. Usually the wave vector of a photon in the optical region is negligibly small. The momentum condition given above therefore reduces to

$$k_f = k_i \qquad (1.14)$$

That is, the momentum of the electron alone is conserved. This selection rule means that only vertical transitions in k- space are allowed between the valence band and conduction band. These transitions can be schematically represented by the figure 1.11. Such transitions are called direct transition. The absorption process occurs in the so-called direct-gap semiconductors. Here the bottom of the conduction band lies at $k = 0$, and hence directly above the top of the valence band. Electrons near the top of the valence band are able to make transitions to states near the bottom
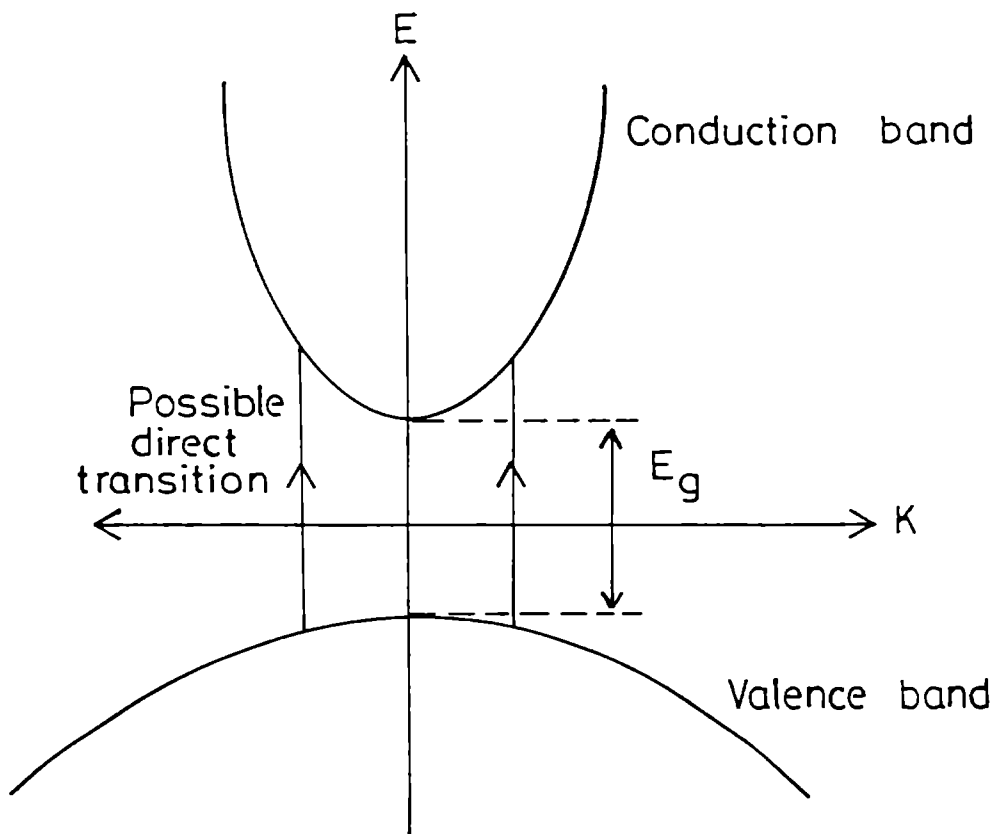
Figure 1.11 Direct transition from the valence band to the conduction band.

of the conduction band, consistent with the selection rule. The absorption coefficient in such transition is given by

$$\alpha = A\,(h\nu - E_g)^{1/2} \qquad\qquad (1.15)$$

where A is a constant involving the properties of the bands, and E_g is the energy gap.

In certain cases, the selection rules forbid direct transitions at $k = 0$, but allow them at $k \neq 0$. The absorption coefficient for such forbidden transition is given by

$$\alpha = A\,(h\nu - E_g)^{3/2} \qquad\qquad (1.16)$$

There are also indirect-gap semiconductors, in which the bottom of the conduction band does not lie at the origin. Figure 1.12 shows the corresponding energy band diagram. In this case the electron cannot make a direct transition from the top of the valence band to the bottom of the conduction band because this would violate the momentum selection rule ($k_f = k_i$).

Such a transition may take place, but as a two-step process. The electron absorbs both a photon and a phonon simultaneously. The photon supplies the needed energy, while the phonon supplies the required momentum (the phonon energy, which is only about 0.05eV, is very small compared to that of the photon, which is about 1eV, and hence may be disregarded. However, the phonon momentum is appreciable). The absorption coefficient for the indirect transition is given by

$$\alpha = A^{'}\,(T)\,(h\nu - E_g)^{2} \qquad\qquad (1.17)$$

Where $A^{'}$ (T) is a constant containing parameters pertaining to the bands and the temperature.

1.7.2 Exciton absorption

In fundamental absorption, it is assumed that the excited electron becomes a free particle in the conduction band, and similarly, the hole left in the valence band is also free. The electron and hole attract each other and may form a bound state, in which the two particles revolve around each other. That is they revolve around their centre of mass. Such a state is referred as an exciton.
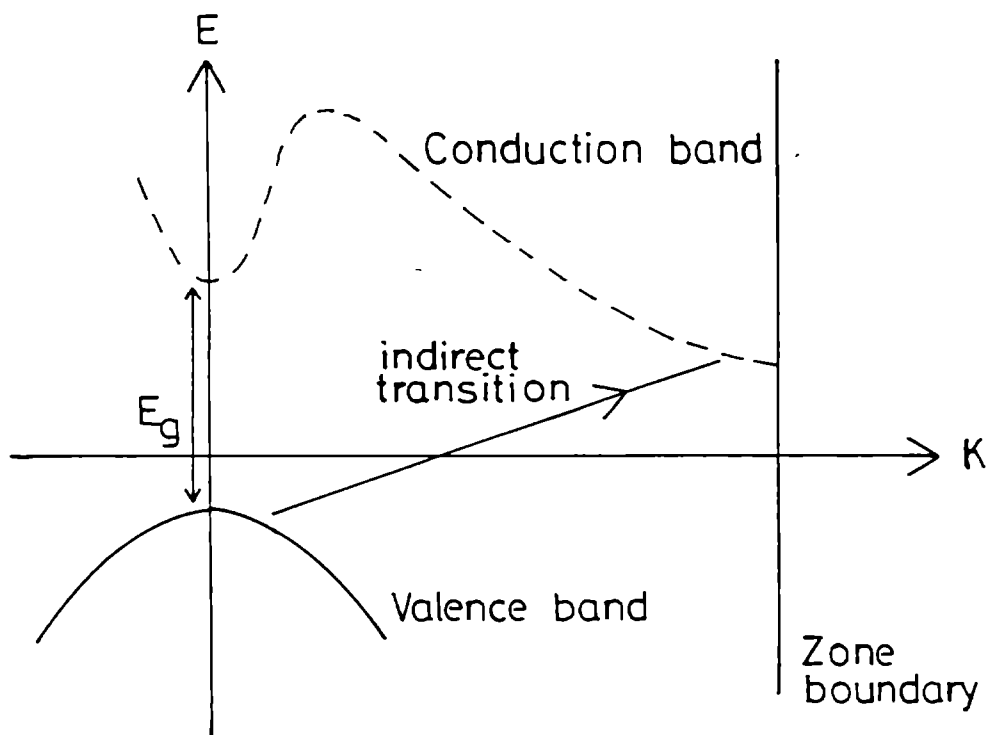
Figure 1.12 Indirect transition from the valence band to the conduction band.

The binding energy of the Exciton is small and is nearly 0.01eV, and hence the Exciton level falls slightly below the edge of the conduction band, as indicated in figure1.13. The Exciton level is in the same neighbourhood as the donor level.

The energy of the photon involved in Exciton absorption is given by

$$hv = E_g - E_{ex}, \tag{1.18}$$

where E_{ex} is the Exciton binding energy. Absorption of an Exciton introduces complications into the fundamental absorption spectrum, particularly near the edge, and renders the determination of the energy gap in semiconductors more difficult. However, Exciton absorption is important in discussion of optical properties of insulators in the ultraviolet region of the spectrum.

1.7.3 Free-Carrier Absorption

Free carriers, both electrons and holes absorb radiation without becoming excited into the other band. In absorbing a photon, the electron (or hole) in this case makes a transition to another state in the same band, as shown in figure 1.14. Such a process is usually referred to as an intraband transition. The free carrier absorption takes place when $hv < E_g$, and frequently this absorption dominates the spectrum below the fundamental edge. For $hv > E_g$, both type of absorption, fundamental and free-carrier absorption occur simultaneously.
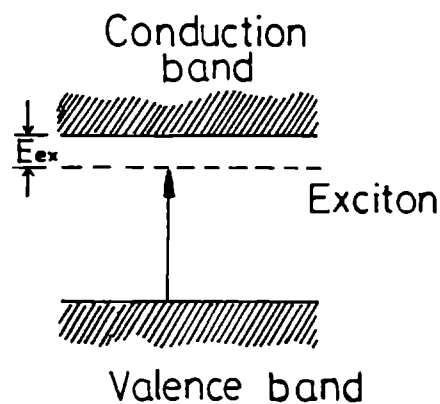
Figure 1.13 Exciton level and the associated absorption.
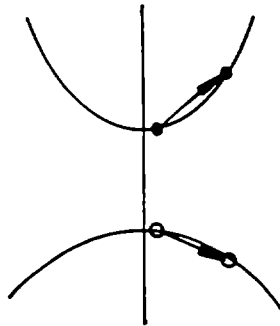
Figure 1.14 Schematic of free carrier absorption.

1.7.4 Absorption process involving impurities

The absorption processes involving impurities often take place in semiconductors. The type and degree of absorption depend on the type of impurity or impurities present, and on its concentration.

Figure 1.15 shows the main classes of such processes. For low energy radiation a neutral donor absorbs a photon and the electron makes a transition to a higher level in the impurity itself or in the conduction band. The transition to higher impurity levels appears as sharp lines in the absorption spectrum. Figure 1.15b shows the transition from the valence band to a neutral acceptor, which is analogous to the donor-conduction band transition as in the case of figure 1.15a.

Figure 1.15c represents a process in which an electron is excited from the valence band to an ionized donor, or from an ionized acceptor to the conduction band. Such processes lead to absorption, which is close to the fundamental absorption, and are seldom resolved from it.

Figure 1.15d illustrates an absorption process, involving transition from an ionized acceptor to an ionized donor. The energy of photon in this case is

$$hv = E_g - E_d - E_a \qquad (1.19)$$

This leads to a discrete structure in the absorption curve, but this is often difficult to resolve because of its proximity to the fundamental edge.
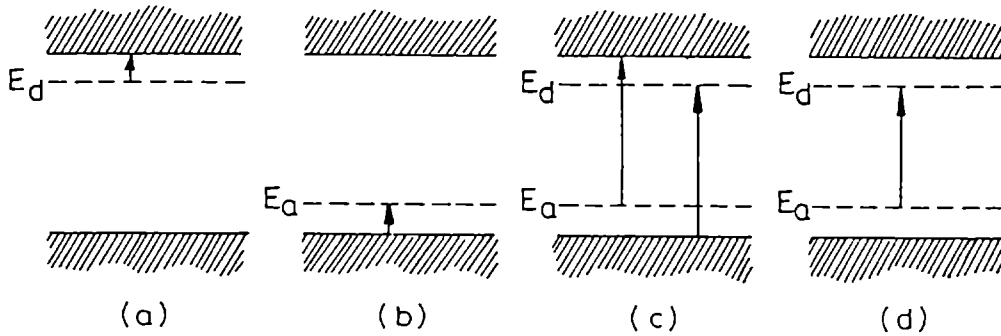
Figure 1.15 Various absorption processes involving impurities.

The impurities may also affect the absorption spectrum in other, indirect ways. For instance, an electron is often found to be trapped by an impurity. This may happen as follows: The impurity first traps an electron, now becoming a charged centre, attracts a hole through the Coulomb force. Thus both an electron and a hole are trapped by the impurity. The spectrum of this Exciton is different from that of the free Exciton, because of the interaction with the impurity.

REFERENCES

1. N.B. Hannay,

    "Semiconductors," (Chapman & Hall, London, 1960).

2. R.A. Smith,

    "Semiconductors," 2nd Edn. (Cambridge University Press, London, 1978).

3. J. Pankove, *"Optical Process in Semiconductors,"*

    (Prentice- Hall, New Jersey, 1971).

4. George Bush and Horst Shade,

    "Lectures on Solid State Physics," (Pregamon Press, New York, 1976).

5. Donald. A. Neamen,

    "Semiconductor Physics and Devices," (IRWIN, Illinois, 1992).

6. M. Ali Omar, *"Solid State Physics- Principles and Applications,"*

    (Addison- Wesley Publishing Company, Philippines, 1975)

CHAPTER 2

THIN FILM PREPARATION METHODS

2.1 INTRODUCTION

Thin films of metals were probably first prepared by Michael Faraday, using electrochemical method. In the earlier stages, scientific interest in these solid films centred on reflective coating on mirrors, antireflection coatings for lenses, multilayer interference filters, automobile headlights, and decorative coatings. Nowadays the thin films are widely used in various fields of science and technology. The need for new and improved optical and electronic devices has stimulated the study of thin film of elements, their oxides as well as binary and ternary compounds; consequently this has accelerated the efforts to develop different thin film deposition techniques. The thin film properties are strongly dependent on the method of preparation. The application and the properties of a given material determine the most suitable technique for the preparation of thin films of that material.

This chapter describes the various methods for preparing thin films for research, development and production purposes. Thin film deposition techniques can be classified broadly into two categories, viz., physical and chemical methods. In physical method, the particles to be deposited have been transferred to vapour state by a physical process, either thermal evaporation, or an impact process. The physical deposition techniques are evaporation, sputtering, ion plating etc. Thin film deposition by chemical methods, includes thin film formation by chemical process in the gas or vapour as well as in the liquid phase. This includes electrodeposition, electroless deposition, pyrolisis, chemical vapour deposition etc. A broad classification of thin film deposition techniques [1-6] is given in table.2.1.

2.2 PHYSICAL METHODS

Under physical methods, vacuum evaporation and sputtering are the important techniques for the deposition of thin films. The deposition of films by these methods occurs mostly at low gas pressure and hence a vacuum chamber is required.

Evaporation in high vacuum

Reactive evaporation

Activated reactive evaporation

Ion plating

Reactive ion plating

Arc evaporation (reactive)

Laser evaporation (reactive)

Reactive sputtering

Cathode sputtering

Magnetron sputtering

rf sputtering

Ion beam deposition

Ionized cluster beam

Plasma decomposition

Chemical vapour deposition

Photo CVD

Plasma enhanced CVD

Electrolytic deposition

Electroless deposition

Electrolytic anodization

Spray pyrolysis

Liquid phase epitaxy

Evaporation

Sputtering

Gas Phase

Liquid Phase

Physical

Chemical

Thin Film Deposition Techniques

Table 2.1

2.2.1 Vacuum Evaporation

Vacuum evaporation is a simple and convenient technique, and is most widely used for the deposition of thin films, both in laboratory and in industry. A material when heated in vacuum will evaporate when its vapour pressure is higher than the surrounding pressure. This is the basic principle in evaporation. The material to be deposited may be heated directly or indirectly. In direct heating the material to be evaporated is always in direct contact with the source. In indirect heating the material to be evaporated is taken in a crucible of glass, quartz or alumina, and the crucible is heated with the heater windings. Obviously this source material should be mechanically and thermally stable at high temperatures and should not react with the material being deposited. The substrate is kept at a distance form the source. The vapour from the source travels through the vacuum, reaches the substrate and condenses to form a film. The vacuum evaporation can be sub divided into different groups, depending on the method used for evaporating the material, as follows:

2.2.2 Resistive Heating

Here the material is evaporated, by electrical resistance heating. Refractory metals like tungsten, molybdenum, and tantalum, which have high melting point and very low vapour pressure, in the form of a boat or wire (helix or basket) are used as the source material. Vapour sources of different designs are used for evaporation, depending on the material to be evaporated. The main disadvantages of the evaporation by simple resistive heating are (a) the reaction of the evaporant material with the source, (b) the difficulty in attaining high enough temperatures for the evaporation of dielectrics, (c) low rate of evaporation, and (d) the dissociation of compounds or alloys upon heating.

2.2.3 Flash Evaporation

This method is used for the preparation of thin films of alloys or compounds. In the case of alloys or compounds due to the difference in vapour pressure of the constituents, the rate of evaporation will be different for each of them. This leads to a difference in the composition of the deposited film as compared to the starting material. In flash evaporation, the boat is heated to a high temperature and then the material to be deposited taken in the form of fine powder is made to fall into this continuously at a slow rate. All the material will evaporate instantaneously and hence the composition is maintained.

2.2.4 Electron Beam Evaporation

Electron beam evaporation is best suited for high temperature materials. Here the material is placed in a water cooled crucible and a fine beam of electrons is focused on to the material. Due to highly localized heating, evaporation takes place from a small volume. This results in congruent evaporation. In the case of compounds like oxides or nitrides, a small quantity of oxygen or nitrogen is fed into the system during the evaporation such that any depletion of the gas due to decomposition will be compensated to maintain the stoichiometry of the film. This process is called reactive electron beam evaporation.

2.2.5 R.F. Heating

Radio frequency heating can be used for the vacuum deposition of materials. By suitable arrangement of the RF coils, evaporation can be achieved, thereby eliminating the possibility of contamination of the film by the source. Preparation of thin films by RF heating is limited because of the coupling needed between the coil and the evaporant and also the difficulty in positioning the coil and the samples properly in a vacuum system for effective coupling. The evaporation rate is difficult to control.

2.2.6 Laser Evaporation

In laser evaporation, lasers are used as the thermal source to vaporize the evaporent materials. The laser source is kept outside the vacuum chamber. Then the laser beam of a few mm diameters is focused on to the target material, and the absorption of energetic radiation results in a thermal shock on the target surface and the material is ablated instantaneously through a plasma plume. The advantage of this technique is that the material composition is faithfully reproduced in the deposited film.

2.2.7 Arc evaporation

In this method, an electric arc between the evaporant and an additional electrode is ignited. Electrodes of the metal to be evaporated are mounted on insulated supports in a vacuum system evacuated to a pressure of 10^{-5}Torr; one of the electrode is rotatable and the other is fixed. Using a standard welding generator, the voltage is applied between the electrodes, and the rotatable electrode is brought into contact with the fixed rod, until a hot spot appears, and then moves away, thus producing an arc. This results in the rapid deposition of the thin film of the electrode

metals on the substrate placed close to the electrode. Films of niobium, tantalum, vanadium and stainless steel can be deposited using this method.

2.2.8 Ion Plating

In this method the substrate is biased to a high voltage during deposition and the material is evaporated either by resistive or electron beam source at a pressure of about 10^{-3}m.bar. Thus a glow discharge is generated in the region between the evaporation source and the substrate. The material that is evaporated becomes ionized during transport, and due to the potential at the substrate, the deposition takes place. Due to the continuous ion bombardment on the growing film, the film adhesion is excellent and this technique is widely used in depositing tribological coatings.

2.2.9 Reactive Evaporation

Reactive evaporation is a variant of Gunther's three temperature method [7]. The basic principle is that for many binary systems, it has been found that a stoichiometric interval exists with a limited degree of freedom in selecting the individual components and substrate temperature for the formation of a particular compound film.

The condensation flux N_k of a given vapour on a given substrate exceeds zero only if the ratio P/P_e exceeds a critical value q_c

$$\text{i.e. } N_k > 0 \text{ if } (P/P_e) > q_c,$$

where P is the actual pressure and P_e is the equilibrium vapour pressure.

At a given substrate temperature, the condition for progressive condensation can be written as

$$N_k = 0 \quad \text{if} \quad N_+ \leq N_{+c}(T)$$

$$N_k > 0 \quad \text{if} \quad N_+ > N_{+c}(T)$$

were N_+ is the incident flux and N_{+c} is the critical value of the incident flux.

If the flux exceeds the critical value N_{+c}, the condensation flux rises rapidly and approaches its maximum value given by

$$N_{k\,max} = \alpha\,(N_+ - N_e)$$

where α is the condensation coefficient and N_e is the re-evaporation flux from the substrate. It is schematically represented in figure 2.1. Here $(P/P_e)^*$ corresponds to the beginning of the nucleation due to surface diffusion.

Assuming a constant incident flux N_+, the conditions for progressive condensation can be expressed in terms of a critical temperature T_c;

$$N_k = 0 \quad \text{if} \quad T > T_c\,(N_+)$$

$$N_k > 0 \quad \text{if} \quad T < T_c\,(N_+)$$

Thus, by analogy with figure 2.1, the condensation can be represented as a function of substrate temperature, and is shown in figure 2.2. Here T^* indicates the beginning of nucleation by surface diffusion.

Suppose the vapour phase consists of two components A and B, both being incident on the substrate under consideration. As the vapour density is low enough, the collision between the particles of the components A and B in the vapour phase can be neglected. However the interaction between the particles can take place in the adsorbed stage on the substrate surface. The interaction may lead to the formation of molecules,

$$A + B \rightarrow AB$$
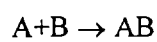
where AB stands for all possible combinations $A_n\,B_m$. A rough estimate of the interaction probability on the surface gives a density

$$n_{AB} = \text{Const.}\;n_A\,n_B\;\overline{D}$$
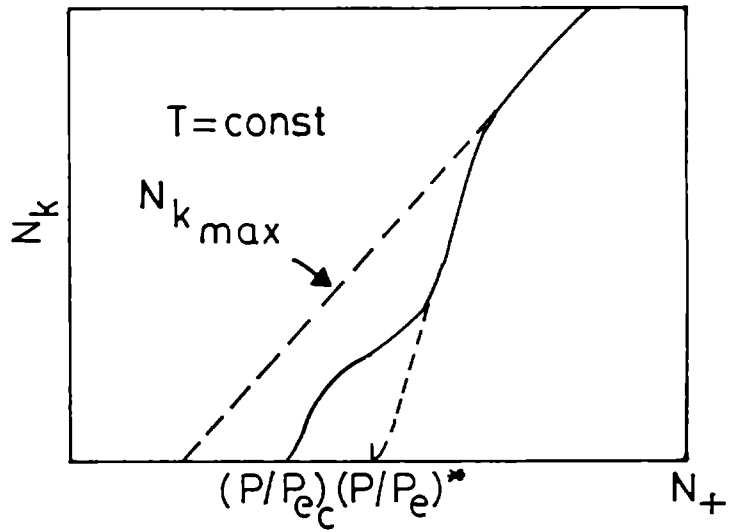
Figure 2.1 Variation of condensation flux N_k with incident flux N_+ of the particles
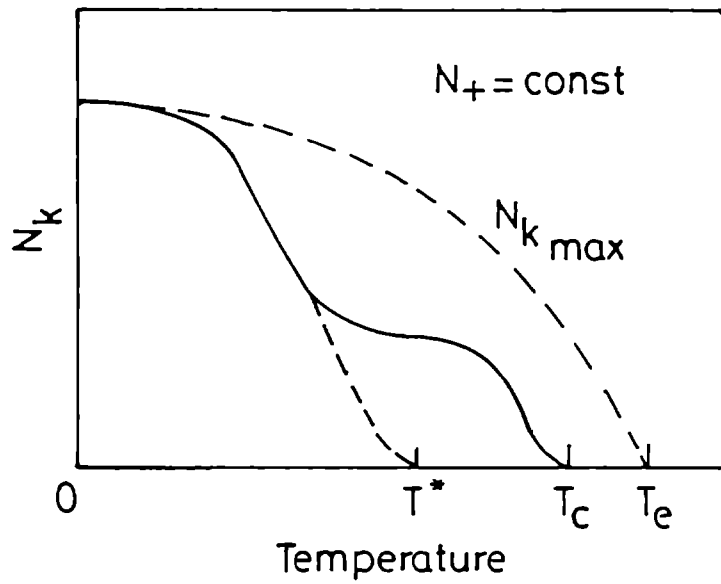
Figure 2.2 Variation of condensation flux N_k with substrate temperature T.

where n_A and n_B are the number of adsorbed atoms of A and B, and $\bar{D}$ the mean diffusion coefficient. It is only a rough calculation, because we are not considering the energies of the colliding particles, as the particles that collide against the substrate with sufficient energy will react to form the compound molecules.

Since the number of adsorbed atoms is proportional to the actual vapour pressure P, or the incident flux N_+ of the particular vapour, the density n_{AB} should also be proportional to the product of incident fluxes (N_{+A} N_{+B}) or vapour pressure (P_A P_B).

In order to estimate the critical values, which now apply, the equilibrium pressures P_{eA}, P_{eB} of the components and the values P_{eAB} of the compound must be considered. P_{eAB} usually corresponds to the dissociation pressure of the compound, and is equivalent to the pressure of the more volatile component (say, A) in equilibrium with the compound. Thus the critical values of one component A in the presence of the other component B should vary as follows.

$$N_{+cA}\ (B) \ll N_{+cA}$$

$$T_{cA}\ (B) > T_{cA}$$

This means that at a given substrate temperature, it will be possible to condense A, in combination with B at a lower critical flux. Or in otherwords, it means that a higher substrate temperature may be used to deposit A in combination with B for a given flux of A.

At a given substrate temperature T, for incident fluxes $N_{+B} < N_{+cB}$, no condensation of any kind is possible while the incident rate N_{+A} is very low. However, at a critical value N_{+cA} (B), sufficient molecules AB are formed on the substrates, and nucleation and progressive condensation of AB starts. This critical value N_{+cA} (B) itself depends on the incident flux of component B. With the further increase of flux N_{+A}, no increase of the condensation flux N_k is possible until, with $N_{+A} > N_{+cA}$, condensation of unreacted A takes place.

Figure 2.3 shows the condensation diagram for two incident components A and B at a given substrate temperature. It can be seen that well defined areas with layers of different compositions can exist as functions of the incident fluxes. There exists one region in particular where only pure compound layers of the composition
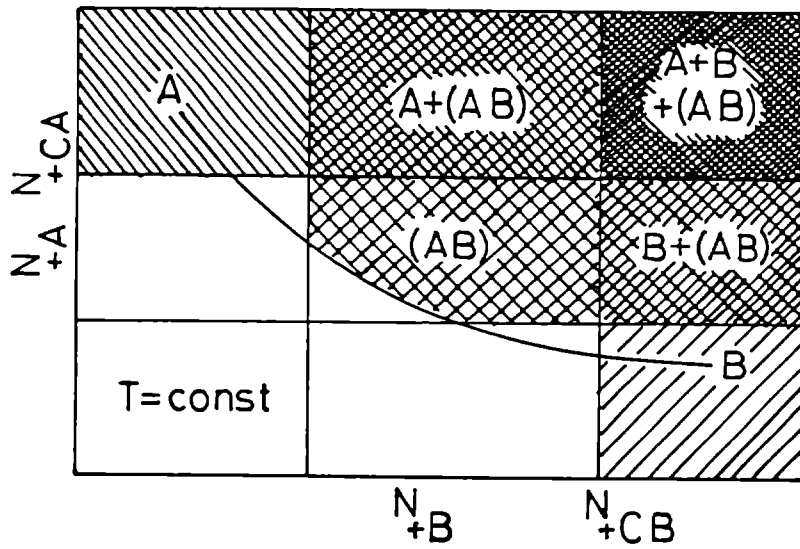
Figure 2.3 Condensation diagram for two incident components A and B

AB is obtained, while the unsaturated components are re-emitted on the vapour phase. This region is determined by the straight lines $N_{+A} = N_{+cA}$, $N_{+B} = N_{+cB}$ and by the curve $(N_{+A} \ N_{+B}) = $ constant, as indicated by the relation $n_{AB} = $ const $n_A n_B$. $\bar{D}$. This special region should occur in all cases, where the condition,

$$P_e \left(\frac{i}{AB} \right) < P_{ei} \ ; \quad (i = A,B)$$

is satisfied, i.e., a significant increase in adsorption energy due to the reaction A+B→AB is necessary. The area of the region is possible only within a limited temperature range. So by separate vapour deposition of two components at a suitable substrate temperature, the deposition of exact stoichiometric compound films is possible. The advantages of the reactive evaporation can be summarized as follows:

1. The need to synthesis the compound from the elements prior to deposition, can be eliminated

2. Very high temperature is needed to evaporate high melting point carbides, nitrides and oxides as such, and if resistive heating is used, the film will be

contaminated as a result of evaporation of the source itself. Reactive evaporation overcomes this difficulty.

3. High rate of deposition of the compounds is possible.

4. The decomposition of the compound upon heating in vacuum and the consequent lack of stoichiometry in the films is avoided.

5. The stoichiometry can be adjusted by simply varying the individual evaporation rates, and thus the carrier concentration and the type of conductivity of the compound can be controlled.

6. Dopants can be evaporated simultaneously and hence the doping level can be controlled.

7. Amorphous films can be prepared by this method, since the lowest substrate temperature is dictated by the condensation temperature of the more volatile component (usually low for O_2, S_2 and Se_2).

8. The film growth can be started and stopped abruptly and hence abrupt interfaces are possible.

Even though the technique can be used for the preparation of many compounds, it suffers from the following drawbacks, which arise from the low chemical reactivity of the particles used for the film formation.

1. The use of large volatile flux entails less loss of the volatile element.

2. When high deposition rates are required, use of large amounts of volatile flux leads to high volatile partial pressure (10^{-4}-10^{-2} Torr) which reduces the mean free path and also scatters the non-volatile beam away from the substrate surface. Also the high pressure in the chamber reduces the evaporation rate of non-volatile components.

3. Because of the high volatile elemental pressure, some unreacted volatile element likely to be entrapped in the growing film, change the film properties, especially at low substrate temperature.

2.2.10 Activated Reactive Evaporation

In the case of certain compounds, the reaction rate of elements to form their compounds may be very low. The reaction rate may be increased in two ways. The first method is by increasing the transilational energy of the particles so that they can overcome the potential barrier. The second method is by lowering the potential barrier itself, so that particles with very low energy can react together.

The translational energy of the particles can be increased by the temperature of the substrate, where the reaction takes place. The substrate temperature cannot be increased beyond a certain range as this may increases the dissociation of the compound thus formed. Also the film formed may re-evaporate from the substrate surface. Another way to increase the translational energy of particles is by increasing the source temperature. But, if the source temperature is increased very much, the evaporation rate will also increase. The evaporation rate must be controlled in reactive evaporation. Hence the most versatile method of increasing kinetic energy of the particles is by ionizing the particles with suitable radiations or electron beams and accelerating them in an electric field.

Bunshah and Reghuram [8] used some of these techniques for the first time to increase the chemical reaction rate; and the technique has been known as Activated Reactive Evaporation (ARE). They used an electric field to activate the reactive gas, by using a low voltage probe. The probe was positively biased around 100V. The secondary electrons from the molten pool of the metal are attracted to this probe. These electrons ionize the reactive gas, generating thick plasma. Due to the presence of this plasma, the reaction rate is very much increased.

In ARE the ions are not accelerated to the substrate and this is because, usually ions are positively charged and will be attracted only to the negatively charged pool of the metal which is in a direction opposite to that of the substrate. Also the applied electric field is confined to a small region above the source of the secondary electrons and ionization of the atoms predominantly takes place beyond this field. So the only increase in translational energy of the atom is from the collisions with electrons. It can be shown that this energy is very low, and hence cannot be the cause for the large increase in chemical reaction rate in ARE.

In ordinary reactive evaporation the particles are not ionized and they have to collide with sufficient translational energy to overcome the potential barrier. But when one of the particles is ionized, the activation energy for chemical reaction becomes very low or equal to zero. This is because of an inverse fifth power attractive force arising from point charge induced dipole interaction between the ion and molecules [9]. This increases the chemical reaction tremendously and hence the high deposition rates. Though chemical reaction rate is very much increased, there is still the problem of amorphous areas and unreacted elements getting entrapped in the

growing film. This can be eliminated by choosing the substrate temperature during deposition. By favourably choosing the substrate temperature, it is possible to re-evaporate the amorphous areas and the unreacted species from the substrate surface, and thus good quality films are obtained. It is also found that with the ratio $T/T_b \approx 0.33$, films with optimum properties are obtained [10-12], where T is the substrate temperature and T_b the normal boiling point of the compound. This particular substrate temperature increases the diffusion into the re-evaporated areas and good quality films can be obtained. If still higher substrate temperature is chosen, the crystalline areas of the film will also re-evaporate, resulting in films of poor quality.

2.3 SPUTTERING

It is one of the earliest techniques used for the deposition of thin films. The basic principle is ejection of surface atoms from a solid on the impingement of energetic particles. This process of ejection of particles by bombarding with positive ions is commonly known as sputtering. The liberated components condense on the surrounding area, and consequently on the substrate surface to form thin film. Nowadays sputtering has become one of the most versatile techniques in thin film technology for preparing thin solid films of almost all materials. Some of the main advantages of the sputtering are (a) high uniformity of thickness of the deposited films, (b) ability of the deposit to maintain the stoichiometry of the original target composition, (c) better reproducibility of the films, and (d) good adhesion to the substrates. Depending on the methods used to eject the atoms/molecules, there can be different types of sputtering.

2.3.1 Glow Discharge Sputtering

The simplest sputtering arrangement is the glow discharge sputtering system. Here an electric field is applied between two electrodes in an inert gas at low pressure $\approx 10^{-2}$m.bar. The material to be deposited is taken as solid disc and is used as the cathode. The substrate can be kept on a platform, which can be floating, biased or grounded. When the cathode is biased to a voltage of 1 to 2KV, at a pressure of about 10^{-2}m.bar, a glow discharge is produced in the chamber between the cathode and anode. The inert gas ions bombard the cathode and knock out the surface atoms through a process of momentum transfer. The rate at which the material is released is dependent on the target material, mass and energy of the incident ion. The pressure

inside the chamber decides the rate of deposition. One disadvantage of the glow discharge sputtering is that the efficiency is normally less than 5%, so that most of the electrons travel towards the substrate without causing ionization and hence the substrate temperature increases. More over it is very difficult to sustain the discharge at low pressure and a high pressure deposition leads to scattering of sputtered particles and hence lower deposition rate.

2.3.2 Magnetron Sputtering

. The difficulties faced in glow discharge sputtering can be overcome using magnetron sputtering. Now it is one of the most widely used methods for the deposition of thin films, for the industrial applications. It makes use of the helical electron motion in the presence of electric and magnetic field. The magnetron sputter cathode is normally designed with permanent magnets placed behind the target material in a water cooled enclosure. This configuration leads to non-uniform erosion of the target; the maximum erosion taking place in the region where the magnetic and electric fields are perpendicular. However the advantage of this method is that the deposition rate is high, and the rise in substrate temperature is low. This can be achieved with a cathode potential of the order of few hundred volts ($\approx$ 500volts), at pressure as low as 5×10^{-4}m.bar. Thus in spite of non-uniform erosion, the magnetron sputtering is a preferred technique while depositing on temperature sensitive substrates.

2.3.3 Scanning Magnetron Sputtering

It reduces the non-uniform erosion of the target material as in the case of magnetron sputtering. Here the magnetic field is scanned on the target surface, using electro-mechanical methods and this results in a better utilization efficiency of the target material.

2.3.4 Bias Sputtering

In this case the substrates are biased with a negative potential with respect to anode, so that it is subjected to an ion bombardment throughout the growth. This effectively cleanse the substrate surface, and the films with good adhesion to the substrates are formed.

2.3.5 R.F. Sputtering

In the case of insulating material, the simple discharge will be ineffective due to the charge build up on the target surface. RF Sputtering uses AC potentials at a

frequency of the order of 13MHz. Due to the difference in the mobility of electrons and ions, the ions are always positioned near the target. The target is maintained at a negative potential due to a capacitor connected in the circuit. Thin films of quartz, aluminium oxide, boron nitrate, mullite, and various glasses can be prepared using RF sputtering. The use of RF sputtering for the deposition of thin films is of great interest because it enables more economical deposition of thin films on to substrates of large area.

2.3.6 Triode Sputtering

It is an alternative method to increase the ionization and sustain the discharge at low pressure. It is made possible by injecting electrons into the discharge from a source other than the target cathode. A hot cathode, which emits electrons through thermionic emission, is used to inject electrons into the discharge system. The total ionization and the ionization efficiency are increased by accelerating these electrons.

2.3.7 Ion Beam Sputtering

One main disadvantage of the sputtering is the high background pressure, which results in the inclusion of gas molecules in the sputtered films. In ion beam sputtering the ion beam is generated using an ion source in a high-pressure chamber. Then it is extracted to the differentially pumped vacuum chamber and directed to a target of the desired material, which is to be sputtered. Here the target and substrate are independent of the acceleration electrode, and therefore the damage due to the collision of ions is much less than in conventional sputtering. The influence of residual gas is much less because the sputtering chamber can be kept at a low pressure, since the ion source is independent of the sputtering chamber. Using this method the films can be prepared at pressure below 10^{-3}Torr.

2.3.8 Reactive Sputtering

In reactive sputtering, the metal is sputtered in the presence of a reactive gas along with the inert gas. The concentration of the reactive gas in the system and the rate of sputtering of the metal would decide the composition of the deposited film. Thus it is possible to deposit a film, which is totally metallic to totally insulating depending on the process conditions.

2.3.9 Unbalanced magnetron Sputtering

Confinement of ionization near the cathode due to transverse magnetic field results in a lower ion density over the substrates. Enhancement of ion bombardment on the substrate in magnetron sputtering is done by unbalancing the magnets such

that some of the magnetic lines of force curve away towards the substrate. Some of the electrons escape along these lines, pulling positive ions along with them by ambipolar diffusion. The energy of bombarding ions can be increased by negatively biasing the substrate. Thus this method retains all the advantages of magnetron sputtering like high deposition rate, low pressure operation etc.; and gives the additional ion bombardment on the growing film.

2.4 ION ASSISTED DEPOSITION

In general thin films deposited by PVD techniques at room temperature are amorphous and tend to have columnar growth. This leads to lower packing density, which leads to deterioration of the properties due to contamination from the atmospheric moisture. An alternative to this is the deposition of thin films at an elevated temperature, which gives additional energy to the adatoms, thereby improving the crystallinity and packing density. However it is not always possible to heat the substrate during deposition to the required temperature. Another method of achieving the effect of substrate temperature is by having ion bombardment during the growth of thin films. By controlling the ion energy and ion density on the substrate, the required microstructure can be achieved.

2.4.1 Kaufman Ion Sources

In ion plating, the pressure in the deposition system is high ($\approx 10^{-3}$m.bar) to cause ionization. This would reduce the mean free path of the vapour, affecting the deposition process. This difficulty can be overcome by introducing a separate ion source into the system. The beam comes out of the ion gun, which is focused onto the substrates. The ion energy and ion density is controlled to achieve the required properties of the films. The disadvantage of such sources is that the ion density is low ($\approx 10^9$cm^{-3}) and the hot filament's life is reduced in reactive gas environment.

2.4.2 Ionized Cluster Beam

Ionized Cluster beam deposition is a recently developed technique that has been widely used for the preparation of high quality films of a wide variety of materials. Clusters are evaporated in a special cell and ionized by electron impact. These ionized clusters will be accelerated against the substrate with a suitable energy. It is assumed that the clusters burst on the substrate and that single atoms with higher mobility diffuse on the substrate surface. The higher energy of the atoms results in an intense mixing of the interface, and hence the adhesion will be improved.

2.4.3 ECR Plasma

Conventional DC and RF glow discharges are low density plasmas (plasma density of the order of 10^{10}cm^{-3}) and operate at rather high pressure $\approx 10^{-3}$m.bar. For many applications, it has been observed that the ion density is an important factor rather than ion energy. Electron cyclotron Resonance (ECR) plasma sources, which uses the principle of resonance of electron frequency in microwave and magnetic field are high density sources (ion density $\approx 10^{13}$cm^{-3}) and with low energy. ECR plasma has been conventionally used in chemical vapour deposition to enhance the reactivity of gas species. Recently ECR plasma is used in PVD systems also. The advantage of ECR source is that it operates at low pressure and it is primarily electrodeless plasma.

2.5 CHEMICAL METHODS

The chemical methods of thin film deposition involve a definite chemical reaction. In general it uses simpler equipment, which are more economical than those used in physical methods. Different kinds of chemical methods are used for the preparation of thin films.

2.5.1 Thermal Growth

A large number of films like oxides, nitrides, carbides can be prepared by heating the metal substrate in the gases of the required type. Preparation of thin films by thermal growth is not a commonly used technique.

2.5.2 Chemical Vapour Deposition (CVD)

It is an important popular technique for the preparation of thin films of a wide variety of materials, elements as well as compounds, on various substrates. In this method the films are formed on substrates, by the reaction of the constituents in the vapour phase. Films of high purity and quality, with required composition and doping levels can be prepared by this method. Several type of chemical reactions, such as chemical transfer, thermal decomposition, reduction, oxidation, nitride and carbide formation etc. are available to carryout the CVD process.

2.5.3 Photochemical Vapour Deposition (Photo CVD)

Photo CVD is a recently developed low temperature deposition technique for the preparation of high quality films. The photochemical deposition takes place when high energy photons selectively excite states in the surface-absorbed or gas phase molecules leading to bond rupture and the production of free chemical species to

form the films or to react to form compound films on the adjacent substrates. UV lamps or lasers are the sources used for the photochemical deposition.

2.5.4 Plasma-Enhanced Chemical Vapour Deposition (PECVD)

PECVD is a versatile technique of depositing a wide variety of thin film materials. Dielectric and semiconducting films such as SiO_2, Si_3N_4, amorphous silicon, polycrystalline silicon etc., can be deposited using PECVD at much lower temperature than are possible with CVD. In this method, plasma produced by RF, DC or microwave fields is used to promote the chemical reaction, the average electron energies in the plasma being sufficient to ionize and dissociate most of the gas molecules.

2.5.5 Electrolytic Deposition

It is basically an electrochemical process and is governed by the law of electrolysis. Electric current is passed through the electrodes, which are immersed in a suitable electrolyte. The material gets deposited on the cathode. The rate of deposition is governed by the laws of electrolysis. By this method, it is possible to deposit films on metallic substrates. The disadvantage of this method is that the film may be contaminated by the electrolyte.

2.5.6 Electroless Deposition

By this method the films can be deposited from a solution, in which no electric potential is applied. The rate of deposition depends on the temperature of the bath and in some cases, the deposition need to be stimulated by a catalyst. This method can be used for large area deposition.

2.5.7 Anodization

This method is used for the deposition of oxide films over certain metals. It is basically an electrochemical process. When the electric current is passed through the electrodes, the anode reacts with the negative ions from the electrolyte and forms an oxide coating. The growth rate of the oxide layer depends on the current density and the temperature of the bath. By this method it is not possible to deposit a film of selected thickness, because most of the metal oxides are insulators.

2.5.8 Liquid Phase Epitaxy

This method can be used for the deposition of high purity epitaxial films of semiconductor compounds. It is based on the crystallisation of semiconducting materials dissolved in a suitable metal of low melting point (viz. Sn, In, Pb, Bi, Ga). A saturated solution of the material at high temperature is prepared, and then allowed

to cool at a suitable rate. The solution becomes super-saturated and a crystalline phase begins to grow over the given substrates. In some cases the solution is removed by some chemical or mechanical means. By this process monocrystalline films with a low number of crystal defects can be prepared.

2.5.9 Spray Pyrolysis

The spray method differs from other chemical solution deposition techniques, in which the film is formed on a substrate kept outside the solution. Here the solution containing soluble salts of the constituent atoms of the compound is sprayed on to the heated substrate, to produce the film either by pyrolytic or hydrolitic chemical reaction of the liquid droplets. It is a simple and inexpensive method for the preparation of uniform coatings over large areas.

2.5.10 Sol-gel technique

Recently this method is widely used for the preparation of thin films. It is simpler and cost-effective and it allows coatings on large surfaces. The substrates are inserted into a solution containing hydrolysable metal compounds (organometallic) and then pulled out at a constant speed into an atmosphere containing water vapour. In this atmosphere, hydrolysis and condensation processes take place. Water and carbon groups are removed by baking at temperature $\approx 500\text{-}600^{\circ}C$.

REFERENCES

1. L. Holland, *Vacuum Deposition of Thin films*, (Chapman Hall, London, 1961.)

2. R.W. Berry, P.M. Hall and M.T. Harris, *Thin Film Technology*, (Van Nostrand, New York, 1968.)

3. K.L. Chopra, *Thin Film Phenomina*, (Mc Graw Hill, New York, 1969.)

4. L.I. Maissel and R. Glang, Eds, *Hand Book of Thin Film Technology*, (Mc Graw Hill, New York, 1970.)

5. K. Rechielt and X. Jiang, Thin Solid Films, **191** (1990) 91.

6. Joy George, *Preparation of Thin Films*, (Marcel Dekker, Inc. New York, 1992.)

7. K.G. Gunther *"The use of thin films in Physical Investigation"* J.C. Anderson, Ed,(Academic Press, New York, 1966) p.213.

8. R. F. Bunshah and A. C. Reghuram, J. Vac. Sci. Tech. **9** (1972) 1389

9. E. W. McDaniel, *Collission Phenomina in Ionized Gases*, (Wiley, New York, 1964)

10. P. S. Vincett, W. A. Barlow and C. G. Roberts, J. Appl. Phys. **48** (1977) 3400

11. P. S. Vincett, Z. D. Popovic and L. McIntyre, Thin Solid Films **82** (1981) 357

12. P. S. Vincett, Thin Solid Films **100** (1983) 371

13. Ed. Schuegraf, *Handbook of Thin Film Deposition Process*, (Noyes Publication, 1990).

14. Donald L. Smith, *Thin Film Deposition – Principles and Practice*, (Mc Graw Hill, 1995).

15. Milton Ohring, *Materials Science of Thin Films*, (Academic Press, 1992)

EXPERIMENTAL TECHNIQUES

3.1 PREPARATION OF COMPOUND THIN FILMS BY REACTIVE EVAPORATION

Reactive evaporation technique, a variant of Gunther's three temperature method [1], was used for the preparation of lead selenide thin films. Lead was evaporated from a molybdenum boat and selenium was evaporated from quartz crucible placed in a conical basket of molybdenum wire.

The rate of evaporation G from a clean surface in vacuum at a temperature T was calculated from the loss of weight per unit area per unit time and is given by Langmuir expression [2]

$$G = P. \left(\frac{M}{2\pi RT} \right)^{\frac{1}{2}} \qquad (3.1)$$

where P is the vapour pressure, M molecular weight of the material and R, the gas constant.

The rate at which the metal atoms arrive at the substrate is best expressed in terms of the deposition rate as observed from the same source at the same temperature and distance, but in the absence of the reactive element flux [3]

$$\frac{dN_m}{A_r.dt} = \frac{N_a \rho_m d'}{M_m} \text{ atoms cm}^{-2} \text{ s}^{-1} \qquad (3.2)$$

where N_a is the Avogadro number, ρ_m, the density of the metal film in gm/cm^3, d' the pure metal condensation rate in cm/sec, M_m the molar mass of the metal in gm/mol, and A_r the receiving surface area in cm^2.

The impingement rate of oxygen molecules is given by

$$\frac{dN_{O2}}{A_r.dt} = 3.513 \times 10^{22} (M_{O2} T)^{-\frac{1}{2}} P_{O2} \text{ molecules cm}^{-2}\text{s}^{-1} \qquad (3.3)$$

where M_{O2} is the molar mass of oxygen, T the gas temperature ($\approx 300K$) and P_{O2} the oxygen partial pressure in Torr.

The impingement rate of the atoms/molecules on the substrates for a given rate of deposition can be calculated using the equations 3.2 & 3.3.

The rate of deposition of the vapour on the substrate also depends on the source geometry, position of the source relative to the substrate and the condensation coefficient. According to Knudsen cosine law, the rate of deposition varies as $\cos\theta/r^2$, for the ideal case of deposition from a uniformly emitting point source to a plane surface, where r is the radial distance of the substrate from the source and θ is the angle between the radial vector and the normal to the substrate surface.

3.1(a)　Vacuum System

The films were prepared in a conventional vacuum system fitted with a 12inch glass bell jar. The working chamber was evacuated to low pressure by a 4inch oil diffusion pump backed by a rotary pump with a pumping speed 200 liters/min. Pirani and Penning Ganges were used to measure the pressure inside the chamber. The evaporation chamber was provided with two high current (100A, 10V) sources for the evaporation of the materials. There were also provisions in the chamber for ion-bombardment cleaning, substrate heating and substrate temperature measurements. The system was also provided with a narrow tube to admit the required gas, which was controlled by a needle valve.

3.1(b)　Substrate Cleaning

Optically flat glass slides were used as substrates. The glass slides were first cleaned with an industrial detergent, then washed in running water, followed by distilled water. Then these slides were rinsed in acetone and were ultrasonically agitated for fifteen minutes in double distilled water. The cleaned substrates were then dried with a hot-air blower and loaded into the vacuum chamber. The substrates were further cleaned by ion-bombardment in the vacuum system for fifteen minutes, prior to the deposition of the film.

3.1(c)　Deposition of the film

The system was initially pumped to a vacuum nearly equal to 10^{-5}m.bar. The substrates were then heated to the required temperature. The temperature was monitored using a fine wire chromel-alumel thermocouple placed in contact with the substrate. High purity (99.999%) lead and selenium were used as the evaporants. A

quartz crucible placed in a conical basket of molybdenum wire was used as the selenium source (S_1). The temperature of the source and hence the flux could be easily controlled by adjusting the current through the molybdenum wire. A boat made of molybdenum sheet (S_2) was used to evaporate lead. The schematic diagram of the set up is shown in Figure 3.1.

When the substrates had attained the required temperature, it was maintained at that temperature for fifteen minutes. Then the current through the selenium source was switched on, and adjusted to a pre-calibrated value, to get a certain selenium flux, keeping the shutter over both the sources. Then the current through the metal (Lead) source was switched on and increased to a pre-determined value, which gave the required metal flux for the deposition of the compound film. The shutter was then removed and the deposition of the compound film was allowed to take place. The individual elements from both the sources met at the substrate surface and combined to form lead selenide. The unreacted elemental atoms/molecules would re-evaporate from the substrate due to the elevated temperature. After completion of the deposition, the shutter was put back in position over the sources and the supply to both the sources switched off. The substrate temperature was then slowly reduced.

For the preparation of oxide films, selenium source was replaced by oxygen source. After the substrate had attained the required temperature, the oxygen was admitted into the chamber. The pressure inside the chamber was controlled by a needle valve, so as to get a pressure $\approx 10^{-3}$m.bar. After 10 minutes the film deposition was done as described earlier.

3.2 PREPARATION OF In_2O_3 AND ITO FILMS BY ACTIVATED REACTIVE EVAPORATION

Certain metals do not readily form their oxide/nitride phase when reactively evaporated in an oxygen/nitrogen atmosphere. This is because of the high activation energy needed for chemical reaction (1-3eV) to form the oxide/nitride phase. Another problem with the reactive evaporation is the low deposition rate. In order to overcome these difficulties, Bunshah [4,5] had developed Activated Reactive Evaporation (ARE).

This thesis reports the preparation of In_2O_3 and ITO thin films by a modified version of the ARE [6]. The set up used for the activated reactive evaporation is shown in the figure 3.2. Here the use of the magnetic field is dispensed with, and

51
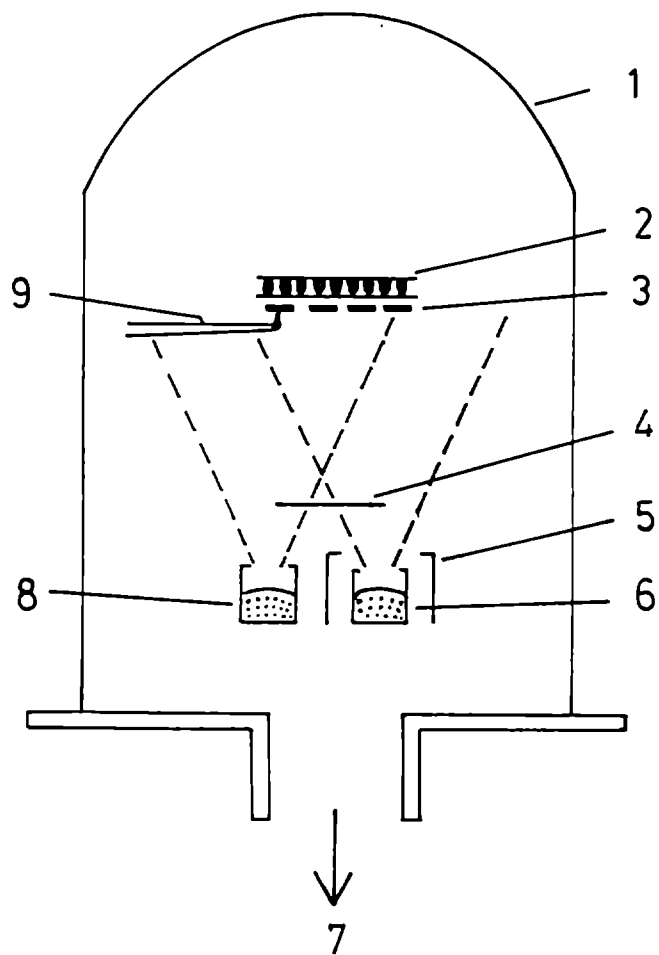
Figure 3.1 Schematic diagram of the experimental set up for reactive evaporation.

1. bell jar 2. substrate heater 3. substrates 4. shutter 5. heat shield

6. metal source (S_2) 7. to pump 8. Selenium source (S_1) 9. thermocouple
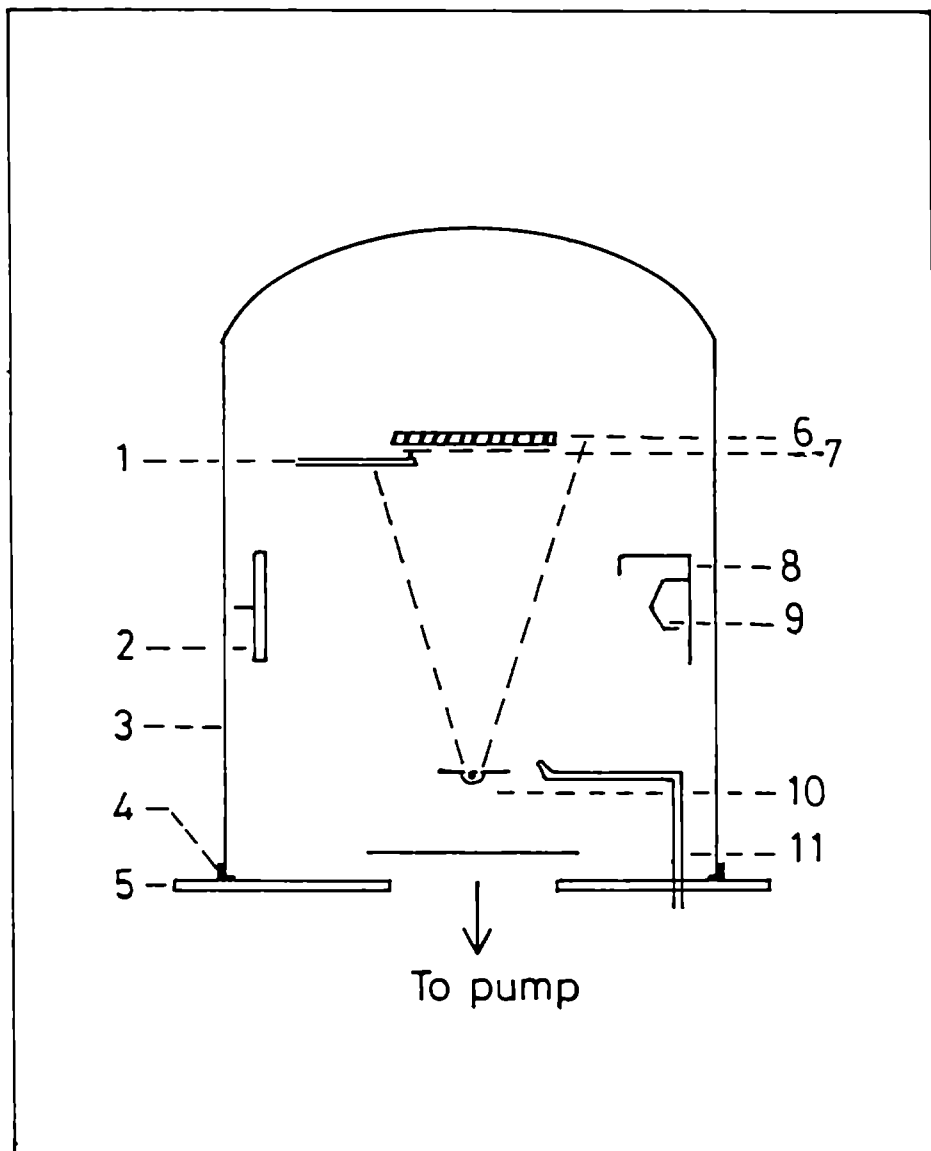
Figure 3.2 Schematic diagram for the experimental set up for ARE

1. thermocouple 2. anode 3. glass bell jar 4. L-gasket 5. base plate

6. substrate heater 7. substrates 8. electron reflector and shield

9. W- filament 10. metal source 11. Cu-tube for O_2 inlet

metallic bell jar can obviously be used. Tungsten electron emitter was used to obtain a high emission current, and a negatively charged reflector behind the emitter was used to direct the electrons towards the anode.

With ordinary reactive evaporation, indium will not form the oxide phase easily on substrates at room temperature. Using the modified ARE technique, it is possible to deposit In_2O_3 and ITO films on substrates at room temperature. The deposition rate was found to be high. Here two tungsten wires of 0.05mm diameter were used as the electron emitters. Anode was made of thick aluminum block of 8.5cm × 8.5cm × 1cm dimensions and was biased at 100V positive with respect to the cathode by a dc supply capable of supplying 2A. The electron emitters were so shielded that small quantities of tungsten evaporating from the filament at such a high temperature would not reach the substrate. With this set up it is possible to maintain the glow discharge down to 5×10^{-4}m.bar of oxygen partial pressure.

3.3 X-RAY DIFFRACTION (XRD)

X-ray diffraction is a non-destructive method to identify the compound and also to determine the structure. To obtain good spectra, the thickness of the sample must be of the order of $2000A^\circ$.

Usually in X-ray diffraction, the Bragg-Brentano geometry is used, where the X-ray beam falls at an angle θ on the film and the detector is at an angle 2θ. The specimen and the detector are rotated at angular velocities ω and 2ω, to get the various diffracting planes. In this geometry when thin films are used, the effective thickness of the films to the incident radiation varies as $t/sin\theta$, where t is the thickness of the film and θ is the angle of incidence of the X-ray beam. Consequently scattered intensities will be angle dependent (enhanced by a factor $t/sin\theta$) and this must be borne in mind when comparing the intensities with the standard powder diffraction data. With proper care, the X-ray diffraction can yield good results and any particular compound in binary or ternary system can be identified without difficulty.

For the present study monochromatic Cuk_α radiation was used. The accelerating voltage applied was 30KV and the tube current was 20mA. The sample was scanned for 2θ values from 20° to 60°.

3.4 ENERGY DISPERSIVE ANALYSIS OF X-RAY (EDAX)

A scanning electron microscope is like a large X-ray tube used in conventional X-ray system. The electrons emitted from the filament are accelerated to high energies where they strike the sample. In the process, X-rays characteristic of atoms in the irradiated area are emitted. By an analysis of their energies, the atoms can be identified and a count of the number of X-rays emitted, the concentration of atoms in the specimen can be determined. In a good energy dispersive spectrometer, the detector resolution is about 150eV, so overlap of the peaks occurs when they are not separated in energy by more than this amount.

3.5 SCANNING ELECTRON MICROSCOPY (SEM)

Scanning electron microscopy is a useful tool for observing the surface features of the films. From the micrograph, grain size and their orientation relative to the substrate surface can be obtained. Scanning electron microscopic studies in conjunction with X-ray diffraction can be used to get a complete understanding of the structural properties of the film.

In scanning electron microscopy, a fine beam of electrons is rastered over the surface of the specimen. The electrons emitted from the surface are collected by appropriate detectors. The output can be used to modulate the brightness of a cathode ray tube (CRT) whose x-y inputs are driven synchronously with the x-y voltages rastering the electron beam. Thus the image produced on CRT is mapped directly to the corresponding point on the sample. The image magnification is simply the ratio of scan length on the CRT to that on the specimen. Resolution of good quality SEM is about 5nm. SEM requires very little in regard to sample preparation, provided that the sample is vacuum compatible. Another requirement is that the samples should be conducting, or else there will be a charge builds up on the sample surface. If the sample is insulating, a thin conducting layer of gold or silver $(50\text{-}100\text{A}^\circ)$ has to be deposited on the surface. However, uncoated insulating samples can be studied with very low beam voltages, though with a compromise on the image resolution. JEOL JSM 35 electron microscope was used to take the SEM micrograph of the samples.

3.6 MEASUREMENT OF FILM THICKNESS

Tolansky's multiple beam interferometric method [7] was used to measure the thickness of thin films. In this method, Fizeau fringes of equal thickness are produced by using a monochromatic light source.

The film whose thickness is to be measured was deposited on a glass substrate with a sharp step between the surface of the substrate and the surface of the film. An over layer of highly reflecting film was then deposited over the film and the bare substrate. A multiple beam interferometer was formed by placing a semi silvered optically flat film on the filmed surface such that both the film surfaces were in contact. A schematic of cross section of the film arrangement for the multiple beam interferometry is shown in figure 3.3a. This interferometer was clamped on a specially made jig with three tilt adjustment screws. Figure3.3b shows the jig for multiple beam interferometry. A typical interferometer arrangement for producing the Fizeau fringes is shown in Figure 3.4a. When the interferometer was illuminated with collimated monochromatic light, fringes with a step at the film boundary is observed. By adjusting the tilt adjustment screws the fringes could be made to run in straight line perpendicular to the step. Figure 3.4b shows the fringes with steps produced by the multiple beam interferometric set up. The fringe spacing and the fringe displacement across the step were measured and used to calculate the film thickness. The thickness of the film is given by

$$t = \frac{d}{D} \cdot \frac{\lambda}{2} \tag{3.4}$$

where D is the fringe spacing, d is the fringe shift and λ the wavelength of the monochromatic light used.

For the production of sharp fringes, the following conditions are to be satisfied.

1. The over layer on the film and the bare substrate must be highly reflective. A reflectivity of 0.94 has been found to be optimum.

2. The thickness of the reflecting surface must be uniform and the film surface must be as close as possible to the semi silvered surface.

3. The divergence of the incident beam must be less than $3°$ and should be normal to the plate.

If narrow, well separated fringes can be produced, film thickness can be measured to an accuracy of $\pm 20A°$.
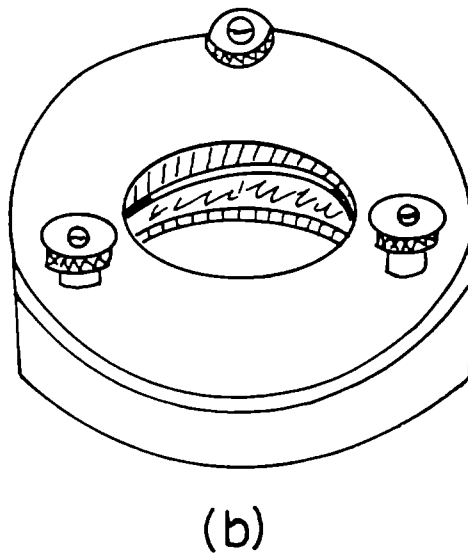
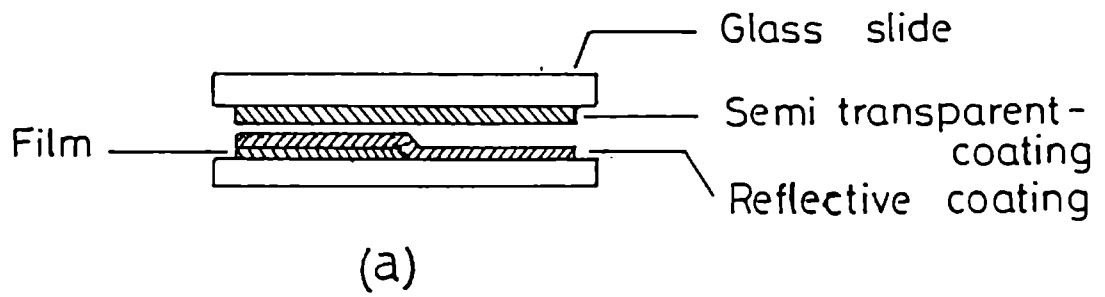Figure 3.3a   Cross section of the film arrangement for the multiple beam

interferrometry.

3.3b   Jig for multiple beam interferometry.

Filter

Beam splitter

Multiple beam interferometer
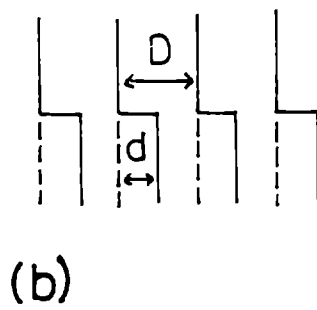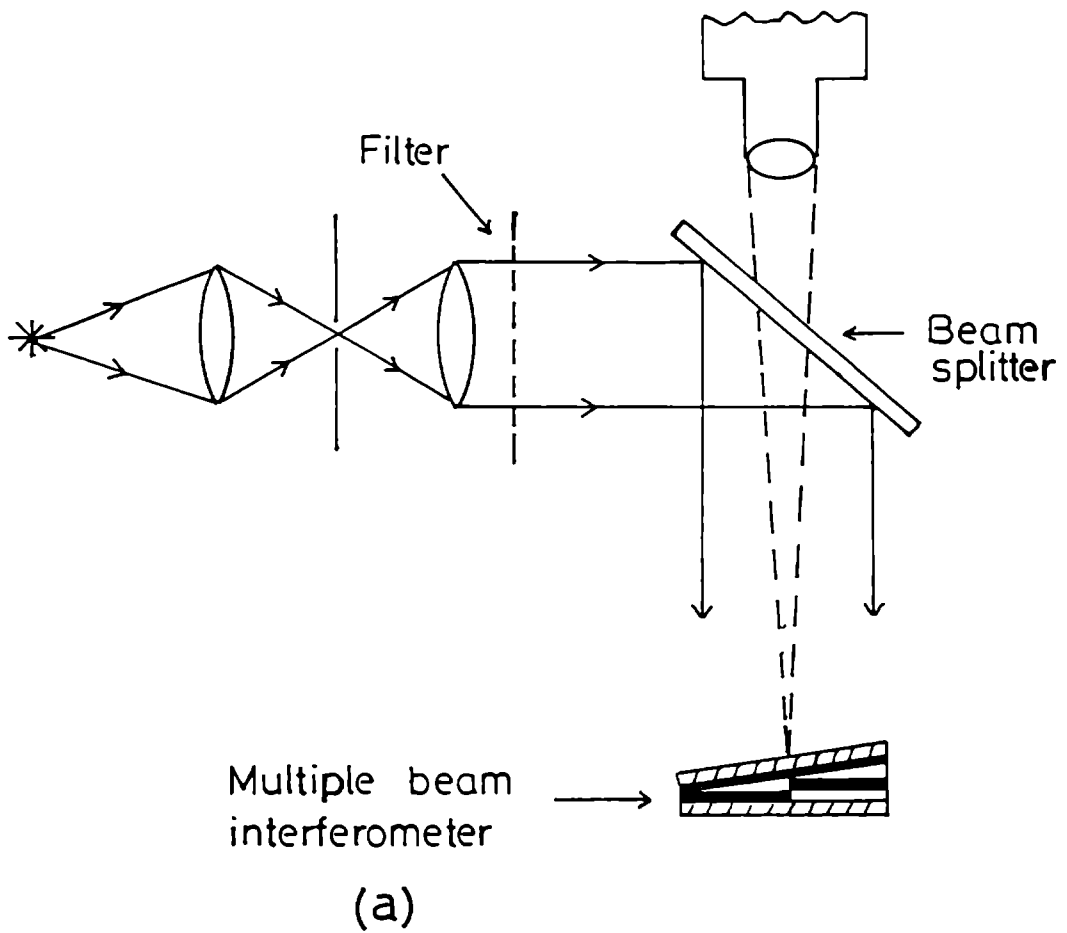
(a)

D

d

(b)

Figure 3.4a Multiple beam interferometer arrangement

3.4b Fringes with steps produced by multiple beam interferometry.

3.7 MEASUREMENT OF ELECTRICAL CONDUCTIVITY

The electrical conductivity of a semiconductor depends on the density of the charge carriers and their mobility. At absolute zero all the semiconductors are considered as insulators. The dependence of the electrical conductivity of semiconductors on temperature is of basic interest not only for understanding the semiconductor properties but also because they are directly utilized in many device applications.

As the temperature is increased from absolute zero, there will be an exponential increase in conductivity of semiconductors, due to the excitation of the electron from the closest donor level to the conduction band. Activation energy for electron transition in this case is the gap between the donor level and the conduction band. If the temperature is further increased, the electrons from the next defect levels are excited and this process continues until all the defect levels are exhausted. In the case of p-type semiconductors transition will take place between valence band and acceptor levels. At sufficiently high temperature excitation of the electrons from the valence band to conduction band takes place and the intrinsic conduction may start. In this region, the activation energy is the band gap between the valence band and conduction band.

Hence the study of the variation of conductivity with temperature gives the information regarding the defect levels as well as the band gap. The energy gap can be determined from the slope of the ln σ Vs 1/T curve, where σ is the conductivity and T is the absolute temperature. Generally the intrinsic conduction starts only at a very high temperature.

Conductivity measurements of highly insulating samples are not very easy, because of the very high resistance. So to measure the current, good quality electrometers must be used in its maximum sensitivity range. This necessitates the heavy shielding of the specimen and the electrometer cable from electrical disturbances. The measurement must be performed in vacuum. Otherwise the humidity present in the atmosphere may short circuit the specimen and gives a higher value of conductivity. A well smoothed dc was supplied to the heater unit, which maintains the samples at various temperatures. One end of the power supply was earthed to eliminate the ripples, if present, masking the required signal. In order to avoid the electrical disturbances, the measuring cell and the heater block were

properly earthed. A fine wire chromel-alumel thermocouple was used to measure the temperature of the sample. The measurement set up and the sample geometry are shown in figure 3.5a

The metal contacts to the specimen to measure the conductivity must be ohmic in nature. The circuit used for measuring conductivity is shown in figure 3.5b. A well smoothed power supply was used to apply the specimen current. The voltage across the specimen was measured with a Keithley 195 DMM and the current was measured using a Keithley 616 digital electrometer.

3.8 CONDUCTIVITY TYPE MEASUREMENT

Hall effect is one means to determine the type of conductivity say, n-type or p-type. But it requires a good deal of sample preparations and is not applicable when the sample is of high resistivity. A simple and convenient technique to test the type of carriers make use of the thermoelectric properties of semiconductors and is known as hot probe method.

When one end of the sample is heated by the hot probe, the electrons at that point gain a high velocity and drifts to the colder end. This produces a disturbance in the equilibrium distribution of the carriers and sets up an electric field which opposes the flow of carriers. This electric field will be positive with respect to the cold end if the carriers are electrons and negative if the carriers are holes.

3.9 MEASUREMENT OF HALL VOLTAGE

One of the most important tools in semiconductor work is the measurement of Hall effect. Conductivity measurements give information about the product of mobility and carrier concentration, but do not serve to separate these quantities. The additional information provided by the Hall effect measurements enables one to determine these quantities separately.

The circuit diagram used for the Hall effect measurement is shown in figure 3.6. A current is passed through the material and a magnetic field is applied at right angle to the direction of the current flow. As a result a voltage develops normal to the direction of the current and applied magnetic field. This voltage is called the Hall voltage (V_H). The sign of this voltage depends on the type of the material being investigated. It is negative when the material is n-type and positive when the material is p-type. The Hall voltage is proportional to the current through the specimen, the
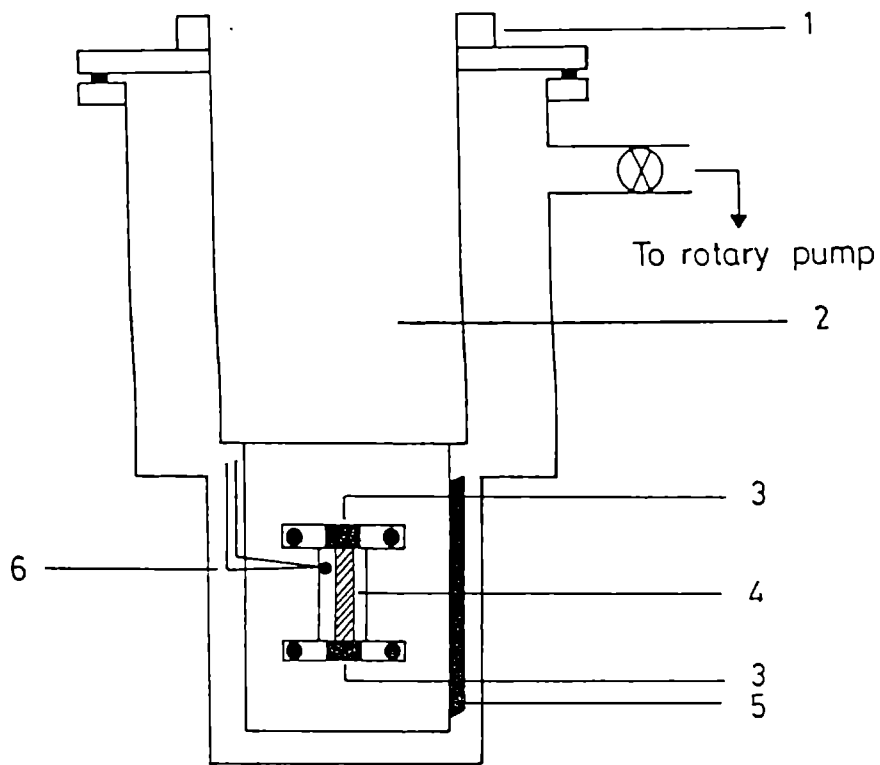
Figure 3.5a Cross section of conductivity measurement cell.

1. Wilson seal 2. Cryogenic fluid 3. Electrodes

4. Specimen   5. Heater   6. Thermocouple
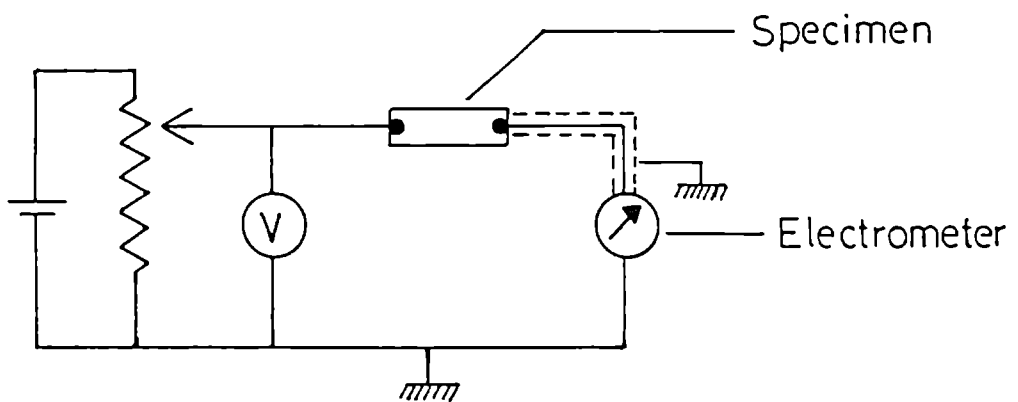
Figure 3.5b Circuit diagram for the measurement of conductivity.

applied magnetic field, and inversely proportional to the thickness of the sample. The proportionality constant is called the Hall coefficient (R_H). It is given as

$$V_H = \frac{R_H IB}{t} \times 10^{-8} \text{ Volts} \qquad (3.5)$$

where I is the current is amperes, B, the magnetic field in gauss, t, the thickness of the specimen in cm, V_H, the Hall voltage in volts and R_H, the Hall coefficient in cm^3/coulomb.

The films for the Hall effect measurements have been deposited on 4cm ×1cm glass substrate using suitable mask.

A schematic diagram of the Hall effect measuring cell is given figure 3.7. The Hall voltage developed across the sample was measured using Keithley 181 nanovoltmeter. The current through the sample was measured using a Keithley 195 digital multimeter. Magnetic field was applied to the sample, using an electromagnet, generating stabilized field. Magnetic field up to 5K gauss was applied. The details of the field stabilized electromagnet can be had from reference 8. Measurements were carried out in a vacuum better than 10^{-2} Torr, using an all metal cell with provision for heating the sample. A fine wire chromel-alumel thermocouple placed in contact with the sample was used to measure the temperature.

Conventional dc method is applicable only if the carrier mobility is greater than a few cm^2 $V^{-1}s^{-1}$, below which single or double ac method is to be used. This is because of the inverse proportionality between the Hall voltage and carrier concentration. In the case of highly resistive samples, it may be very difficult to send an appreciable amount of current, so as to get a reasonable Hall voltage, without producing Joule heating. In such case, the measurement of the required signal may become difficult, due to the increased noise.

3.10 MEASUREMENT OF THERMOELECTRIC POWER

Another important method for studying semiconductors is the measurement of thermoelectric power. The schematic representation of the measurement of the thermoelectric power is shown in figure 3.8. A temperature difference ΔT between the ends of a specimen gives rise to an emf of $Q\Delta T$ millivolts. This defines Q, the thermoelectric power.
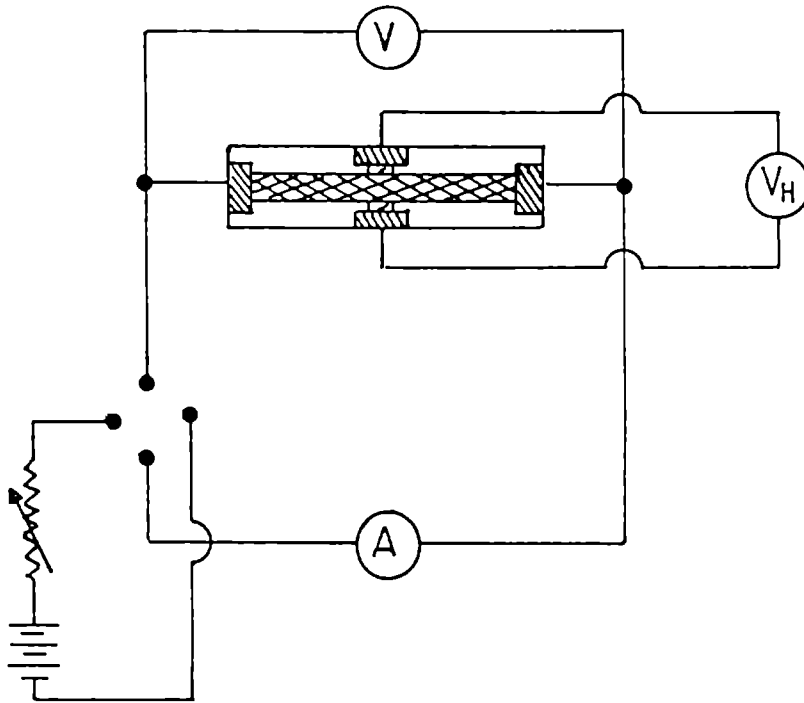
Figure 3.6 Circuit diagram for the measurement of Hall voltage.
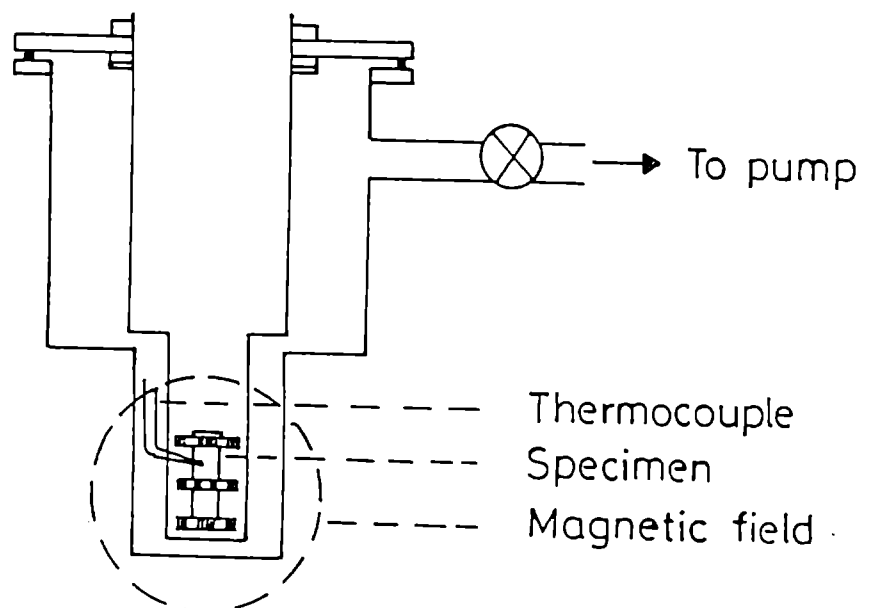
Figure 3.7 Schematic diagram of the Hall effect measurement cell.
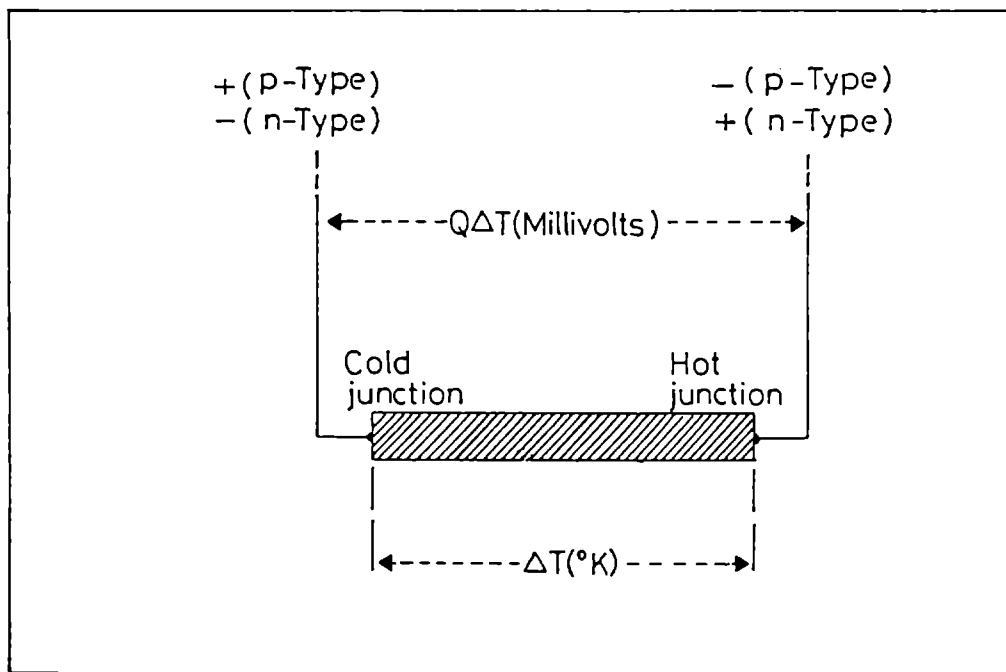
Figure 3.8 Schematic diagram of the measurement of thermoelectric power

Thermoelectric effect has significant applications in both science and technology. Practical applications of this effect include measurement of the temperature, generation of power, cooling and heating. Thermoelectric power of a semiconductor depends up on the scattering mechanism, carrier density, type of carriers and effective mass, and perhaps the forbidden energy gap. The set up for the measurement of thermoelectric power is shown in figure 3.9a and 3.9b. It is in such a way that one end of the film can be connected to heater attachment and the other end to a cold finger. With this arrangement, one end of the specimen can be cooled and the other end can be heated. Fine wire chromel-alumel thermocouples were attached to the ends of the sample using teflon strips to get firm contact. The thermocouple voltage was measured to determine the temperature of each end of the sample and hence the average temperature and temperature difference ΔT. The thermo emf developed across the film was measured using a Keithley 195 digital multimeter, through suitable contacts made to the ends of the sample. All these measurements were taken under a vacuum better than 10^{-2}Torr.
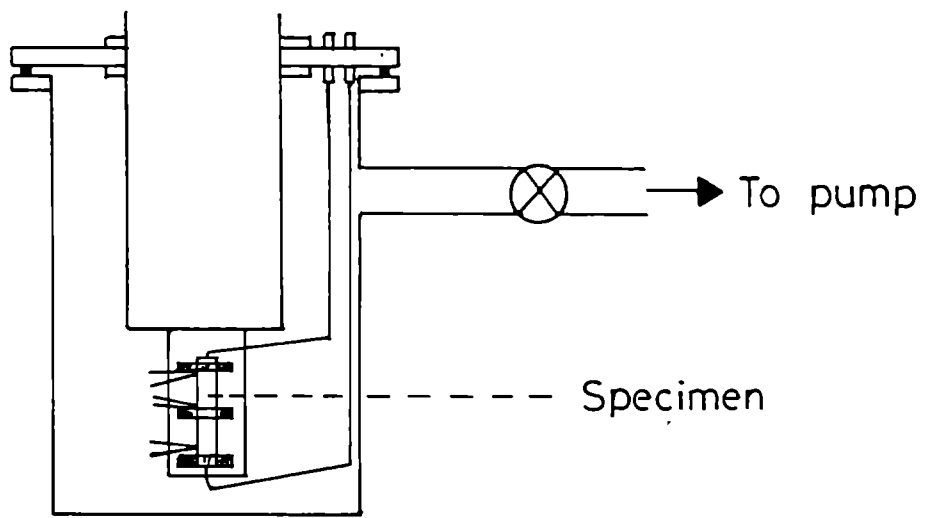
(a)
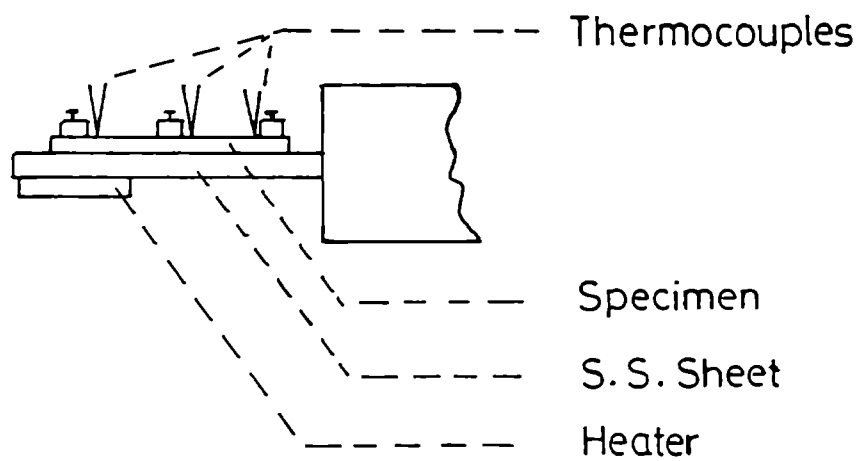
(b)

Figure 3.9a Sectional view of the thermoelectric power measuring cell.

3.9b Side view of the sample mount.

3.11 DETERMINATION OF OPTICAL CONSTANTS OF THIN FILMS

The study of the optical properties of solid is a powerful tool in understanding the electronic and atomic structure of solids. Measurement of optical constants, the refractive index (n), the extinction coefficient (k) and the absorption coefficient ($\propto$) has crucial importance from the point of view of basic and applied research. This is because, these constants are determined by the structure and bonding of atoms in the solid. Hence the measurement of these quantities as a function of wavelength can give valuable information regarding the structure and bonding. Moreover any application of the materials in optics or opto-electronics, n & k are the most important quantities.

Commonly used methods for measuring the optical constants are spectroscopic ellipsometry, simultaneous measurement of transmission and reflection, and measurement of reflection/transmission only. The spectroscopic ellipsometry offers a precise determination of optical constants, particularly at photon energies well above the fundamental edge.

But the method is applicable only in the region of wavelength where polarizers and analyzers are available. Moreover elaborate mathematical calculation is needed. One advantage of this method is that the material need not be transparent to the radiation used.

Simultaneous measurement of transmission and reflection is the most used method for the measurement of the optical constants. This method is applicable in any region of the spectrum if suitable light source and detectors are available and also if the materials is fairly transparent. In the highly absorbing region of the spectra of the material, reflectivity measurements is the only available method.

In the present study, the optical constants are calculated using a method based on the transmission spectrum, developed by Swanepoel [9]. The practical situation for a thin film on a transparent substrate is as shown in figure 3.10. The film has thickness d and complex refractive index η= n-ik, where n is the refractive index and k the extinction coefficient which can be expressed in terms of the absorption coefficient α using the relation.

$$k = \frac{\alpha\lambda}{4\pi} \qquad\qquad (3.6)$$
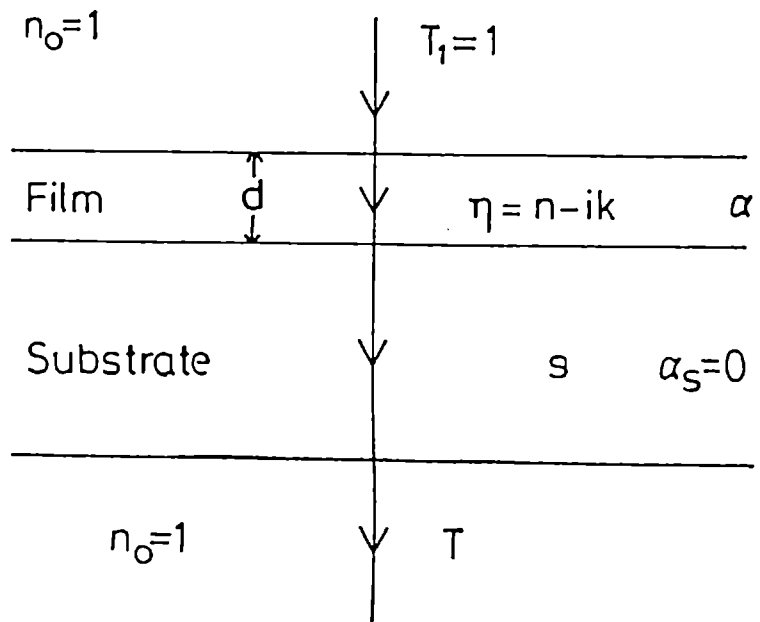
Figure 3.10 System of an absorbing thin film on a thick finite transparent substrate.
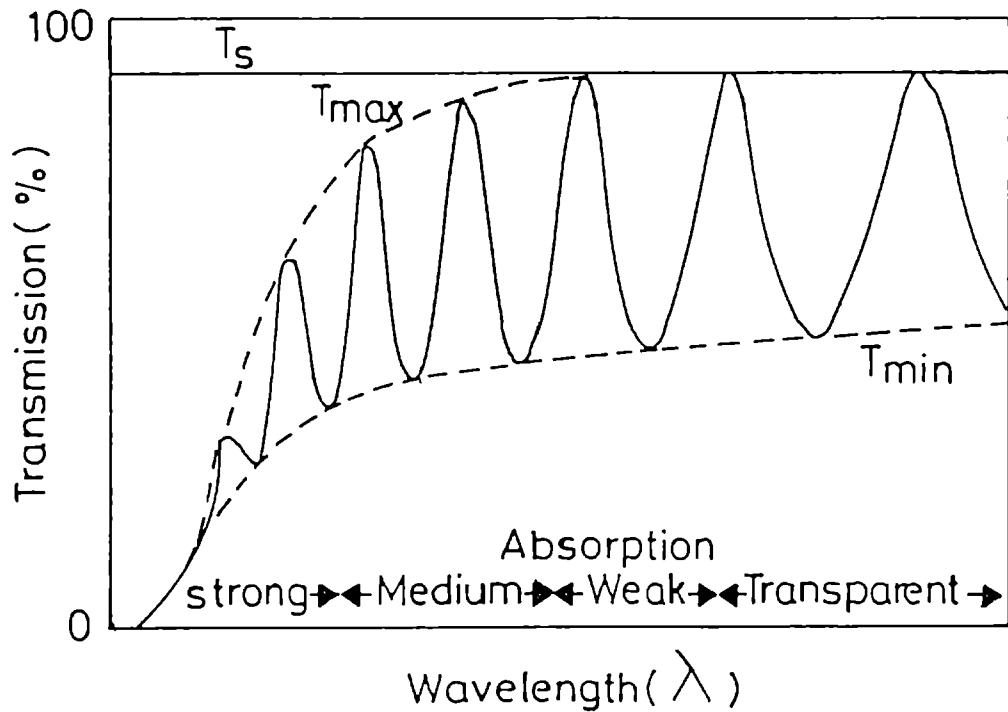
Figure 3.11 Typical transmission spectrum for a thin film of uniform thickness.

where λ is the wavelength of light. The transparent substrate had a thickness of several orders of magnitude larger than d, refractive index s and absorption coefficient α_s = 0. The system is surrounded by air with refractive index n_0 = 1. If the substrate and film surfaces are perfectly smooth and the film thickness d is uniform, interference effects give rise to a spectrum as shown in figure 3.11. These fringes of the transmission spectrum of a thin film surrounded by non-absorbing media can be used to calculate the optical constants of thin film.

Considering the thick substrate alone in the absence of a film, the interference free transmission is given by the expression,

$$T_s = \frac{(1-R)^2}{(1-R^2)}$$

where $R = \left[\frac{(s-1)}{(s+1)}\right]^2$

or $\quad T_s = \frac{2s}{s^2+1}$ $\qquad$ (3.7)

and $\quad s = \frac{1}{T_s} + \left(\frac{1}{T_s^2} - 1\right)^{\frac{1}{2}}$ $\qquad$ (3.8)

The transmission T for the case of figure 3.11 is a complex function. Taking all the multiple reflections at the three interfaces into account, in the case $k^2 \ll n^2$ the expression for the transmission T for normal incidence is given by

$$T = \frac{Ax}{B - Cx\cos\phi + Dx^2} \qquad (3.9)$$

where

$A = 16n^2s$ $\qquad$ (3.10a)

$B = (n+1)^3 (n+s^2)$ $\qquad$ (3.10b)

$C = 2(n^2-1)(n^2-s^2)$ $\qquad$ (3.10c)

$D = (n-1)^3 (n^2-s^2)$ $\qquad$ (3.10d)

$\phi = 4\pi nd/\lambda$ $\qquad$ (3.10e)

$x = \exp(-\alpha d)$ $\qquad$ (3.10f)

The envelops around the interference maxima (T_{max}) and minima (T_{min}) are now considered to be a continuous function of λ, where

$$T_{max} = \frac{Ax}{B - Cx + Dx^2} \tag{3.11}$$

$$T_{min} = \frac{Ax}{B + Cx + Dx^2} \tag{3.12}$$

The spectrum can roughly be divided into four regions. In the transparent region $\alpha = 0$ and the transmission is determined by n and s through multiple reflections. In the region of weak absorption α is small but starts to reduce the transmission. In the region of medium absorption α is large and the transmission decreases mainly due to the effect of α. In the region of strong absorption the transmission decreases drastically due to the influence of α.

In the transparent region $\alpha = 0$ or x = 1. Substituting equation (3.10) into (3.11) yields,

$$T_{max} = \frac{2s}{s^2 + 1} \tag{3.13}$$

which is identical to equation (3.7). This equation can be used to calculate s in the transparent region. Substituting equations (3.10) in (3.12) for x = 1 yields,

$$T_{min} = \frac{4n^2 s}{n^4 + n^2(s^2 + 1) + s^2}$$

or

$$n = [M + (M^2 - s^2)^{\frac{1}{2}}]^{\frac{1}{2}} \tag{3.14}$$

where $M = \frac{2s}{T_{min}} - \frac{s^2 + 1}{2}$

T_{min} is thus a function of both n and s, and n can be calculated form T_{min} using equation (3.14). In the region of weak and medium absorption. $\alpha \neq 0$ and x<1. Subtracting reciprocal of equation (3.11) from equation (3.12) yields an expression that is independent of x,

$$\frac{1}{T_{min}} - \frac{1}{T_{max}} = \frac{2C}{A}$$
(3.15)

Substituting equation (3.10) into (3.15) and solving for n yields

$$n = [N + (N^2 - s^2)^{1/2}]^{1/2}$$
(3.16)

where $N = 2s \dfrac{T_{max} - T_{min}}{T_{max}T_{min}} + \dfrac{s^2 + 1}{2}$

From T_{max} and T_{min}, $n(\lambda)$ can be calculated using equation (3.16) and since $n(\lambda)$ is known, x can be calculated in different ways. Solving equation (3.11) gives

$$x = \frac{E_M - [E_M^2 - (n^2 - 1)^3 (n^2 - s^4)]^{1/2}}{(n-1)^3 (n - s^2)}$$
(3.17)

where $E_M = \dfrac{8n^2 s}{T_{max}} + (n^2 - 1)(n^2 - s^2)$

Solving equation (3.12) gives

$$x = \frac{E_m - [E_m^2 - (n^2 - 1)^3 (n^2 - s^4)]^{1/2}}{(n-1)^3 (n - s^2)}$$
(3.18)

where $E_m = \dfrac{8n^2 s}{T_{min}} - (n^2 - 1)(n^2 - s^2)$.

The reciprocals of equations (3.11) and (3.12) give

$$x = \frac{F - [F^2 - (n^2 - 1)^3 (n^2 - s^4)]^{1/2}}{(n-1)^3 (n - s^2)}$$
(3.19)

where $F = \dfrac{8n^2 s}{T_i}$

and $T_i = \dfrac{2T_{max}T_{min}}{T_{max} + T_{min}}$

where T_i represents the interference free transmission.

In the region of strong absorption the interference fringes disappear.   Values of n can be estimated by extrapolating the values calculated in the other parts of the

spectrum. For very large α the curves T_{max}, T_i and T_{min} converge to a single curve T_0. Then

$$x \approx \frac{(n+1)^3(n+s^2)}{16n^2s}T_0 \qquad (3.20)$$

The refractive index of the substrate can be determined by measuring the interference-free transmission of the clean substrate alone and using equation (3.8) to calculate s.

Since $n(\lambda)$ is calculated, $x(\lambda)$ can be determined from any of the curves T_{max}, T_i or T_{min} using their respective formulae. Measuring the thickness d of the film, $\alpha(\lambda)$ can be calculated form $x(\lambda)$ using the equation $x = \exp(-\alpha d)$

For the measurements, a Hitachi U-3410, UV-Vis-NIR spectrophotometer, which can cover the wavelength range from 2600nm to 185nm, was used. This instrument has got fairly high resolution and a spectral bandwidth of 2nm was used in the instrument.

REFERENCES

1. K.G. Gunther; *"Use of Thin Films in Physical Investigation"*, J.C. Andeson (Ed), (Academic Press, New York, 1966) p. 213.

2. S. Dushmen, *"Scientific Foundations of Vacuum Techniques"*, (John Wiley, New York, 1962) p.17

3. R. Glang, *" Hand Book of thin film Technology"*, L.I. Maissel and R. Glang (Eds.) (Mc Graw Hill, New York, 1970) p.1-81.

4. R.F. Bunshah and A. C. Reghuram, J Vac. Sci. & Tech. **9** (1972) 1389

5. H.S. Randhawa, M. D. Mathews, and R.F. Bunashah, Thin Solid Films **83** (1981) 267

6. J. George, B. Pradeep and K. S. Joseph, Rev. Sci. Instrum. **57** (1986) 2355

7. S. Tolansky, *" Multiple Beam interferometry of Surface and Films "* (Oxford University Press, London, 1948)

8. J. George, K. S. Joseph, B. Pradeep, T. I. Palson and V. Narayanankutty Am. J. Phys. **57** (1989) 184

9. R. Swanepoel, J. Phys. E: Sci. Instrum. **16** (1983) 1214.

TRANSPARENT CONDUCTING OXIDES: AN OVERVIEW

4.1 INTRODUCTION

The interest in transparent conductors has tremendously increased, since the first report of a transparent conducting cadmium oxide film by the thermal oxidation of sputtered films of cadmium [1]. Thin film of metals such as Au, Ag, Cu, Fe etc. having thickness $\approx$ 100Å have also been found to have similar properties. But these films in general, are not very stable and their properties change with time. On the other hand coatings based on semiconductor materials have a large number of applications because of their stability and hardness being superior to those of thin metallic films.

Simultaneous occurrence of high optical transparency ($\geq$80%) in the visible region and the low resistivity (lower than $10^{-3}\Omega$cm) is not possible in intrinsic stoichiometric material. The only way to obtain good transparent conductors is to create electron degeneracy in wide band gap (>3eV) oxides by controllably introducing non-stoichiometry and/or appropriate dopants. These conditions can be obtained in oxides of indium, tin, zinc, cadmium and their alloys, in thin film form. Number of techniques for depositing these transparent conducting oxides (TCO) has been developed, some at large scale production level.

Wide range of applications of these coatings in electronic, opto-electronic and mechanical devices has generated interest in research related to the growth and characterization of these materials. These thin film devices include the following: resistors, solar cells, solar heat collectors, gas sensors, anti-static coatings for instrument windows and anti-reflection coatings. The high transparency in the visible region, together with the high reflectivity in the IR region makes them very attractive for use as transparent heat reflecting materials.

Heterojunction solar cells with an integral conducting transparent layer offer the possibility of fabrication of low cost solar cells with performance, suitable for large scale terrestrial applications. The conducting transparent film permits the transmission of solar radiation directly to the active region with little attenuation. At the same time transparent conducting films can serve simultaneously as a low

resistance contact to the junction and can act as an anti-reflection coating for the active region. Solar cells utilizing these types of coatings are now being widely fabricated, for example SnO_2/Si, In_2O_3/Si, ITO/Si, and $ITO/SiO_x/Si$. Indium Tin Oxide (ITO) can also use as a transparent and conducting electrode for devices working in the near IR region. Heterojuctions of these types such as ITO/InP, ITO/GaSb. ITO/GaAlSb, may be the potential candidates for such applications.

The use of these films as gas sensors is based on the fact that the conductance change in semiconductor materials are large and are caused primarily by the changes in carrier concentration due to charge with the species adsorbed from the gas phase. The electron concentration in the semiconductor gas sensor can vary in the conduction band, approximately linearly with pressure, over a range of up to eight decades, while the variation in carrier mobility is very small. It is this large and reversible variation in conductance with active gas pressure that has made these semiconductor materials, attractive for the fabrication of gas sensing electronic transducers [2-3].

A recent study has shown that the metallic oxide coating onto glass containers appreciably reduces the coefficient of friction of the glass surfaces, facilitating the movement of the containers through high speed fitting lines. It has now become common practice to apply these metallic oxide coatings to glass containers immediately after the forging [4].

In addition to the main applications, TCO films are used in a variety of other applications such as production of heating layers for protecting vehicle windscreen from freezing and misting over [5], optical wave guide based electro-optic modulators [6], photo cathode in phtoelectrochemical cells [7], surface layers in electroluminescent devices [8], laser damage resistant coatings and antistatic surface layers on temperature control coatings in orbiting satellites etc. [9].

Most of the research work on the fabrication of transparent conducting oxides has been restricted to oxides of indium, tin, and their combinations. Some work has been going on other materials such as CdO, ZnO and Cd_2SnO_4. Recently some work on gallium indium oxide ($GaInO_3$) has indicated that this material can also be used as a transparent conductor. Doping of $GaInO_3$ with Ge or Sn results in properties comparable with those of ITO [10]. Some of the properties of certain transparent conductors are listed in table 4.1.

Compound	Structure	Cell dimensions (Å°)			Resistivity (Ω cm)	Band gap (eV)	Dielectric constant	Refractive index
		a	b	c				
SnO_2	Rutile	4.737	------	3.186	10^{-2}-10^{-4}	3.7-4.6	12(E∥a) 9.4(E∥c)	1.8-2.2
In_2O_3	Bixebyte	10.117	----	-------	10^{-2}-10^{-4}	3.5-3.75	8.9	2.0-2.1
ITO	Bixebyte	10.117-10.31	------	-------	10^{-3}-10^{-4}	3.5-4.6	-----	1.8-2.1
Cd_2SnO_4	Sr_2PbO_4	5.568	9.887	3.193	10^{-3}-10^{-4}	2.7-3	-----	2.05-2.1
ZnO	Wurtzite	3.242	-------	5.194	10^{-1}-10^{-4}	3.1-3.6	8.5	1.85-1.9

Table 4.1 Some properties of transparent conducting oxides at room temperature

Given in this chapter a brief review on the preparation techniques, electrical properties and optical properties of transparent conducting oxides.

4.2 TRANSPARENT CONDUCTING OXIDES: BASIC PROPERTIES

4.2.1 Tin Oxide

Tin oxide (SnO_2) has a tetragonal rutile structure with space group D^{14}($P4_2$/mnm) [11]. The unit cell contains six atoms – two tin and four oxygen atoms, as shown in   figure 4.1. Each tin atom (cation) is at the center of six oxygen atoms (anions) placed approximately at the corners of a regular octahedron, and every oxygen atom is surrounded by three tin atoms approximately at the corners of an equilateral triangle.   The lattice parameters are a = b = 4.737Å and c = 3.185Å

The electrical conduction in SnO_2 results from the existence of defects in the crystal, which may act as donors or acceptors. These are generally produced because of either oxygen vacancies or interstitial tin atoms or other intentionally added impurities. If SnO_2 were completely a stoichiometric one, it would have been an insulator or at most an ionic conductor. A perfectly stoichiometric SnO_2 can be made conducting by creating oxygen deficiencies by heating the sample in a slightly reducing atmosphere or by chemical doping. However in practical, the material is never stoichiometric and is invariably anion deficient. This is due to the formation of oxygen vacancies. These vacancies are responsible for the high conductivity of SnO_2.
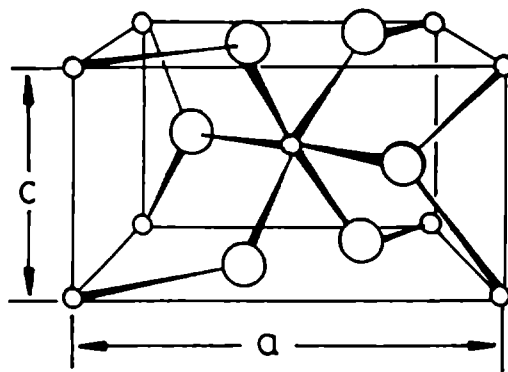
Figure 4.1 Unit cell of the crystal structure of SnO_2. O - indicate oxygen atoms and o- indicate tin atoms.

4.2.2 Indium Oxide

Indium Oxide (In₂O₃) single crystal has a cubic bixebyte structure also called c-type rare earth structure. It belongs to the space group (T^7_h,Ia3). The lattice parameter of In_2O_3 is 10.117 Å. The co-ordination number of indium atom is six-fold and four-fold for the oxygen atom. The unit cell of In_2O_3 contains 80 atoms and as such the structure is highly complicated. However Hamberg and Granqvist [12] and Fan and Goodenough [13] have proposed a simple band structure to explain the conduction mechanism in In_2O_3. According to Hamberg et al [12] In_2O_3 has a parabolic band characterized by effective mass m_c^* for the conduction band and m_v^* for the valence band. Figure 4.2 shows the assumed band structure of In_2O_3. Here E_{go} denotes the direct band gap.

Fan et al [13] and Vincent [14] have suggested that the conduction band is mainly from the In:5s electrons and the valence band is from O^{2-}:2p electrons. For stoichiometric In_2O_3, the Fermi energy E_F is located halfway between the valence band and conduction band. Usually In_2O_3 is reduced and the oxygen vacancies give rise to shallow donor states just below the conduction band. In such case the E_F lies between the donor level and the conduction band minimum.

Usually In_2O_3 is a non-stoichiometric compound. This non-stoichiometry results in an n-type semiconductor or even a semimetal at high electron concentration. The defect structure of In_2O_3 has been studied by De Wit et al [16].

$$E_c^o(k) = \frac{\hbar^2 k^2}{2 m_c^*} + E_{go}$$

$$E_v^o(k) = -\frac{\hbar^2 k^2}{2 m_v^*}$$

Figure 4.2 Band structure of undoped In_2O_3. Shaded area denotes the occupied states.

The oxygen vacancies are assumed to be the point defects in In_2O_3. According to Frank and Kostlin [17], when some oxygen is lost from In_2O_3, the material can be represented as In_2O_{3-x} ($V_o^{\cdot\cdot}$) $e_{2x}^{\cdot}$; where x is normally less than 0.01, $V_o^{\cdot\cdot}$ denotes doubly charged oxygen vacancies and $e^{\cdot}$ denote e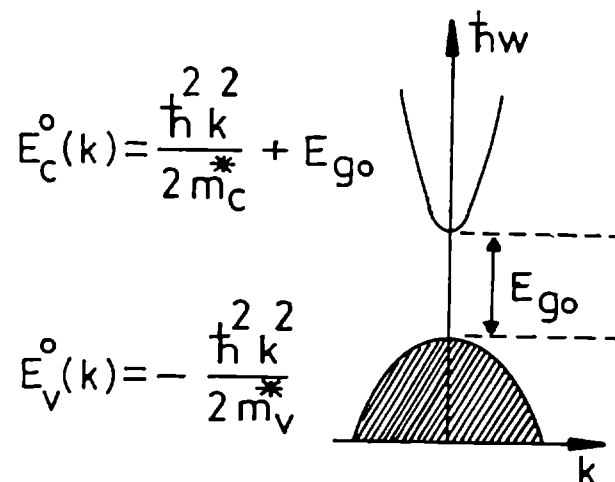lectrons which are needed for charge neutrality on the macroscopic scale. The donor level introduced by stoichiometric defects are generally in the range 0.008eV to 0.03eV, depending on the donor concentration. The donor level lies below the conduction band for low donor concentration. At high donor concentration, an impurity band thus formed overlaps the bottom of the conduction band, producing a degenerate semiconductor.

4.2.3 Indium Tin Oxide

Tin doped Indium Oxide, commonly called indium tin oxide (ITO) films, retains a crystal structure of In_2O_3. The lattice constant of ITO is usually larger than that of the undoped In_2O_3. It is found to depend on the deposition parameters. The lattice constant of In_2O_3 is 10.117Å. For ITO, it is found to vary up to 10.31Å, as observed by many workers [18-20]. The increase in lattice constant is due to the substitutional incorporation of tin ions in interstitial positions. The ITO films in general, exhibits a strong (111) or (100) preferred orientation depending on the preparation conditions.

The properties of ITO can be understood by superimposing the effect of tin doping on the host lattice of In_2O_3. The structure of In_2O_3 is highly complicated and as such the band structure of ITO is not easy to calculate. Hamberg et al [12] assumed a parabolic band structure for ITO like In_2O_3. In the case of ITO partial filling of the conduction band as well as the shift in the energy of the bands relative to their locations in In_2O_3 takes place. It is shown in figure 4.3. In_2O_3 is usually oxygen deficient and these oxygen vacancies give rise to a shallow donor level just below the conduction band. In the case of tin doped In_2O_3, Sn:5s level is stabilized just below E_c. Unlike oxygen vacancies V_O, a two electron donor level, Sn:5s level is a one electron donor level. In ITO films V_O and Sn:5s donor levels co-exist and both contribute conduction electrons as shown in figure 4.4. When In_2O_3 is doped with Sn, tin enters substitutionally in the cation sub lattice. Hence we have Sn^{4+} replacing In^{3+} and acting as an n-type donor. The oxygen vacancies normally do not contribute when there is a large percentage (>10%) of tin. For higher values of doping, the

$$E_c^o(k)=\frac{\hbar^2 k^2}{2m_c^*}+E_{go}$$
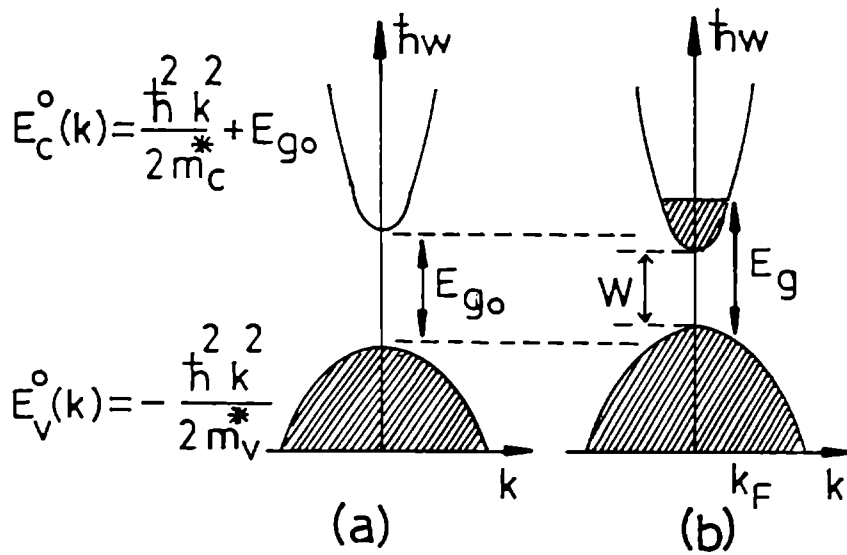
$$E_v^o(k)=-\frac{\hbar^2 k^2}{2m_v^*}$$

Figure 4.3 Band structure of (a) undoped In_2O_3 and (b) Sn doped In_2O_3. Shaded area denote occupied states.
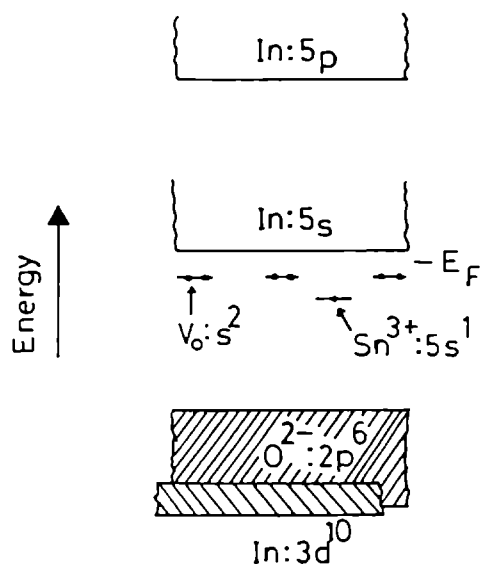
Figure 4.4 Schematic energy band model of Sn-doped In_2O_3.

compensation of part of the donor levels of non-stoichiometric origin starts, and it makes the impurity band narrower and increases the activation energy for conduction.

4.2.4 Cadmium Stannate

Cadmium stannate has two phases, namely Cd_2SnO_4 and $CdSnO_3$. Crystals of Cd_2SnO_4 is generally orthorhombic, whereas $CdSnO_3$ can exist both in rhombohedral and orthorhombic structure. Rhombohedral $CdSnO_3$ has an ilmenite structure, while orthorhombic $CdSnO_3$ has a distorted perovskite structure. Both are wide band gap n-type semiconductors. Films deposited on unheated substrates are normally amorphous in nature, while films deposited on substrates at an elevated temperature are found to be polycrystalline. The films in general exhibit a texture along (100) direction perpendicular to the substrate.

The films of cadmium stannate have been prepared by various techniques. Sputtering and spray deposition are the commonly used techniques for the preparation of this film. In sprayed films, the $CdSnO_3$ phase is formed at substrate temperature $700\text{-}750^\circ C$, whereas at $Ts \geq 800^\circ C$, the Cd_2SnO_4 phase is deposited. These films show a sheet resistance as low as $10\,\Omega/square$ and $100\ \Omega/square$ respectively with a good visible transmittance $\sim 80\%$.

4.2.5 Zinc Oxide

Zinc oxide is technologically an important material. It occurs in nature as the mineral zincite. It crystallizes in the hexagonal wurtzite lattice. The zinc atoms are nearly in the position of hexagonal close packing. Every oxygen atom lies within a tetrahedral group of four zinc atoms, and all these tetrahedra point in the same direction along the hexagonal axis giving the crystal its polar symmetry. The lattice constants are a = 3.24Å, and c = 5.19Å. The fundamental band gap of zinc oxide, calculated from the band structure model is nearly 3.5eV.

Zinc oxide has one of the largest electrochemical coupling coefficients of all non-ferroelectric materials, resulting in its extensive use as transducers in surface acoustic wave devices and microwave delay lines.

The zinc oxide films retain the bulk wurtzite structure and are composed of columnar crystallites with grain size $\sim 100\text{-}300$Å. Sputtered zinc oxide films have strong c-axis orientation, perpendicular or parallel to the substrate depending mainly on the substrate material, while the preferred orientation depends on the deposition parameters.

4.3 GROWTH TECHNIQUES

A variety of thin film deposition technique have been employed to deposit transparent conducting oxides such as indium oxide (IO) tin oxide (TO), antimony doped tin oxide (ATO), fluorine doped tin oxide (FTO), tin doped indium oxide(ITO), zinc oxide(ZO), indium doped zinc oxide (IZO), cadmium oxide(CO) and cadmium stannate (CTO). Since the electrical and optical properties of these oxides depend strongly on the microstructure, stoichiometry and the nature of impurities present. Each deposition technique with its associated parameters yields films of different properties.

4.3.1 Evaporation

Vacuum evaporation and reactive evaporation have been employed to deposit various transparent conducting films. The important control parameters are the evaporation rate, substrate temperature, source to substrate distance and oxygen partial pressure.

Thin films of IO [21,22], TO [23] and ZO [24] have been prepared by the oxidation of the respective metal films. The conductivity and transparency are controlled primarily by the oxidation temperature, which varies from 350-500°C. Reactive evaporation of IO, TO and ITO [25,26] films has been achieved by the vacuum evaporation of the corresponding metal or alloy in an oxygen atmosphere on to substrates heated to about 300-500°C. In activated reactive evaporation (ARE), the reaction between the evaporated species and the gas is activated by establishing thermionically assisted plasma in the reaction zone. Dense plasma is generated in the reaction zone by employing tungsten emitter and a low voltage anode assembly. This technique has been used to deposit high quality transparent conducting thin films of indium tin oxide, antimony doped tin oxide, indium oxide, tin oxide and zinc oxide [27-30].

Oxides of indium, tin, cadmium and zinc can also be deposited by thermal evaporation, electron beam evaporation and flash evaporation from the corresponding oxides[31-34]. When pure or mixed oxides are evaporated, they get reduced and form opaque films of lower oxides. Transparent conducting oxide films are then obtained either by the post oxidation or by the introduction of oxygen during evaporation. In the case of oxidation during deposition, the substrate temperature and the oxygen partial pressure are the main control parameters.

4.3.2 Sputtering

It is one of the most widely used techniques for the deposition of transparent conducting oxide thin films. Both reactive and non-reactive form of DC sputtering, RF sputtering, magnetron sputtering and ion beam sputtering has been used. A_r - O_2, N_2 - O_2 or O_2 are generally used as the sputtering gas, although in some case H_2 has been added to reduce the target and/or film.

Thin films of IO, TO, ITO, CdO etc. were prepared by reactive sputtering by various authors [35-38]. Usually, but not always, the as-sputtered films were found to be amorphous, especially if deposited on unheated substrates. Elevated substrate temperature or a post deposition heat treatment gives polycrystalline films. These films are generally found to exhibit strong preferential orientation, which depends primarily on the sputtering rate and sputtering pressure. In order to obtain the optimum transparent conducting properties, the reactively sputtered films normally require a post deposition heat treatment in either oxidizing or reducing ambient depending on the initial sputtering conditions.

Sputtering from the oxide target to form transparent conducting oxide films offers a better control over the stoichiometry. Highly transparent and conducting films can be deposited using this technique. Hot-pressed, pure or mixed oxide targets are generally used. An improvement in the crystallinity, mobility, visible transmittance and IR reflectance is observed by introducing oxygen over a narrow range of pressure into the chamber during sputtering.

Ion beam sputtering is also used for the deposition of TCO films like IO, TO, ITO etc. Unlike RF sputtering, this method involves minimal intrinsic heating and electron bombardment, and hence constitutes a low temperature deposition method. Using this method, it is possible to produce high quality transparent conducting oxide films on substrates at room temperature [39].

4.3.3 Reactive Ion plating

This method offers the deposition of transparent conducting oxide films on substrates at low temperature [40,41]. It involves reactive evaporation or magnetron sputtering of metals or alloys aided by a low power RF discharge directed towards the substrate. The resulting bombardment of energetic ions or atoms provides energy to the surface of the substrates and of the growing film, eliminates the need for

substrate heating. The presence of ionized reactive species also facilitates their reaction with the evaporated or sputtered atoms.

4.3.4 Chemical Vapour deposition (CVD)

It is one of the most important techniques for producing thin films. It involves a reaction of one or more gaseous reacting species on a solid surface, that is substrate. Metallic oxides are generally grown by the vaporization of suitable organometallic compound.

Tin oxide films are usually deposited by the vaporization of suitable organometallic compounds and their in situ oxidation with O_2, H_2O and H_2O_2. Stannous and stannic chloride, tetramethyl tin, dimethyl tin dichloride and dibutyl tin diacetate are the most commonly used organometallic compounds for the growth of tin oxide films [42-44]. Organometallic compound suitable for the CVD of In_2O_3 is uncommon and expensive. Still this technique is sued for the preparation of In_2O_3 films on large scale. ITO films were also prepared by the same method. Ryabova et al [45] reported a low resistivity $\sim 10^{-4}\Omega$ cm for ITO films prepared by CVD.

(Indium acetylacetonate + tin acetylacetonate) and (indium 2-ethylhexanoate + tin chloride) are commonly used as the starting material for the deposition of ITO films by CVD. Preferential orientation is found to depend on the starting material. ZnO films have also been grown using a CVD technique for piezoelectric, electro-optic and guided wave device applications [46].

4.3.5 Spray Pyrolysis

This is one of the most widely used techniques to deposit transparent conducting oxide films, because it is simple and economical. It is based on the pyrolytic decomposition of a metallic compound dissolved in a liquid mixture when it is sprayed onto a previously heated substrate.

The transparent conducting films of TO, ATO, FTO [47,48] etc. have been deposited by spraying an alcoholic solution usually of $SnCl_4$ and some times of $SnCl_2$, $SnBr_4$ or tetrabutyl tin. Fluorine doping is achieved by adding NH_4F and sometimes trifluoroacetic acid or HF. Similarly $InCl_3$ is used as a source of indium in indium oxide or ITO [49,50]. Tin doping is achieved by adding $SnCl_4$. Transparent conducting zinc oxide films can also be prepared using the same method [51]. Aqueous solution of zinc acetate is usually used as spray solution.

4.3.6 Other Techniques

In addition to the above mentioned preparation techniques, several other techniques which are used to deposit transparent conducting oxide films, include the following:

(a) Pulsed laser evaporation

Transparent conducting oxide films of IO, ITO, TO etc. [52-54] have been prepared using the laser evaporation. Grivas et al [52] used an excimer laser for depositing IO films and Adurodija et al [53] have used the same method to prepare good quality ITO films on glass substrates at room temperature. They obtained a visible transmission $\sim$ 85% and resistivity $\sim$ $4.5 \times 10^{-4} \Omega$cm for the films prepared at room temperature. Dai et al [54] has reported the deposition of SnO_2 films from SnO_2 target using Nd:glass laser. They obtained SnO_2 films on glass substrates at room temperature with (200) orientation and resistivity $3 \times 10^{-3} \Omega$cm with a visible transmittance $\sim$ 75%.

(b) Sol-gel method

This method is also used for the preparation of TO, IO, ITO [55-60]. The sol-gel dip coating is simpler and coast effective and it allows coating of large surfaces. The substrates are inserted into a solution containing hydrolysable metal compounds and then pulled out at a constant speed into an atmosphere containing water vapour. In this atmosphere, hydrolysis and condensation take place. Water and carbon groups are removed by baking at temperature $\sim$ 500°-600°C.

For the deposition of SnO_2, stannous chloride is dissolved in ethyl or isopropyl alcohol. The solution is well stirred, refluxed for one hour, and aged for another two hours. After hydrolysis, the substrates to be coated are dipped in the solution and pulled out at constant speed. Firing at a higher temperature, nearly 600°C gives transparent conducting films of SnO_2. Mattox [55] used a solution of SnO_2 and In_2O_3 as precursors made by dissolving tin isopropoxide $(Sn(OC_3H_7)_4)$ and indium isopropoxide(In $(OC_3H_7)_3$) powders in anhydrous ethanol for the preparation of ITO. For the preparation of ZnO films Chu et al [59] have used zinc acetate dihydrate, ethylene glycol, n-propyl alcohol and glycerol for preparing sol.

(c) Electroless chemical growth technique

This technique is mainly used for the growth of chalcogenide films. It has also been used for the deposition of transparent conducting oxide films. In this

process the substrate is immersed in an acquous solution of metal chloride. Solid phase of metal hydroxide or metal hydrous oxide are formed, which on heating yield the metal oxide.

Thin films of TO and doped TO [56,61] have been prepared using this method. Goyal et al [62] used this technique to deposit In_2O_3 and ITO films. Typical starting solution for In_2O_3 is $InCl_3$, $Na_3C_6H_5O_7$, $AgNO_3$ and distilled water. NaOH is added to this solution to adjust the pH. For ITO coatings, the Sn is added in the form of $SnCl_4$.

4.3.7 Conclusions

Various deposition techniques such as CVD, spray pyrolysis, sputtering, evaporation, activated reactive evaporation, etc. can be employed for the growth of transparent conducting oxide films. The properties of the resulting films depend markedly on the deposition parameters of each technique. The important features related to various techniques are as follows:

(1) Spray Pyrolysis can be employed for the growth of low-cost films for large-area applications where uniformity is not the primary requirement.

(2) The ion-assisted and ARE growth technique is particularly suitable for deposition on polystyrene-like materials where substrate heating is not possible.

(3) For the growth of reproducible device quality films, CVD and sputtering have been extensively used in one form or another. However, deposition rates of CVD methods are usually greater than those of sputtering techniques. The sputter deposition technique, although more complex and more expensive, is preferred as it permits better control of film deposition and thickness.

(4) Techniques such as vacuum evaporation, dip coating, electroless deposition, etc. are of academic interest only and are not suitable for the production of device-grade films.

4.4 ELECTRICAL PROPERTIES

The electrical properties of TCO films depend on the different growth parameters involved in different techniques. Some of the important parameters, which influence the electrical properties, are substrate temperature, film thickness, post-deposition annealing, gas flow rate, doping concentration etc. The effect of some of these parameters on the electrical properties of various TCO films are as follows:

4.4.1 Tin Oxide

Several workers have tried to optimize the substrate temperature in order to grow highly conducting oxide films. It is observed that for films prepared at high substrate temperature, the sheet resistance is much smaller than that prepared at low temperature. Moreover the variation in resistivity with temperature is less in films deposited at higher substrate temperature. It suggests that the grain boundary scattering potential decreases as the substrate temperature increases. Shanti et al [47] have studied in detail, the effect of substrate temperature on tin oxide films grown on glass substrates, by spray pyrolysis. The mobility is found to increase with substrate temperature. It can be explained on the basis of grain boundary scattering. With increase in substrate temperature, the grain size increases [61] causing a decrease in grain boundary potential and hence an increase in mobility. The decrease in grain boundary potential is also responsible for an increase in carrier concentration, with substrate temperature.

The resistivity of SnO_2 film is reported to be almost independent of film thickness if it is greater than 200nm. It is found that the resistivity increases with decrease in thickness. The decrease in resistivity with thickness is more pronounced for films deposited at low substrate temperature. Similar behaviour is observed for IO, ITO, ZO, CO, etc.

The oxygen flow rate which determines the properties of TCO films is an important parameter. In the case of SnO_2 films prepared by CVD [62], the sheet resistance decreases with oxygen flow rate. Initially it decreases, reaches a minimum and then increases. The high value of sheet resistance for low oxygen flow rate may be due to the presence of highly resistive SnO and/or Sn_3O_4 phases. The decreases in concentration of these phases with increased oxygen flow rate reduce the resistivity. A similar behaviour in sheet resistance is observed in films prepared by sputtering also. In all these cases, the mobility and carrier concentration reaches a maximum at the point where the resistivity reaches a minimum. Above the optimised value of P_{O2}, the carrier concentration decreases because of the incorporation of oxygen atoms and thereby reducing the number of oxygen vacancies.

The scattering mechanism involved in conduction process in transparent conducting oxide films is not well established. But many workers have explained their results on the basis of different scattering process. According to Shanthi et al

[47] the mobility increases with increase in temperature, in the range 200-300K for spray deposited SnO_2 films. Here the increase in mobility is attributed to the presence of grain boundary scattering. Normally all the TCO films are degenerate with very high carrier concentration. In such case the effect of mobility on different type of scattering can be classified on the basis of carrier concentration (N); (i). $N<10^{18}cm^{-3}$, in this case the mobility is governed by the barrier effect of the grain boundaries and (ii) $N>10^{19}cm^{-3}$, here the mobility depends only on the transport properties, and the contribution of grain boundaries is almost negligible (iii) $10^{18}cm^{-3} <N<10^{19}cm^{-3}$, here the two contributions, namely bulk properties and grain boundary effects based on film degeneracy, should be considered. It is reported that in films with $N>10^{20}cm^{-3}$ the ionized impurity scattering becomes dominant. Dewall et al [63] has reported that the mobility of undoped SnO_2 films decreases with increase in temperature in the range 0-300°C. This decrease of mobility is probably due to the predominance of lattice scattering on this temperature range.

4.4.2 Indium Oxide Films

Indium oxide is one of the most widely used TCO films, owing to its superior electrical and optical properties. It may be due to the fact that the mobility is much higher than that of SnO_2. All the undoped In_2O_3 films are n-type and highly degenerate. The conduction is due to free electrons originating from oxygen vaccines and/or excess indium atoms in the films, forming the ionized impurity centers.

In the case of a vacuum evaporated In_2O_3 film, it is observed that the resistivity decreases at first and then increases again as the substrate temperature is increased. Here the carrier concentration initially remains constant and then it decreases with increase in substrate temperature. It confirms that the free carrier concentration is mainly because of oxygen vacancies, as suggested by Fan et al [13] and Bosnell et al [64]. In general the crystalline size as well as the crystalline nature of the film improves with increase of substrate temperature.

Oxygen partial pressure during deposition is another parameter, which strongly influences the electrical properties of In_2O_3 film. It is because of the fact that the carrier concentration mainly depends on the oxygen vacancies.

Different types of scattering mechanism have been suggested for conduction of In_2O_3 film. Noguchi et al [65] has observed a weak dependence of mobility on temperature, for films grown by reactive evaporation. In this case the scattering due

to grain boundary is ruled out, because the observed mean free path is smaller than the grain size. Ionized impurity scattering can play a dominant role, because of the presence of oxygen vacancies and /or excess indium atoms.

4.4.3   Indium Tin Oxide (ITO)

ITO films are obtained by doping tin into In_2O_3. Sn^{4+} substitute for the In^{3+} cation, creating a donor level in the energy band gap. Tin doping is found to decrease the electrical resistivity significantly. All the tin doped In_2O_3 films are n-type and completely degenerate. The electrical parameters depend on the dopant concentration.

For In_2O_3 films prepared by spray pyrolysis, the resistivity found to decrease with dopant level up to 5wt%, but increases at higher dopant levels [66]. Similar behaviour has also been observed for ITO films deposited by DC sputtering[67], electron beam evaporation[68] and thermal evaporation [69]. The optimum tin concentration for obtaining lowest resistivity has been found to vary in films prepared by different techniques.

Many workers have observed a decrease in carrier concentration and increase in resistivity beyond 10wt%Sn. According to Kostlin et al [70], for higher dopant levels, tin ions occupy the nearest neighbouring sites more frequently and thereby compensates the donor action. Mizuhashi [71] explained such results in terms of too much distortion of crystal lattice. Manifacier [72] attributed the increase in resistivity to an increase in disorder, which decreases the mobility and free carrier concentration. The decrease in mobility with increase of dopant levels is due to the enhancement of scattering mechanisms, such as ionized impurity scattering.

The contribution of ionized impurity scattering increases with increase of dopant level. For ITO films doped below Sn/In = 0.10, the dominant scattering mechanism is found to be ionized impurity. Tin ions act as ionized impurity scattering centers in addition to the oxygen vacancies and/or excess indium atoms.

In the case of ITO also, substrate temperature is found to affect the electrical properties. The resistivity initially decreases as the substrate temperature increases. This type of dependence of resistivity on the substrate temperature may be due to the fact that crystallinity of the film improves with increase in substrate temperature [73], and hence an increase in conductivity. At higher substrate temperature, the resistivity

increases again. It may be due to the oxidation of InO_x: Sn films. Similar variation in resistivity has been observed by many workers [74,75].

Another factor affecting the electrical property is film thickness. In most cases it is observed that the conductivity and Hall mobility increase with increasing film thickness. The low value of mobility in very thin films can be explained on the basis of scattering at inter crystalline boundaries. The decrease in carrier concentration with thickness may be due to the decrease in defect contribution to the carrier concentration. The increase in conductivity with increase in thickness is due to the improvement in the crystallinity [75-77].

In the case of films prepared by sputtering, the sputtering power and oxygen partial pressure affect the electrical properties [78,79]. The resistivity is found decreasing with increasing sputter power. For low value of sputter power, the target surface is oxidized non-stoichiometrically. Sputtered particles can be further oxidized during their transport from target to substrate or on the substrate surface itself. For high sputter power, the number of sputtered atom increases. So more oxygen atoms are used to oxidize these sputtered species, and the number of oxygen atoms available to oxidize the target decreases. The surface of the target becomes more metallic and so the deposited film has low resistivity.

Post deposition heat treatment also plays an important role in the electrical properties of ITO films. Many workers have studied the effect of annealing on the electrical properties [80,81]. Very high oxygen concentration in ITO increases the electrical resistivity, while too low oxygen content makes the film more metallic. Annealing the film either in a reducing atmosphere or in an oxidizing atmosphere can optimize the concentration of oxygen. Annealing a high resistance film in a reducing atmosphere lowers the oxygen content, thereby making it more conductive. It is also observed that the conductivity decreases for films deposited at low oxygen partial pressure after annealing in oxygen and no marked change in conductivity for films grown at high oxygen partial pressure [82].

4.4.4 Zinc Oxide

It is a II-VI n-type wide band gap semiconductor. In undoped ZnO, the n-type conductivity is due to the deviation from the stoichiometry. The free charge carriers result from the shallow donor levels are associated with the oxygen vacancies and interstitial zinc. The electrical properties of zinc oxide films strongly depend on the

deposition method, thermal treatment and oxygen chemisorption, substrate temperature etc.

For zinc oxide films conductivity is found to increase with increase in substrate temperature up to 350°C. Above 350°C it is found to be decreasing [83]. The increase in electrical conductivity may be due to the increase in carrier concentration in this temperature range. The decrease in conductivity above 350°C is consistent with the decrease in carrier concentration, may be due to the complete oxidation. Many other workers observed similar type of variation [84-86].

Miami et al [87] have reported that, for ZnO films prepared by RF magnetron sputtering, there is no change in the electrical properties of ZnO films exposed to air at room temperature for months. At the same time he has observed a change in the electrical resistance, when the film is heat-treated under vacuum. The increase in resistivity is smaller than that of the heat-treated films in air or oxygen. The electrical resistance of the film is found to increase by three to ten orders of magnitude after heating the film in air. The increase in resistance can be attributed to the chemisorption of oxygen on the surface of the film.

4.4.5 Cadmium Stannate Films (CTO)

Cadmium stannate or cadmium tin oxide is an n-type semiconductor with a wide band gap. Thin films of Cd_2SnO_4 have metal like electrical conductivity $\sim10^3$ $\Omega^{-1}cm^{-1}$, high carrier concentration $\sim10^{20}cm^{-3}$ and mobility $\sim 45cm^2V^{-1}s^{-1}$. The electrical properties depend mainly on the deposition technique, substrate temperature, post deposition annealing etc.

Substrate temperature is an important parameter in the growth of CTO films. Amorphous films are formed when substrates are kept at room temperature [88]. At high substrate temperature $\sim 400°C$, polycrystalline films are obtained [89]. For spray deposited CTO films [89], the conductivity increases with increase in substrate temperature. It is consistent with the increase in the carrier concentration.

The film thickness also affects the resistivity of CTO films. It is found that the resistivity decreases with film thickness up to 2000Å and, for films with thickness >2000Å, it shows almost a constant value. It is consistent with those for other TCO films.

4.4.6 Conclusion

In general, the electrical properties of transparent conducting oxide films depend on the growth techniques and the parameters involved. The common features of the electrical properties of TCO films are:

1. Generally transparent conducting oxide films are n-type.

2. Substrate temperature has a significant effect on the electrical properties of TCO films. Higher substrate temperature creates more oxygen vacancies and hence higher conductivity in these oxide films.

3. The electrical properties of these films are influenced by the process of diffusion of oxygen either into the film or out of it. Post deposition annealing in different ambient such as H_2, NH_4 etc. may further improve the electrical properties.

4. The conduction mechanism in TCO films is governed by carrier concentration. In films having carrier concentration greater than $10^{20} cm^{-3}$, both carrier concentration and mobility are independent of temperature, indicating degenerate semiconductor behaviour. In general when the carrier concentration is less than $10^{18} cm^{-3}$, conduction is always limited by grain boundary scattering. When carrier concentration is greater than $10^{20} cm^{-3}$, ionized impurity scattering is the dominant scattering mechanism.

5. The electrical properties of transparent conducting oxide films improve when they are doped with suitable impurities. In general, it results in an increase in carrier concentration as well as mobility. When excess impurities are added, it forms clusters in the lattice, and distorts. In addition it produces additional scattering centers also. The mobility, in general, increase with doping, reaches a maximum value, and then decreases at higher dopant concentration.

6. Of all the TCO coatings, ITO and fluorine-doped tin oxide have the best electrical properties. Recently aluminium-doped zinc oxide films have also emerged as an alternative to ITO and $F:SnO_2$, due to the comparable electrical properties of Al:ZnO.

4.5 OPTICAL PROPERTIES

The range of transparency, the transmission and reflection of TCO films depend on various parameters such as growth condition, thickness, doping concentration, etc.

4.5.1 Tin Oxide

SnO_2 films show both direct and indirect transition. The direct and indirect band gap of the film is estimated to be ~ 4.2eV and 3.1eV respectively. According to Afify et al [90] the band gap of the SnO_2 films are independent of film thickness. But the values of the band gap, both, direct and indirect, vary with the substrate temperature. Many authors have observed an increase in band gap with increase in substrate temperature [91,92]. It is observed that the transmission increases, whereas the absorption decreases continuously with an increase in oxygen flow rate. With increased oxygen partial pressure, the film possesses mainly SnO_2 phase.

While considering the effect of thickness on the optical properties of SnO_2, Agashe et al [93] observed a reduction in the average transmission with increase in thickness of spray deposited films. Melsheimer et al [94] has observed that the increase in thickness not only decreases the transmission but also shifts the absorption edge towards the larger wavelength region. It is because of the lower number of free carriers. The decrease in the number of free carriers is expected to shift the band edge towards longer wavelength on the basis of Burstein-Moss theory[95,96].

4.5.2 Indium Oxide

Indium oxide thin films are superior to SnO_2 films, because they can be prepared with higher conductivity and IR reflectivity. These films are transparent in the range 0.4-2μm. The transparency and other optical parameters depend on many factors such as growth process, thickness, conductivity, etc.

In_2O_3 is found to show both direct and indirect transition. The direct band gap is found to vary between 3.35eV and 4.2eV depending on the deposition parameters and techniques, whereas the indirect band gap is found to vary between 2.5eV and 3eV. Not much work has been reported on the study of refractive index (n) and extinction coefficient (k) of In_2O_3 film. The reported values of n for In_2O_3 film vary between 1.8 and 2.1. The transmission is normally around 80% thought the visible range, and it can extend up to 1μm. The reflectivity increases to more than 80% beyond 10μm. The electrical parameters of the film also affect the optical properties. The film with highest sheet resistivity shows highest transmission. It is because of the fact that the transmission depends on the conductivity of the film, which in turn depends on the free carrier absorption.

4.5.3   Indium Tin Oxide

The optical properties of In_2O_3 films are greatly influenced by doping. The most commonly used dopant of In_2O_3 is Sn. ITO is having excellent optical and electrical properties. Many workers have studied the optical properties of ITO as a function of doping and other growth parameters [21,53,97,98].

ITO film also shows both direct and indirect transition like TO and IO. Here the effect of Sn doping is that it increases both direct and indirect band gap. It is due to the fact that the Sn doping increases the carrier concentration and hence a widening of the band gap. According to Hamberg et al [12] and Roth et al [99], in addition to band gap widening, there can be band gap narrowing also, because of electron-electron and electron-impurity scattering. These effects are quite significant in ITO films. The band gap narrowing has also been reported to be proportional to $N^{2/3}$, where N is the carrier concentration.

A reduction in refractive index of ITO film [100,101] with increase in carrier concentration is expected according to

$$n^2 = \varepsilon_{opt} - \frac{4\pi Ne^2}{m^* \omega_0^2}$$

(4.1)

This decrease in n is due to the addition of tin, which in turn increases the carrier concentration.

Ohhata et al [100] have studied the effect of annealing on refractive index. It is found that the annealing decreases the refractive index, because the annealing increases the free carrier concentration and conductivity, which in turn, decreases the refractive index. Same phenomenon is observed by Pommier et al [76] while studying the variation of n with substrate temperature.

The transmission characteristics of the ITO films are comparable with IO or TO. But the reflection properties in the IR region are better for ITO films than SnO_2. The Plasma wavelength of ITO film shifts towards the shorter wavelength. The carrier concentration and sheet resistance also influence the transmission and reflection properties of ITO. The IR reflectance increases with increase in carrier concentration.

The reduction in sheet resistivity results in a decrease in transmission. The effect of thickness is found to be less sensitive for ITO films compared to IO or TO films. It is observed that the dependence of transmission on thickness is not exponential, which is contrary to the expected behaviour of transmission as per the relation.

$$T = (1-R)^2 \exp(-\alpha t), \qquad\qquad (4.2)$$

the non-exponential variation of transmission suggests that the physical properties of these films change with thickness.

Nath et al [73] have studied the effect of Sn concentration on the transmission of ITO films. It is found that the addition of Sn to In_2O_3 does not change the transmission significantly up to 15wt% Sn. Above 15wt%, T decreases, mainly because of the free carrier absorption, Yuanri et al [102] have observed that the transmission in the visible range near the band edge increases with increase in carrier concentration. It is due to the fact that an increase in carrier concentration results in shifting of the absorption band edge towards the shorter wavelength. This Burstein-Moss shift reduces the contribution of inter-band absorption, thus increasing the overall transmission at the shorter wavelength.

Oxygen partial pressure is another factor that controls the optical properties. It is observed that the transmission is very poor for low oxygen partial pressure [103]. With increase in oxygen pressure, the transmission increases rapidly and then becomes almost constant. The IR reflection remains constant for low oxygen partial pressure and it drops suddenly with increase in oxygen pressure. The reduction in reflectivity is due to the decrease in the number of carriers and mobility owing to the high oxygen partial pressure. Similar results have been reported by Latz et al [104].

From the dependence of the properties of oxygen partial pressure, we can conclude that there is a minimum oxygen partial pressure for complete oxidation of metallic components. Theuwissen and Declerck [105] have studied the effect of oxygen partial pressure on the transmission of ITO thin films grown by DC reactive sputtering using an In-Sn target. It has been observed that the transmission remained at about 10% for oxygen partial pressure up to 1.2×10^{-3}Torr, after, which transmission sharply increased to about 90% and remained in the range 80-90% for

oxygen partial pressure up to 3×10^{-3} Torr. For P_{O2}, less than 1.2×10^{-3} Torr, the oxidation of target is not possible because all the oxygen atoms were consumed in oxidation of the sputtered metal ions. As such the deposited films are also non-stoichiometric. At very high oxygen partial pressure ($>1.7 \times 10^{-3}$ Torr) the target gets completely oxidized, and no further scope for the sputtered particles to be oxidized. In this range of oxygen partial pressure although the transmission is good, the conductivity is poor.

Post-deposition annealing in various ambient influences the optical properties of ITO films by removing sub-oxides and by changing the carrier concentration. Weijtens et al [106] have observed an increase in carrier concentration and band gap, for DC magnetron sputtered films, annealed in nitrogen atmosphere. Generally annealing increases the transmission in the lower wavelength region and reduces the optical transmission in higher wavelength region. The enhancement of transmission in the lower wavelength can be explained on the basis of Burstein-Moss shift. The annealing increases the carrier concentration, thereby shifting the absorption edge towards the shorter wavelength. The reduction in transmission in the longer wavelength can be explained on the basis of the relation.

$$\alpha = \frac{C\lambda^2 N}{\mu}$$ (4.3)

where C is a constant and μ is the mobility. The increase in carrier concentration results an increase in the value of α. As α depends on the square of wavelength λ, the wavelength dependence of α becomes stronger. So the transmission decreases readily with increasing wavelength in the near IR region.

4.5.4 Cadmium Stannate (CTO)

It is having comparable properties to that of IO, TO, ZO, etc. Not much work has been done on CTO films. Leja et al [107] have observed a direct band gap~3eV for CTO films. Like IO, TO and ITO, the optical properties of CTO is also affected by deposition technique, deposition parameters, annealing, etc. The variation of optical properties with the above parameters are very similar to that of IO, TO and ITO.

CTO film is transparent in the range from 0.5eV to 2.5eV. The transparency decreases beyond 2.5eV because of inter band absorption. The film is having an average transmission greater than 80% in the visible region. In CTO, the transmission is less dependent on sheet resistivity compared with ITO films. The effect of increasing thickness is also not very significant [40].

The substrate temperature has a significant effect on the transmission properties of CTO films. Ortiz [89] has studied the effect of substrate temperature on the transmission of CTO films. It is found that the transmission increases up to a substrate temperature 430°C, and then remains constant. The observed reduced transmission at lower substrate temperature may be due to the presence of sub-oxides and other surface inhomogenities. A similar increase in transmission with substrate temperature is observed by Shiller et al [108] for magnetron-sputtered films. A shift in the direct absorption edge is observed with increase in substrate temperature. This may be due to an increase in carrier concentration which results in band-gap widening.

An important parameter that influences the sputtered films is the oxygen partial pressure. Transmittance of the film deposited in pure argon drops rapidly in the NIR region. This is because of the presence of high carrier density of the films produced in pure argon. Optical absorption studies of these films suggest that the absorption edge shifts towards the shorter wavelength with decreasing oxygen concentration.

The effect of heat treatment in reducing atmosphere at high temperature is found to increase the conductivity, which in turn influences the optical property, because of the change in carrier concentration. Pisarkiewicz et al [109] have studied the effect of annealing on film prepared by reactive DC sputtered CTO films. The films were sputtered in pure oxygen, then annealed in a reducing atmosphere at 500°C. It resulted an improvement in transmission and a shift in absorption edge towards the shorter wavelength. It suggested that the annealing produced an improvement in the overall properties of the CTO film.

4.5.5 Zinc Oxide

Thin films of zinc oxide are being actively investigated as an alternative candidate for applications as a transparent conducting and IR reflective coatings. The films are in general transparent in the wavelength range 0.3-2.5μm. The plasma edge

lies in the range 2.4μm depending up on the carrier concentration in the film. The value of the band gap varies from 3.2eV to 4eV. The optical properties of ZnO and doped ZnO film have been studied by many workers [51, 59,110,111].

The refractive index in the visible region is ≈2. It is observed that the value of k increases at the lower wavelength region and higher wavelength region. Increase in lower wavelength region is due to the inter band absorption and the increase in the higher wavelength side is due to free carrier absorption. A similar behaviour is observed by many workers [112, 113].

Both oxygen partial pressure and substrate temperature play a crucial role in controlling the optical as well as the electrical properties [114]. For oxygen concentration >2% the films are highly transparent, but non-conducting. On the other hand, for oxygen concentration <2% the films are conducting but opaque, for low substrate temperature say up to 470 K. Above 470K, the films are transparent conducting up to 523K. Above 523K the films are transparent and non-conducting irrespective of the oxygen concentration.

The doping also affects the optical properties of Zinc Oxide film. Major et al [113] have studied the effect of tin doping in Zinc Oxide. Still the film exhibits a high transmittance (~80%) in the visible region. Transmission falls very sharply in the UV region. The absorption edge is observed to shift slightly towards the shorter wavelength. This shift is very small than the expected Burstein-Moss shift. This is an indication of band gap narrowing in ZnO films. It is found that the reflectance in the IR region strongly depends on the indium concentration. It increases with increase in indium concentration. Another useful dopant used in ZnO is aluminium. Aluminium doped Zinc oxide is a potential candidate that can be used as a TCO material [115-117]. Hu et al [115] have studied the properties of Al:ZnO films prepared by CVD on substrates at 367°C. The undoped films are transparent throughout the visible and NIR region and has plasma wavelength at ≈ 8.2 μm. The doped samples are still transparent in the visible region, but the plasma edge shifts to 1.28μm. The optical properties of the doped samples are dominated by high free carrier concentration in the film. The maximum reflexivity observed in doped samples is 82%. An increase in substrate temperature to 420°C is found to increase the IR reflectivity to 90%.

Electrical measurements on Al:ZnO films show that the doping increase the carrier concentration to 10^{21}cm^{-3}, which is an order higher than the In doped ZnO films. Moreover, the mobility is also significantly high. Both the high carrier concentration and mobility make Al:ZnO films superior to In:ZnO film for IR reflector applications.

4.5.6 Conclusion

The optical properties of TCO films are strongly dependent on the growth condition and doping concentration. The semiconducting TCO film shows the following important features:

1. There are both direct and indirect allowed transitions. The values of the band gap depend on the growth condition and doping concentration.

2. The absorption edge, in general, shift towards the short wavelength region, with increase in carrier concentration. This can be explained in terms of Burstein-Moss model. Band-gap narrowing is also observed in films with very high carrier concentration ($>10^{20}$) due to electron-electron and electron-impurity scattering.

3. The substrate temperature strongly influences the optical properties. This is due to the fact that the extent of oxidation is decided by the substrate temperature and hence the carrier concentration.

4. ITO and FTO are widely used for practical application. ITO is used for opto-electonic application, whereas FTO is used in large surface, such as heat mirror. Transmission characteristics of ITO and FTO are comparable, whereas IR reflection property of ITO is superior to that of FTO. More over the properties of ITO are less sensitive to the thickness.

5. CTO and ZnO have transparencies comparable to SnO$_2$ and ITO film in the visible region, but the reflection properties are inferior.

6. Undoped ZnO films are not of practical interest, as these films are unstable at high temperature.

7. Al-doped ZnO film shows stable electrical and optical properties. Typical transmission and reflection values are of the order of 85% and 90%. It is a promising material for uses as a transparent conducting oxide.

REFERENCES

1. K. Badaker, Ann. Phys. (Leipzig) **22** (1907) 749.

2. K.L. Chopra, S. Major and D.K. Pandya, Thin Solid Films **102** (1983) 1.

3. H.L. Hartnagel, A.L. Dawar, A.K. Jain and C. Jagadish,

   "Semiconducting transparent Thin Films," (IOP Publishing Ltd. 1995).

4. R. Puyane (Ed.), *"Proceeding of Battele Seminar on Coatings on glass (Geneva),"* Thin Solid Films **77** (1980) 1.

5. H. Yoshida, H. Furubayashi, Y. Inque and T. Tonomura,

   J. Vac. Soc. Japan **19** (1976) 13.

6. R.T. Chen, D. Robinson, Appl. Phys. Lett. **60** (1992) 1541.

7. H.T. Tien, J. Higgins, J. Electrochem. Soc. **127** (1980) 1475.

8. N. Miura, T. Ishikawa, T. Sasaki, T. Oka, H. Ohatat, H. Matsumato, and

   R. Nakano, Japan J. Appl. Phys. **31** (1992) 46.

9. G. Hass, J.B. Heancy and A.R. Toft, Appl. Optics **18** (1979) 1488.

10. R..J. Cava, S.Y. Hou, J.J. Krajewski, J.H. Marshall, W.F. Pack, D.H. Rapkine and R.B. Van Dover, Appl. Phys. Lett **65** (1994) 115.

11. R.W.G. Wyckhoff, *"Crystal Structure"* Vol. 1, 2nd End.,

    (Wiley, New York, 1963).

12. I. Hamberg and C.G. Granqvist, J. Appl. Phys. **60** (1986) 123.

13. J.C.C. Fan and J.B. Goodenough, J. Appl. Phys. **48** (1977) 3524.

14. C.A. Vincent, J. Electrochem. Soc. **119** (1972) 515.

15. J.H.W. De Wit, J. Solid State Chem. **20** (1977) 143.

16. J.H.W. De Wit, G. Van Unen and M. Lahey,

    J. Phys. Chem. Solids **38** (1977) 819.

17. G. Frank and H. Kostlin, Appl. Phys. A **27** (1982) 197.

18. S. Kulaszewicz, Thin Solid Films **76** (1981) 89.

19. H.W. Lehmann and R. Widmer, Thin Solid Films **27** (1975) 359.

20. M. Rottmann, H. Henning, B. Ziemer, R. Kalahne and K.H. Heckner,

    J. Mater. Sci. **31** (1996) 6495.

21. V. Damodara Das, S. Kiruparvathy, L. Damodare and N. Lakshminarayan,

    J. Appl. Phys. **79** (1996) 8521.

22. M. Girtan, G.I. Rusu and G.G. Rusu, Mater. Sci. and Eng. B 76 (2000) 156.

23. M Watanabe, Jpn. J. Appl. Phys. **9** (1970) 1551.

24. M. Watanabe, Jpn. J. Appl. Phys. **9** (1970) 418.

25. D. Laser, Thin Solid Films 90 (1982) 317.

26. P. Thilakan and J. Kumar, Phys. Stat. Sol. (a) 160 (1997) 97.

27. P. Nath and R.F. Bunshah, Thin Solid Films 69 (1980) 63.

28. D.E. Brodie, R. Singh, J.H. Morgan, J.D. Leslie, L.J. Moore and A.E. Dixon

    "Proceedings of 14th IEEE Photovoltaic specialists conference,"

    (San Diego, 1980) p. 468.

29. H.S. Randhawa, M.D. Mathews and R.F. Bunshah,

    Thin Solid Films 83 (1981) 267.

30. M. D. Benoy and B. Pradeep, Bull. Mater. Sci. **20** (1997) 1029.

31. C.A. Pan and T.P. Ma, Appl. Phys. Lett. **37** (1980) 163.

32. A. Balasubramanian, M. Radhakrishnan and C. Balasubramanian,

    Thin Solid Films **91** (1982) 71.

33. K.G. Gopachandran, B. Joseph, J.T. Abraham, P. Koshi and V.K. Vaidyan,

    Vacuum **48** (1997) 547.

34. I.A. Quazi, P. Akhter, and A. Mufti, J. Phys. D: Appl. Phys. **24** (1991) 81.

35. H. Steffes, C. Imawan, F. Solzbacher and E. Obermeier,

    Sensors and Actuators B **68** (2000) 249.

36. A.N.H. Al. Ajili and S.C. Bayliss, Thin Solid Films **305** (1997) 116.

37. Li-Jian Meng, A. Macarico and R. Martins, Vacuum **46** (1995) 673.

38. M. Rottmann, K.H. Heckner, J. Phys. D.: Appl. Phys. **28** (1995) 1448.

39. M.R. Graham, J.R. Bellingham and C.J. Adkins, Phil. Mag. B **65** (1992) 669

40. R.P. Howson, M.I. Ridge and A.C. Bishop, Thin Solid Films **80** (1981) 137.

41. W.K. Choi, H.J. Jung and S.K. Koh, J. Vac. Sci. Tech. A **14** (1996) 359.

42. K.B. Sundaram and G.K. Bhagavat, Thin Solid Films **78** (1981) 35.

43. S.C. Ray, M.K. Karanjai and D. Das Gupta,

    Thin Solid Films **307** (1997) 221.

44. O. Tabata, T. Tanaka, M. Waseda, and K. Kinuhara,

    Surface Science **80** (1979) 230.

45. L.A. Ryabova, V.S. Salun and I.A. Serbinov, Thin Solid Films **92** (1982) 327

46. T.A. Polly, W.B. Carter and D.B. Poker, Thin Solid Films **357** (1999) 132

47. E. Santhi, V. Dutta, A. Banerjee and K.L. Chopra,

    J. Appl. Phys. **51** (1980) 6243

48. S. Shanthi, C. Subramanian and P. Ramasamy,

    J. Crystal Growth **197**(1999) 858.

49. A. Raza, O.P Agnihotri and B.K. Gupta, J. Phys. D **10** (1977) 1871.

50. K.S. Ramaiah, V.S. Raja, A.K. Bhatnagar and R.D. Tomlinson,

    Semicond. Sci. Technol. **15** (2000) 676.

51. P. Nunes, B. Fernandes, E. Fortunato, P. Vilarinho and R. Martins,

    Thin Solid Films **337** (1999) 176.

52. C. Grivas, D.S. Gill, S. Mailis, L. Boutsikaris and N.A. Voinos,

    Appl. Phys. A **66** (1998) 201

53. F.O. Adurodija, H. Izumi, T. Ishihara and H. Yoshioka,

    Jpn. J. Appl. Phys. **38** (1999) 2710.

54. C.M. Dai, C.S. Su and D.S. Chuu, Appl. Phys. Lett. **57** (1990) 1879.

55. D.M. Mattox, Thin Solid Films **204** (1991) 25.

56. S. Supothina, and M.R. De Guire, Thin Solid Films **371** (2000) 1.

57. H. Jmai, A. Tominaga, H. Hirashima, M. Toki and N. Asakuma,
J. Appl. Phys. **85** (1999) 203.

58. S.S. Kim, S.Y. Choi, C.G. Park and H.Y. Jin,
Thin Solid Films **347** (1999) 155.

59. Sheng - Yuan Chu, Tser – Min Yan and Shen-Li Chen,
J. Mater. Sci. Lett. **19** (2000) 349.

60. Y. Natsume and H. Sakata, Thin Solid Films **372** (2000) 30.

61. T. Muranoi and M. Furukoshi, Thin Solid Films **48** (1978) 309.

62. N. Srinivasa Murthi and S.R. Jawaleker, Thin Solid Films **108** (1983) 277.

63. H. Dewall, and F. Simonis, Thin Solid Films77 (1981) 253.

64. J.R. Bosnell and R. Waghorne, Thin Solid Films **15** (1973) 141.

65. S. Noguchi and H. Sakata, J. Phys. D: Appl. Phys. **13** (1980) 1129.

66. V. Vasu and A. Subrahmanyam, Thin Solid Films **193** (1990) 696.

67. D. B. Fraser and H. D. Cook, J. Electrochem. Soc. **119** (1972) 1368.

68. S.A. Agnihotry, K.K. Saini, T.K. Saxena, K.C. Nagpal and S. Chandra,
J. Phys. D: Appl. Phys. **18** (1985) 2087.

69. M. Mizuhashi, Thin Solid Films **76** (1981) 97.

70. H. Kostlin, R. Jost, W. Lems, Phys. Stat. Sol. **29** (1975) 87.

71. M. Mizuhashi, Thin Solid Films **70** (1980) 91.

72. J.C. Manifacier, Thin Solid Films **90** (1982) 297.

73. P. Nath, R.F. Bunshah, B.M. Basol and M. Staffud,
Thin Solid Films **72** (1980) 463.

74. S. Noguchi and H. Sakata, J. Phys. D: Appl. Phys. **114** (1981) 1523.

75. S. Kulaszewicz, W. Jarmoc, and K. Turowska,
Thin Solid Films **112** (1984) 313.

76. R. Pommier, C. Gril and J. Maruchi, Thin Solid Films 77 (1981) 91.

77. M. Buchanan, J.B. Webb and D.F. Williams, Thin Solid Films 80 (1981) 373.

78. A. Kawada, Thin Solid Films **191** (1990) 297.

79. M. Hoheisel, S. Heller, C. Mrotzek and A. Mitwalsky,

     Solid State Comm. **76** (1990) 1.

80. M. Penza, S. Cozzi, M.A. Tagliente, L. Mirenghi, C. Martucci and A. Quirini,

     Thin Solid Films **349** (1999) 71.

81. Y. Shigesato, S. Takaki and T. Haranon, J. Appl. Phys. **71** (1992) 3356.

82. K. Enjouji, K. Murata and S. Nishikawa, Thin Solid Films **108** (1983) 1.

83. A.P. Roath and D.F. Williams, J. Appl. Phys. 52 (1981) 6685.

84. Y. Natsume, H. Sakata, T. Hirayama and H. Yangida,

     J. Mater. Sci. Lett. **10** (1991) 810.

85. M.F. Ogawa, Y. Natsume, T. Hiranyama and H. Sakata

     J. Mater. Sci. Lett **9** (1990) 1351.

86. M.S. Tomar and F.J. Garcia, Thin Solid Films 90 (1982) 419.

87. T. Miami, H. Nanto, S. Shooji and S. Takata,

     Thin Solid Films **111** (1984) 167.

88. A.J. Nojik, Phys. Rev. B **6** (1972) 453.

89. R.A. Ortiz, J. Vac. Sci. Technol. **20** (1987) 7.

90. H.H. Afify, R.S. Momtaz, W.A. Badawy and S.A. Nasser

     J. Mater. Sci. Mater. Electron. **2** (1991) 40.

91. F. Demichelis, E.M. Mezzetti, V. Smurro, A. Tayliaferro and E. Tresso,

     J. Phys. D: Appl. Phys. **18** (1985) 1825.

92. A. De and S. Ray, J. Phys. D: Appl. Phys. **24** (1991) 719.

93. C. Agashe, M.G. Takwale, B.R. Marathe and V.G. Bhide,

     Solar Energy Materials 17 (1988) 99.

94. J. Melsheimer and D. Zifgler, Thin Solid Films 109 (1983) 71.

95. E. Burstein, Phys. Rev. **93** (1954) 632.

96. T. S. Moss, Proc. Phys. Soc. **B67** (1964) 775.

97. A. Salehi, Thin Solid Films **324** (1998) 214.

98. X.W. Sun, L.D. Wang and H.S. Kwok, Thin Solid Films **360** (2000) 75.

99. A.P. Roth, J.B. Webb and D.F. Williams, Phys. Rev. B **25** (1982) 7836.

100. Y. Ohhata, F. Shinoki and S. Yoshida, Thin Solid Films **59** (1979) 255.

101. R.T. Chen and D. Robinson, Appl. Phys. Lett. **60** (1992) 1541.

102. C. Yuanri, X. Xinghao, J. Zhaoting, P. Chuancai and X. Shuyun,

 Thin Solid Films **115** (1984) 195.

103. J.C.C. Fan, Thin Solid Films **80** (1981) 125.

104. R. Latz, K. Michael and M. Scherrer, Jpn. J. Appl. Phys. **30** (1991) 149.

105. A.P. Theuwissen and G.J. Declerck, Thin Solid Films **121** (1984) 109.

106. C.H.L. Weijtens and P.A.C. Vanloon, Thin Solid Films **196** (1991) 1.

107. E. Leja, T. Stapinski and K. Marszalek, Thin Solid Films **125** (1985) 119.

108. S. Schiller, G. Beister, E. Bnedke, H. Becker and H. Schicht,

 Thin Solid Films **96** (1982) 113.

109. T. Pisarkiewicz, K. Zakrzewska and E. Leja, Thin Solid Films **153** (1987) 479.

110. A. Wang, J. Dai, J. Cheng, M.P. Chudzik, T.J. Marks, R.P.H. Chang and

 C.R. Kannewurf, Appl. Phys. Lett. **73** (1998) 327.

111. G. Gordillo, J. Olarte and C. Calderon, Phys. Stat. Sol.(b) 220 (2000) 293.

112. A. Sarkar, S. Ghosh, S. Chaudhuri and A.K. Pal,

 Thin Solid Films **204** (1991) 255.

113. S. Major, A. Banarjee and K.L. Chopra, Thin Solid Films **125** (1985) 179.

114. N. Tsuji, H. Komiyama and K. Tanaka, Jpn. J. Appl. Phys. 29 (1990) 835.

115. J. Hu, R.G. Gordon, J. Appl. Phys. **71** (1992) 880.

116. Y. Igasaki and H. Saito, J. Appl. Phys. **70** (1991) 3613.

117. Ma Jin, Ji Feng, Z. De-heng,Ma Hong-lei and Li Shu-ying,
Thin Solid Films **357** (1999) 98.

PREPARATION AND CHARACTERISATION OF In_2O_3 THINFILMS

5.1. INTRODUCTION

Indium oxide (In_2O_3) thin film is one of the most widely used transparent conductors. In_2O_3 films are generally polycrystalline with cubic bixbyte structure, also called c-type rare earth oxide structure [1-3]. They belong to the space group (T_h^7Ia3). The lattice parameter of In_2O_3 is $10.117A^o$. The co-ordination is six-fold for the indium atom and four-fold for the oxygen atom. One can assume that there are two crystallographically non-equivalent indium sites, that one of these is associated with an In-O separation of $2.18A^o$, and that oxygen atoms lie nearly at the corners of a cube with two body diagonal opposite corners, unoccupied. The other is associated with non-equal In-O separation of 2.13, 2.19 and $2.23A^o$, and oxygen atoms lying nearly at the corners of a cube with two face-diagonal opposite corners unoccupied. The unit cell of In_2O_3 contains 80 atoms, and as such the structure of In_2O_3 is highly complicated.

In_2O_3 is a non-stoichiometric compound under various conditions with an In/O ratio larger than 2/3. The non-stoichiometry results in an n-type semiconductor or even a semi metal at high electron concentration. It shows a direct band gap usually greater than 3eV. The optical transmission in the visible region is around 80-90%.

An interesting behaviour of In_2O_3 is that its properties depend on the preparation condition[4]. Numerous studies have been carried out over many years to prepare indium oxide films for transparent conducting applications. Many studies have reported the properties of these films prepared by reactive evaporation[5,6], activated reactive evaporation [1], magnetron sputtering[7,8], chemical vapour deposition [9], spray pyrolysis[10,11], laser ablation [12], and sol gel method[13].

Simultaneous occurrence of high electrical conductivity and optical transparency in the visible region makes the transparent conducting oxide films very useful for a number of applications such as solar cells, opto-electronic devices, and liquid crystals. In addition, the transparent conducting oxide films find applications as transparent heating elements, antistatic coatings for instrument windows, heat

reflecting mirrors for glass panes in windows and incandescent bulbs, antireflection coatings, gas sensors, and protective and wear-resistant coatings for glass containers [14-16].

The electrical properties of the transparent conducting oxides depend on the oxidation state of the metal component. Perfectly stoichiometric oxides are either insulators or ionic conductors. Transparent conducting oxide films usually lack stoichiometry due to oxygen vacancies, which induce n-type carriers. When the concentration of oxygen vacancies are high, an impurity band forms, which overlaps the bottom of the conduction band, producing a degenerate semiconductor[17]. Too high oxygen deficiency decreases the crystalline properties of the films and therefore their electrical properties. While too few oxygen vacancies decrease the carrier density and hence the electrical property of the film.

This chapter reports the study of the electrical and optical properties of In_2O_3 films prepared by activated reactive evaporation, on glass substrates at room temperature. The Hall effect measurements show that the films are n-type.

5.2. EXPERIMENTAL

Indium oxide films were prepared by activated reactive evaporation. It is a versatile technique for depositing the transparent conducting oxides and compound semiconductors. The deposition of indium oxide was performed in the vacuum system as described in section 3.2. Optically flat glass slides were used as substrates. Substrates were cleaned with an industrial detergent, followed by running water and 10 minutes ultrasonic agitation in distilled water. Substrates were dried with hot air and loaded into the chamber. The evaporation was carried out in the presence of oxygen plasma. The oxygen plasma was created inside the vacuum chamber. The system was first evacuated to a vacuum of 10^{-5}m.bar. Then industrial grade oxygen was admitted into the vacuum chamber through the needle valve to a pressure nearly 5 x 10^{-4}m.bar. Then the anode supply was turned on initiating the discharge. A bluish glow filled the whole chamber, and a steady discharge current was maintained between 1.6A and 2A. 5N purity indium was then evaporated to the oxygen plasma using a resistively heated molybdenum boat. During deposition, some oxygen would be consumed and hence a slight adjustment of the needle valve was necessary to maintain the oxygen pressure at 5 x 10^{-4}m. bar.

The impingement rate of indium and oxygen atoms on the substrate surface was calculated using the equation 3.2 and 3.3. The following deposition conditions were used for the deposition of In_2O_3 films,

.

Indium impingement rate $\approx$ 2.76- 2.97 x 10 ^{15}atoms cm^{-2} s^{-1}

Oxygen impingement rate $\approx$ 1.09 x 10 ^{17} mol cm^{-2} s^{-1}

The deposition rate of indium oxide film was 400-500A°/minute. Reproducible films were obtained under these conditions. The films were identified by X-ray diffraction. The thickness of the film was measured using Tolansky's multiple beam interferometric method discussed in section 3.6. Conductivity and Hall effect measurements were carried out using conventional four probe method. The electrical contacts were made using evaporated indium. The transmission spectrum was recorded from 2600nm to cut off using Hitachi U 3410 UV-Vis- NIR spectrophotometer. The refractive index (n), and absorption coefficient (α) were calculated using the method developed by Swanepoel, as explained in section 3.11

5.3. STRUCTURAL CHARACTERISATION

Micro structural characterisation was carried out by X-ray diffraction. The thickness of the film used for the X-ray diffraction studies was around 300nm. Figure 5.1 shows the X-ray diffraction pattern of a typical In_2O_3 film. The d values were calculated from the X-ray diffraction pattern. The calculated d values and the relative intensities were given in table 5.1, along with the standard powder diffraction data for In_2O_3[18]. All the diffraction lines were comparable with the standard pattern of In_2O_3, except one peak at 2θ = 27.33° with d = 3.246A°. A similar peak corresponding to 2θ = 27.4° had been observed by Girtan also[4]. It may be due to the deviation from the cubic symmetry. Since all the observed peaks were identified with the standard pattern, it can be concluded that the prepared films were polycrystalline in nature and were having a cubic bixbyte structure of In_2O_3.

5.4. ELECTRICAL PROPERTIES

The films prepared for electrical measurements were of thickness about 350nm. A conventional four-probe method was used to measure the conductivity and Hall coefficient[19]. All these measurements were done under a vacuum better than 10^{-2}m.bar, in an all metal cell as described in section 3.9. Ohmic contacts to the
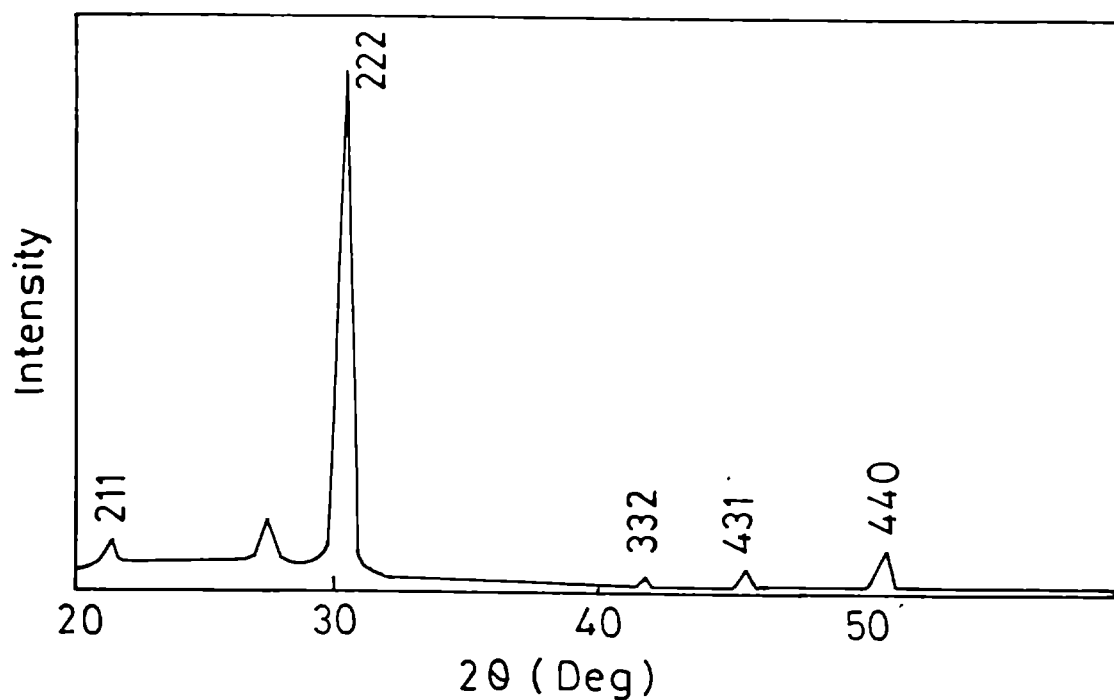
Figure 5.1 X-ray diffraction pattern of In_2O_3 film prepared at room temperature.

(hkl)	Standard pattern		Prepared film	
	d A°	I/I_o	d A°	I/I_o
211	4.130	14	4.148	9.8
.....	....	...	3.246	14
222	2.920	100	2.919	100
332	2.157	6	2.159	3.16
431	1.984	10	1.983	3.9
440	1.788	35	1.789	9.1

Table 5.1 X-ray diffraction data for the In2O3 thin film prepared at
room temperature

samples were made using evaporated indium. The ohmic nature of the contacts were confirmed by the linear current-voltage characteristics through out the temperature range studied. The conductivity of the film was measured by passing a known current through the film and measuring the voltage across the film. The current and voltage were measured using Keithly 195 DMM. A stabilised magnetic field was applied across the sample and Hall voltage developed was measured using keithley 181 nanovoltmeter. The length to breadth ratio of the samples used for the measurements was always greater than 4, so that the influence of the film geometry was negligible. Each measurement was repeated several times and found to be reproducible. The Hall coefficient R_H of the film was calculated using the relation,

$$R_H = \frac{V_H d}{IB} \times 10^8 \text{ cm}^3/\text{Coulomb} \qquad (5.1)$$

where V_H is the Hall voltage in volts, d the thickness of the film in cm, I the current in amperes and B, the magnetic field in Gauss. The carrier concentration (n) of the samples was calculated from the relation ,

$$n = \frac{1}{R_H e} \text{ cm}^{-3} \qquad (5.2)$$

where e is the electronic charge. The Hall mobility μ_H was calculated using the relation

$$\mu_H = \sigma R_H \text{ cm}^2 \text{ V}^{-1} \text{ s}^{-1} \qquad (5.3)$$

where σ is the conductivity of the sample.

The conductivity and Hall effect measurements were carried out as a function of temperature ranging from room temperature to 353K. The Hall effect measurements show that the films were n-type. Measurement at room temperature showed the resistivity $\rho = 1.35 \times 10^{-3}$ ohm-cm , mobility $\mu = 15$ cm^2 V^{-1} s^{-1}, carrier concentration n = 2.97 x 10^{20} cm^{-3} and sheet resistance $R_\square = 38.6\Omega$ / square.

Figure 5.2 shows the variation of conductivity (σ) with the inverse of the temperature. It was found that the conductivity decreased with increase in temperature. The decrease in conductivity might be due to the increased defect scattering owing to the higher carrier concentration of these films. Boechko et al[20], Dmitrieva et al[21] and Sher et al[22] had also observed a similar temperature dependence of the conductivity.

Figure 5.3 shows the variation of mobility with temperature. It was found that the mobility decreased with increase in temperature, in a similar way as the conductivity varied with temperature. The temperature dependence of the mobility was related to the scattering mechanism of the free carriers, say ionised impurity scattering, due to the presence of oxygen vacancies and/or excess indium atoms, which resulted in a very high free carrier concentration of the order of 10^{20}cm^{-3}. Noguchi and sakata[23] reported that for In$_2$O$_3$ films the mobility is independent of temperature in the range 77-300K. Here the mobility decreased as the temperature was increased from 300-355K. It may be due to the lattice and/or ionised impurity scattering. Moreover the electrical properties of the transparent conducting oxide films strongly depend on the method of preparation, oxygen partial pressure during deposition etc.
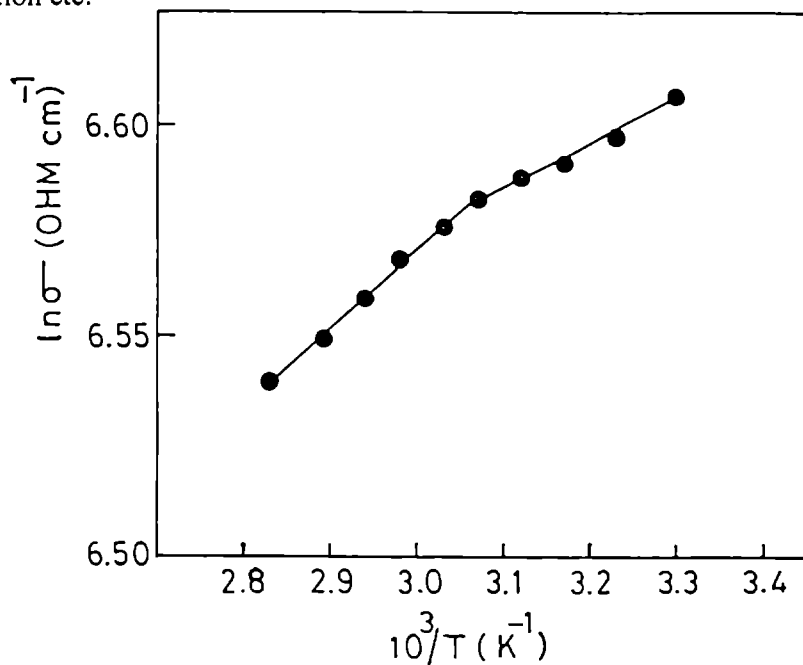
Figure 5.2 Variation of conductivity (σ) with temperature(lnσ Vs 10^3/T).
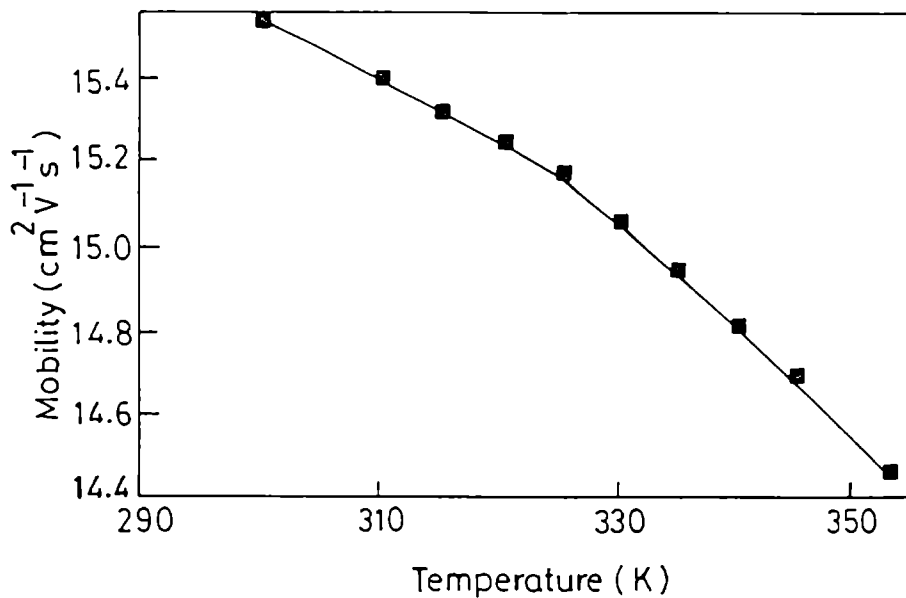
Figure 5.3 Variation of Hall mobility(μ) with temperature(T).

Figure 5.4 shows the variation of Hall coefficient (R_H) with temperature(T). It was found that the R_H was independent of temperature. This suggest that the film was degenerate[24]. The carrier concentration was found to be 2.97 x 10 ^{20}cm^{-3} at room temperature. The In_2O_3 film had such a high value of carrier concentration, which was excited thermally from the donor levels, originating from the defects near the bottom of the conduction band. The Fermi energy E_F can be evaluated using the formula,

$$E_F = \left(\frac{h^2}{8m^*}\right) \left(\frac{3n}{\pi}\right)^{2/3}$$

(5.4)

where m* is the reduced effective mass and h, the Planks constant. Taking the value of m* as $0.3m_o$, from the literature of In_2O_3[25], we obtained E_F = 0.54eV. This is much greater than kT $\approx$ 0.025eV. This again shows that the film was highly degenerate.

Figure 5.5 shows the variation of thermoelectric power(S) with temperature(T). Samples with thickness $\approx$ 200 nm were used for the thermoelectric
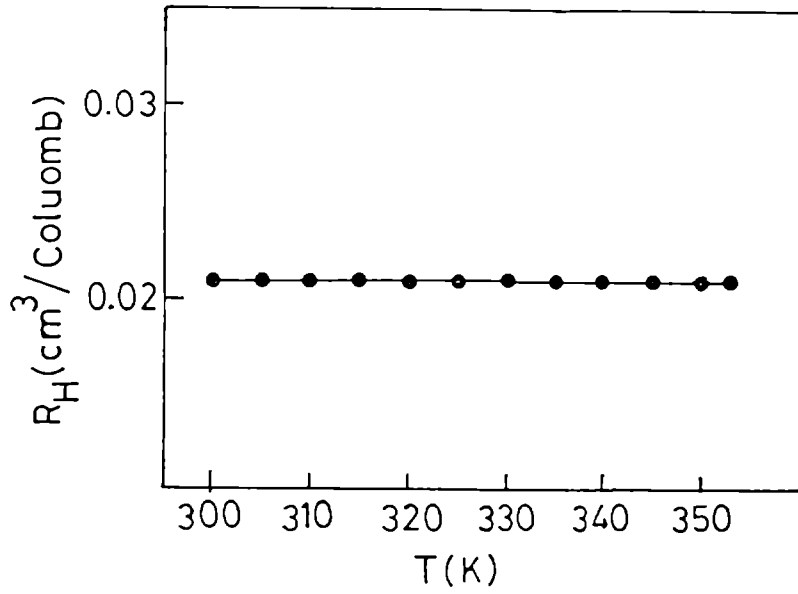
Figure 5.4 Variation of Hall coefficient(R_H) with temperature(T).
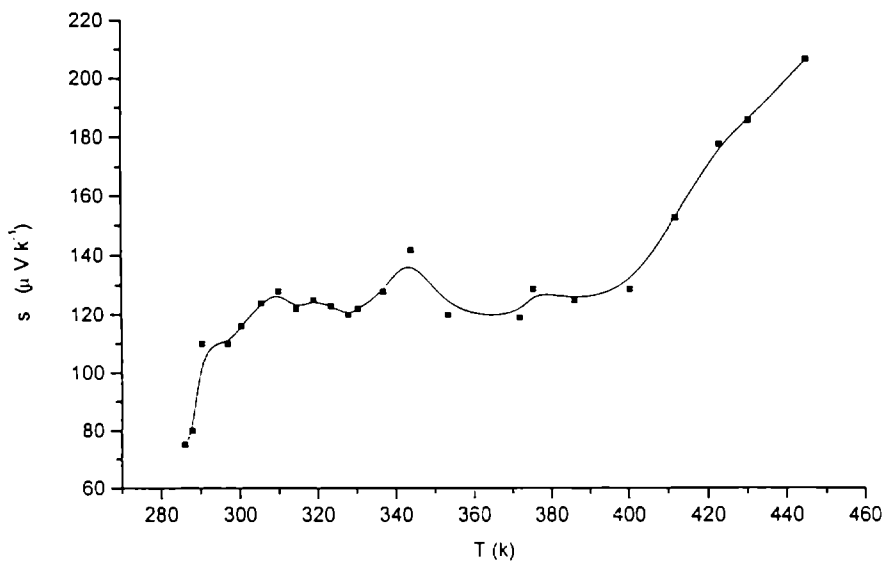
Figure 5.5 Variation of thermoelectric power (S) with temperature (T).

measurements. The temperature of each end of the sample was measured using thermocouple buds attached to the ends. The potential difference between both ends of the samples due to the temperature gradient was measured. The details of the experimental set up were given in section 3.10. The thermoelectric power shows an increase with increase in temperature. But this rise in thermoelectric power was very small in the range of temperature from 300K to 400K. This increase in thermoelectric power with increase in temperature is, due to the degenerate nature of the material.

5.5. OPTICAL PROPERTIES

The optical studies were done using In_2O_3 films having thickness $\approx$ 350nm. The transmission spectrum was taken using Hitachi U 3410 UV-Vis-NIR spectrophotometer. The refractive index of the films was calculated from the interference maxima and minima. Knowing the value of refractive index, the absorption coefficient in the fundamental absorption region could be calculated.

Figure 5.6 shows the transmission spectrum of a typical In_2O_3 film prepared at room temperature. It showed an average transmittance of 80% over a wave length range of 500nm to1680nm. A sharp decrease in the transmittance in the lower wavelength region was due to the fundamental absorption and the decrease in transmittance at higher wavelength region was due to the free carrier absorption[5], a phenomenon that is common in all transparent conductors having higher carrier concentration.
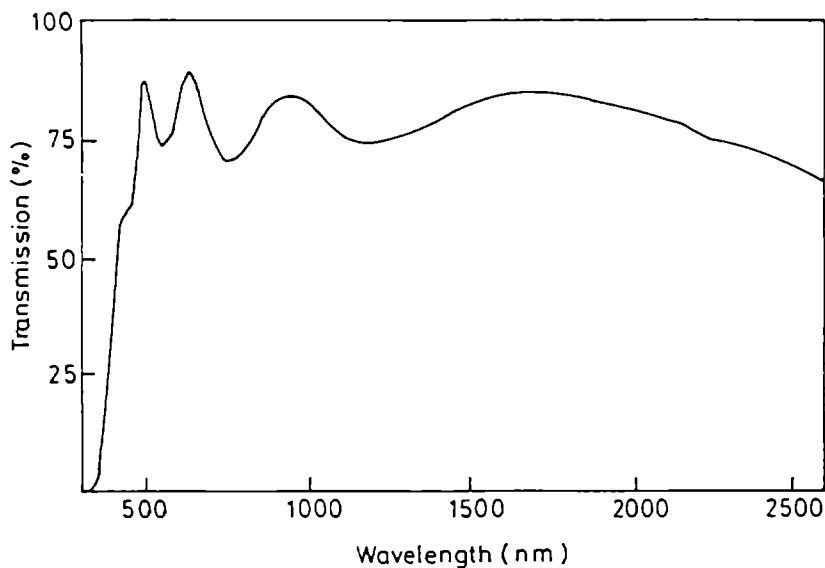
Figure 5.6 Transmission spectrum of a typical In_2O_3 thin film.

Figure 5.7 shows the variation of refractive index(n) with the wavelength. In the 1000nm to 2000nm wavelength region, the refractive index was found to be almost constant and the average value of the refractive index was nearly 2. It is in close agreement with the reported values in the literature[26,27]. Towards the higher energy side, the refractive index is found to be increasing.

The absorption coefficient data were analysed using the theory of Barden et al[28] and Smith[29]. The theory predicts that the absorption coefficient(α) due to band to band transition can be expressed as

$$\alpha = A \ (h\nu - E_g)^r \text{ for direct transition,} \qquad (5.5)$$

where r = 1/2 for the allowed and r = 3/2 for the forbidden transition.
For indirect transition,

$$\alpha = B(h\nu - E_g' \pm E_p)^r, \qquad (5.6)$$

where E_g' is the indirect energy gap and E_p is the absorbed(+) or emitted(-) phonon energy. In this case r = 2 represents allowed and r = 3 represents a forbidden transition.

Figure 5.8 shows the variation of absorption coefficient(α) as a function of photon energy(hν). The absorption has its minimum value at its low energy and increases with the increase in optical energy.

Figure 5.9 shows the plot of $(\alpha \ h\nu)^2$ as a function of photon energy(hν). Due to the linearity of the curve, it was confirmed that the absorption near the fundamental edge was due to the direct allowed transition. Moreover from figure 5.8 it is clear that the value of α is of the order of $10^4 cm^{-1}$, which is a characteristic of direct allowed transition according to Smith[29]. Being the measurements were done at room temperature, exciton bands were not likely to be present. Hence it may be believed that the transition in In_2O_3 was due to band to band transition. The extrapolation of the linear part of the graph to $\alpha = 0$ gives a band gap = 3.52 ± 0.01 eV. This is in good agreement with the band gap reported for bulk In_2O_3[30].
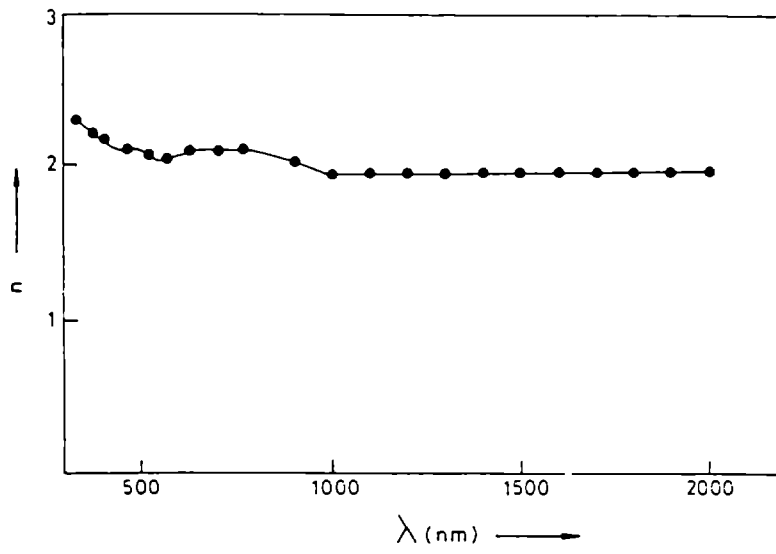
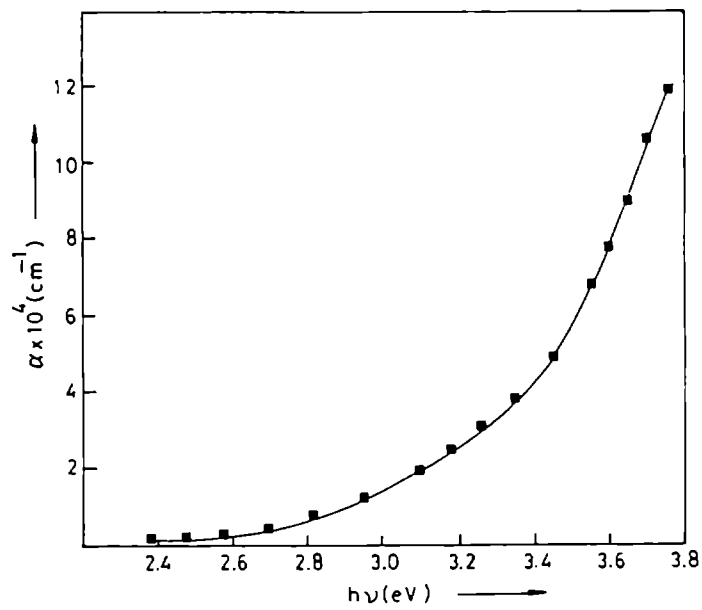Figure 5.7 Variation of refractive index(n) with wavelength(λ).

Figure 5.8 Variation of absorption coefficient(α) with photon energy(hν).
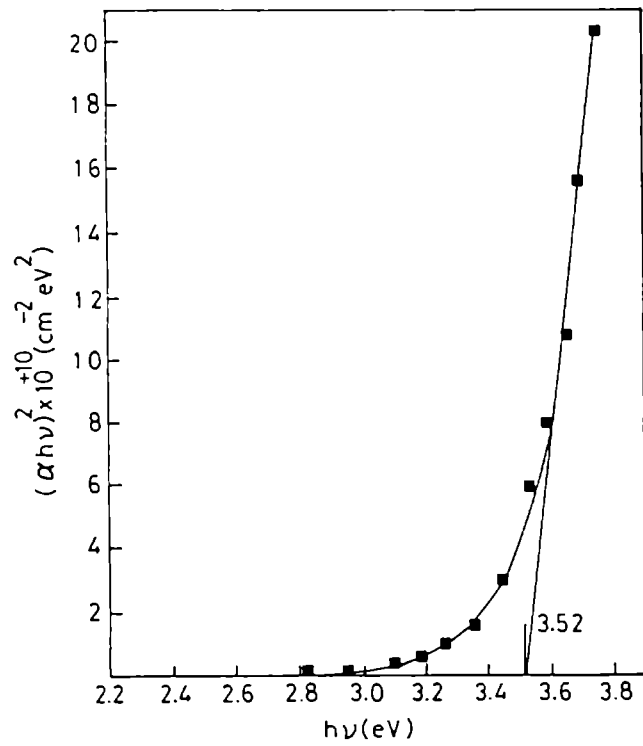
Figure 5.9 Variation of $(\alpha h\nu)^2$ against the photon energy (hν).
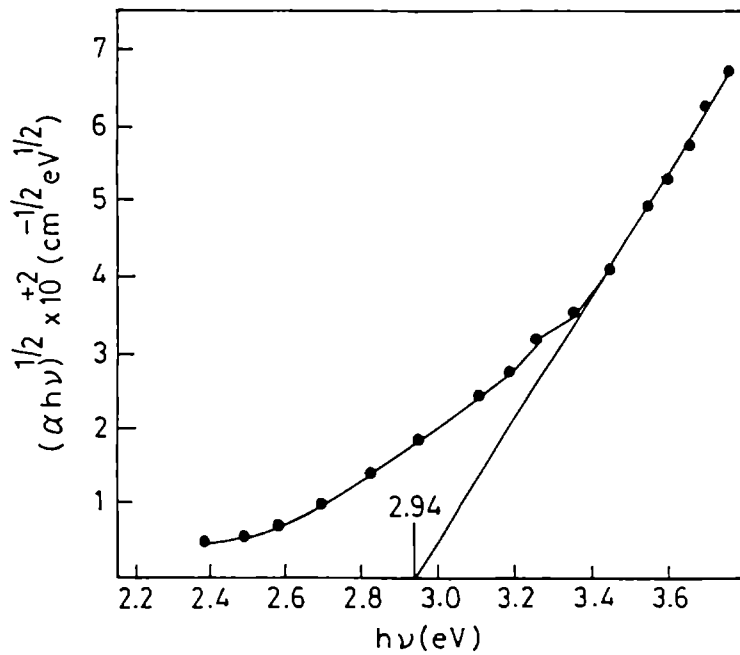

Figure 5.10 Variation of $(\alpha h\nu)^{1/2}$ against the photon energy (hν).

It is also reported that In_2O_3 shows indirect transition. Figure 5.10 shows the variation of $(\alpha\ h\nu)^{1/2}$ as a function of photon energy $(h\nu)$. The linear nature of the curve suggests an indirect allowed transition. The extrapolation of the linear part to $\alpha = 0$ gives a band gap $= 2.94 \pm 0.01$ eV, which is also in good agreement with the reported values[31].

5.6 FIGURE OF MERIT :

Common to all transparent conductor applications it is essential to optimise the electrical and optical parameters. Depending on type of device requiring a transparent electrode, the optical transmission and electrical conduction of the electrode should exceed certain minimum values. Ideally both the parameters should be as large as possible, but their inter-relationship usually excludes the simultaneous achievement of both these criteria. In order to compare the performance of various transparent conductors, the most widely used figure of merit is defined as [32]

$$\varphi = T^{10}/R_{\square} \qquad (5.7)$$

where T is the transmittance and $R_{\square}$ is the sheet resistance. Using this relation the figure of merit is calculated and is found to be 2.78×10^{-3}. A comparison of the figure of merit of transparent conducting films prepared by different techniques is given in table 5.2

5.7 CONCLUSION :

Polycrystalline In_2O_3 films have been prepared on glass substrates at room temperature by activated reactive evaporation. Hall effect measurements show that the films are n-type. The mobility measured at room temperature was $15 cm^2\ V^{-1}\ s^{-1}$, the carrier concentration was $2.97 \times 10^{20} cm^{-3}$ and the resistivity was 1.35×10^{-3}ohm-cm.It shows both direct and indirect allowed transition with band gap of the order of 3.5eV and 2.9eV respectively. The films show a low resistivity and high transmittance which are comparable to those of the doped In_2O_3 and SnO_2 films. This method offers a relatively high deposition rate of the order of 450 to 500 A°/minute. This involves no post deposition heat treatment which makes this method attractive for the preparation of transparent conducting oxide films.

118

Material	Preparation technique	Sheet resistance	Mobility $cm^2V^{-1}s^{-1}$	Carrier concentration cm^{-3}	Transmittance T%	Figure of merit φ_{TC}	Reference
In_2O_3	ARE	38.6	15.5	2.97×10^{20}	80	2.78×10^{-3}	Present work
In_2O_3	Thermal evaporation	88	72	3×10^{20}	80	1.22×10^{-3}	5
In_2O_3: Sn	ARE	20	20-30	1×10^{21}	90	1.74×10^{-2}	33
In_2O_3:F	Ion plating	40	13	7×10^{20}	80	2.68×10^{-3}	34
In_2O_3:Sn	Spray	3.1	......	....	88	8.98×10^{-3}	35

Table 5.2 Comparison of the properties of transparent conducting oxide films.

REFERENCES

1. P.Nath and R.F. Bunshah, Thin Solid Films **69** (1980) 63

2. H. K. Muller, Phys. Stat. Sol. **27** (1968) 723

3. C. E. Wickersham and J. Greene, Phys. Stat. Sol.(a) **47** (1978) 329

4. M. Girtan, G. I. Rusu, Mater. Sci. and Eng. B **76** (2000) 156

5. M. Mizuhashi, Thin Solid Films **70** (1980) 91

6. F. M. Ammanullah, K. J. Prathap and V. H. Babu,
   Thin Solid Films **254** (1995) 28

7. D. V. Morgan, Z. H. Aliyu, R. W. Bunce and A. Salehi,
   Thin solid Films **312** (1998) 268

8. A.H.M. Zahairul Alam, Y. Takashima, K. Sasaki, and T.Hata,
   Thin Solid Films **279** (1996) 131

9. P. Tuner, R. P. Howson and C.A. Bishop, Thin Solid Films **83** (1981) 253

10. J. C. Manifacier, Thin Solid Films **90** (1982) 297

11. H. Kostlin, R. Jost and W. Lems, Phys. Stat. Sol. (a) **29** (1975) 87

12. C. Grivas, D. S. Gill, S. Mailis, L. Boutsikaris and N. A. Vainos,
    Appl. Phys. A **66** (1998) 21

13. Hiroaki Imami, A. Tominaga and Hiroshi hirashima,
    M .Toki and N. Asakuma, J. Appl. Phys. **85** (1999) 203

14. P. T. Mosely, Meas. Technol. **8** (1997) 223

15. K.L. Chopra, S. Major and D.K. Pandya, Thin Solid Films **102** (1983) 1

16. H. L. Hartnagel, A.L. Dawar, A.K. Jain and C. Jagadish,
    Semiconducting Transparent Thin Films, (Institute Of Physics publishing,
    London,1995)

17. Baba Ali, G. Sorenen, J. Ouerfclli, J.C. Bernede and H. El. Maliki,
    Appl. Surf. Sci. **152** (1999) 1

18. JCPDS File No. **6-416**

19. E. H. Puutley, The Hall Effect and Related Phenomena,
    (Whitefriars Press, London, 1960) **p.** 24

20. V. F. Boechko and V.I. Isarev, Inorg. Mater. **11** (1975) 1288

21. A. K. Dmitrieva, L.D. Dudkin, R.S. Erofecv, A. B. Ivanova and
    E. I. Shcherbina, Inorg. Mater. **14** (1978) 326

22. A.A. sher, I. N. Odin and A. V. Novoselova, Inorg. Mater. **20**(1984) 1109

23. S. Noguchi and H. Sakata, J. Phys. D, **13** (1980) 1129

24. N. B. Hannay, *Semiconductors,* (Chapmann and Hall, 1960) **p.** 32

25. R. Clanget, Appl. Phys. **2** (1973) 247

26. A. N. H. Al. Ajili and S.C. Bayliss, Thin Solid Films **305** (1997) 116

27. W. Fukerek, and H. Kersten, J. Vac. Sci. Technol.A **12** (1994) 523

28. J. Bardeen, F. J. Blatt and L. H. Hall, *Proceedings of the Photoconductivity*
    Conference, Atlantic city (Wiley, New York, 1956)

29. R. A. Smith, *Semiconductors* (Cambridge University Press, 1978) **p.** 314

30. J. M. Jarzebski and J. P. Marlon, J. Electrochem. Soc. **123** (1976) 333

31. R. L. Weiher and B. G. Dick, J. Appl. Phys. **35** (1964) 3511

32. G. Hacke, J. Appl. Phys. **47** (1976) 4086

33. P. Nath R. F. Bunshah, B. M. Basol and O. M. Staffsud,
    Thin Solid Films **72** (1980) 463

34. J. N. Avaritsiotis and R. P. Howson, Thin Solid Films **80** (1981) 63

35. J. C. Manifacier, L. Szepessy, J. F. Bresse, M. Perotin and R. Stuck,
    Mater. Res. Bull. **14** (1979) 109

CHAPTER 6

PREPARATION AND CHARACTERISATION OF

INDIUM TIN OXIDE (ITO) THIN FILMS

6.1 INTRODUCTION

Interest in transparent conducting oxide films can be traced back to 1907, with the first report of a transparent conducting cadmium oxide film [1]. Since then there has been a growing technological interest in materials with these unique properties. Although in practice, transparency with acceptable reduction in conductivity can be obtained for very thin metallic films, high transparency along with high conductivity cannot be attained in intrinsic stoichiometric materials. The only way through which this can be achieved is by creating electron degeneracy in wide band gap (Eg ≥ 3eV) materials by controllably introducing non-stoichiometry and/or appropriate dopants. These conditions can be achieved in various oxides of indium, tin, cadmium, zinc and their combinations.

It is now known that non-stiochimetric and doped oxide films of tin, indium, cadmium, zinc and their various alloys exhibit high transmittance and nearly metallic conductivity [2]. These transparent conducting metal oxide films have been widely used in variety of electronic, opto-electronic and industrial devices such as solar energy conversion devices, liquid crystal displays (LCD), cathode ray tubes (CRT), heat mirrors, gas sensors, wear resistant coatings and laser damage resistant coatings in high power laser technology etc. More recently tin doped indium oxide films have been used as transparent contacts in solar cells, light emitting diodes, photo diodes, phototransistors and lasers [2-7]. Their wide application is due to the mechanical and chemical stability of the films, their good adhesion to various substrates, resistance to the action of aggressive media, high transparency in the visible spectral range and high conductivity.

In view of the technological importance, a great deal of basic research and development has been carried out on the electrical and optical properties of indium oxide based materials. Rupprecht [8] carried out one of the first investigations on the

indium oxide (In_2O_3) film. Since then different technique have been used for the properties of these oxide films.

Of all the transparent conducting oxide films, tin doped indium oxide, commonly called indium tin oxide (ITO) is the most popular one. It is an indium oxide based material that has been doped with tin to improve the electrical properties. The ITO films were n-type and exhibits in most cases the cubic bixebyte [$(Mn, Fe)_2O_3$] structure of In_2O_3. The high conductance of ITO film was generated by the high doping level of Sn dopants and oxygen vacancies in the In_2O_3 lattice. Due to the high energy band gap, ITO films appear highly transparent in the visible region. Normally the band gap of ITO films lies between 3.5eV and 4eV.

ITO films were degenerate n-type and the free carrier concentration can be increased up to a level of about $10^{21}cm^{-3}$. The free carriers were liberated from a combination of doubly charged oxygen (O^-) vacancies and tetravalent Sn atom (Sn^{4+}). The tetravalent Sn atoms sit in the trivalent In sites and gives one free electron per molecule, where as the oxygen vacancies creates two free electron per molecule in In_2O_3. The dopant effect in ITO films was governed by microstructure and defect chemistry of the material. It has been reported that Sn atoms in amorphous ITO films were not electrically active; i.e. it does not contribute to the free carrier density. When these films were recrystallized, Sn becomes electrically active. In polycrystalline ITO films, the effect of Sn doping on the electronic transport properties strongly depends on the Sn concentration. If the percentage of Sn increases beyond a certain limit, the increasing fraction of Sn remains inactive. In that case Sn doping creates not only donor centers, but also scattering centers, which do not supply carriers to the material [9]. According to Frank and Kostlin [10], these defect complexes arise from the attraction of interstitial oxygen atoms by Sn dopant, forming a bond, which is stabilized by a second nearby Sn ion. In this way tin-oxygen complexes were postulated in a defect model for ITO, which they successfully account for measured carrier concentration in ITO films deposited by spray Pyrolysis as a function of oxygen partial pressure.

In obtaining a high-quality ITO film, the key properties are high conductivity, high transmittance to visible light, and high reflectance in the IR radiation. If the film is made to have the highest transparency, it may have the highest sheet resistance or vice versa. In order to obtain optimum characteristics; i.e. high transmission in the

visible region and low sheet resistance, the parameters such as thickness of the film, dopants and the other deposition conditions have to be optimized. It is well known that the properties of ITO films intimately associated with the microstructure and chemical composition, which are controlled by the deposition methods and growth conditions [11-14].

Despite the different technologies available for the deposition of ITO films, highly transparent and conducting films could only be attained at a relatively high substrate temperature (greater than 200°C). Of all the techniques, sputtering, ion plating and activated reactive evaporation (ARE) have yielded the best results. Using these methods, it is possible to deposit ITO films on substrates at low temperature.

This chapter reports the preparation of ITO thin films on glass substrates at room temperature by activated reactive evaporation. The electrical and optical properties with substrate temperature and thickness were studied.

6.2 EXPERIMENTAL

Indium tin oxide (ITO) thin films were prepared on glass substrates kept at room temperature, by activated reactive evaporation. 99.999% pure indium and tin were used for evaporation. Resistively heated molybdenum boat was used to evaporate the material, in a conventional vacuum system. The evaporation was carried out in the presence of oxygen plasma. To produce oxygen plasma, the vacuum chamber was first evacuated to a vacuum of 10^{-5}m.bar. Then industrial grade oxygen was admitted into the chamber through a needle value, to a pressure nearly 5×10^{-3}m.bar. Then anode supply was turned on, initiating the discharge. A bluish glow filled the whole chamber, and a steady discharge current was maintained. Then indium and tin (In + 10 wt % Sn) taken in a molybdenum boat was evaporated to the oxygen plasma. A slight adjustment of the needle valve was necessary to maintain the oxygen plasma. The details of the experimental technique are given in section 3.2

Optically flat glass slides were used as substrates. Substrates were cleaned with an industrial detergent, followed by running water and ten minutes ultrasonic agitation in distilled water. The substrates were dried in hot air and then fixed on a substrate holder, whose temperature can be varied from room temperature to 400°C. Then this substrate holder was loaded into the vacuum chamber.

The structural characterization was done using X-ray diffraction (XRD), energy dispersive analysis of X-ray (EDAX) and scanning electron microscopy

(SEM). Conductivity and Hall effect measurements were carried out using van der Pauw method by D 2500 Hall van der Pauw system of MMR technologies. Samples used for these measurements were 1cm ×1cm in size and thickness 350nm. The ohmic contacts were made using silver paste. The transmission spectrum was recorded from 2600nm to 250nm.Refractive index was calculated from the interference pattern using Swanepoels method. Then the absorption coefficient (α), near the absorption edge was calculated. From the analysis of the absorption coefficient, the band gap was calculated.

6.3. STRUCTURAL STUDIES

Tin doped indium oxide films were prepared by activated reactive evaporation. To confirm whether the sample is doped with tin or not, EDAX was taken. Figure 6.1 shows the EDAX of a typical ITO film prepared on glass substrates at room temperature. It shows the presence of tin. It confirms the doping in the prepared samples.
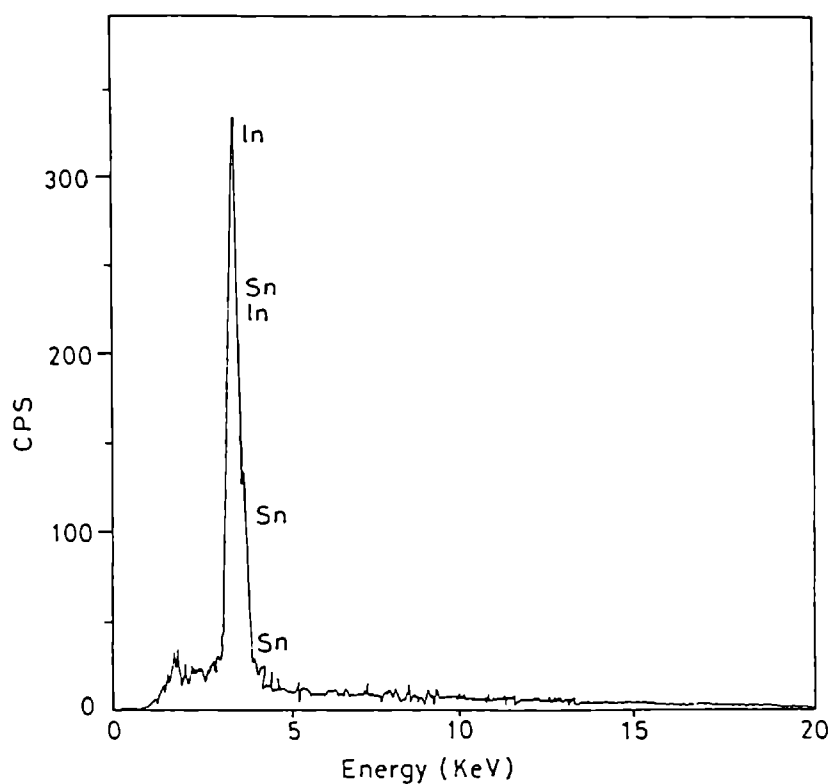
Figure 6.1 EDAX of a typical ITO film prepared at room temperature.

Structural characterization of the films was done by taking the X-ray diffraction. The films used for these studies were having a thickness nearly 350nm. The diffraction patterns were recorded using monochromatic Cu K_α radiation.

Figure 6.2(a-e) show the X-ray diffraction pattern of ITO films prepared at different substrate temperatures. Figure 6.2a is the XRD pattern of the film prepared at room temperature. It can be seen that the film was polycrystalline, with the cubic structure of In_2O_3. All the peaks in the XRD pattern represents In_2O_3 and no peak was found corresponding to any sub oxides of indium or any oxides of tin. So we can confirm that the prepared film was tin doped indium oxide. The d values were calculated from the XRD pattern. The calculated d values and the relative intensities are given in table 6.1 along with the standard data given in JCPDS file (No. 6-416).

The grain size was calculated using the Debye-Scherrer formula,

$$\frac{0.9\lambda}{\beta \cos\theta}$$

(6.1)

where λ is the wavelength of the X-ray used, β the full width at half maximum. The average grain size was found to be $\approx$ 20nm. The lattice parameter 'a' was also calculated from the XRD pattern. It was found to be 10.17A°, comparable to that of In_2O_3, which is 10.12 A°. A slight increase in the lattice constant may be due to incorporation of tin ions in the interstitial position [12].

The XRD pattern of ITO film prepared on glass substrates at room temperature agrees well with that of the standard data given in table 6.1. It indicates that the films were polycrystalline in nature. Fig. 6.2b shows the XRD pattern of the film prepared at 100°C. It also agrees well with that of the standard powder diffraction data. XRD pattern of the film prepared at 150°C is shown in figure 6.2c. From the figure it is seen that the intensity of (222) peak (which is having a maximum intensity in the standard powder diffraction data for ITO) is getting decreased while the intensity of (400) peak is found to be increased. The XRD pattern of ITO film prepared at 200°C shows a further reduction in intensity for (222) peak and the intensity for (400) peak again increased, which is shown in figure 6.2d. The XRD pattern of the film prepared at 250°C is shown in figure 6.2e. Here we observe a very little intensity for the (222) peak. But the (400) peak becomes most

prominent. Hence we can conclude that while increasing the substrate temperature above 200°C, it is showing an orientation towards (400) plane, which is parallel to the substrate surface. The orientation becomes more prominent at higher substrate temperature. This can be evidenced by comparing figure 6.2c to 6.2e.

The d values of the films prepared at different substrate temperature were calculated from the XRD pattern and are given in table 6.1, along with the standard data. All the diffraction lines were matched well with the standard data for ITO.

The grain size was calculated from the XRD spectrum, by measuring the full width at half maximum of the peaks. The grain size of the film prepared at different substrate temperature, using the peaks corresponding to (222), (400) and (440) planes is given in table 6.2. The observed smaller average grain size may be associated with the deposition process. In activated reactive evaporation procedure, a bombardment of the substrate and the growing ITO films with high-energy particles took place. This may cause surface damage and disturbance to the thin film growth. A similar phenomenon can be seen in DC sputtering also [15].
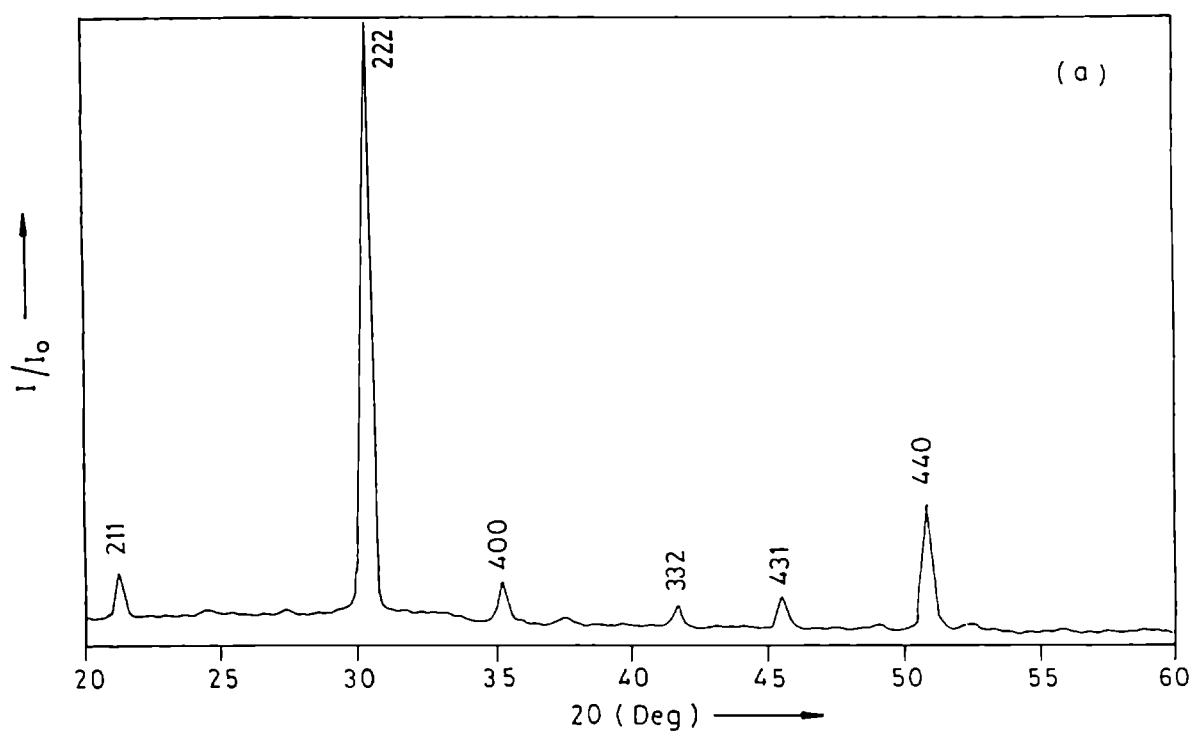
Figure 6.2a X-ray diffraction pattern of ITO thin films prepared at room temperature.
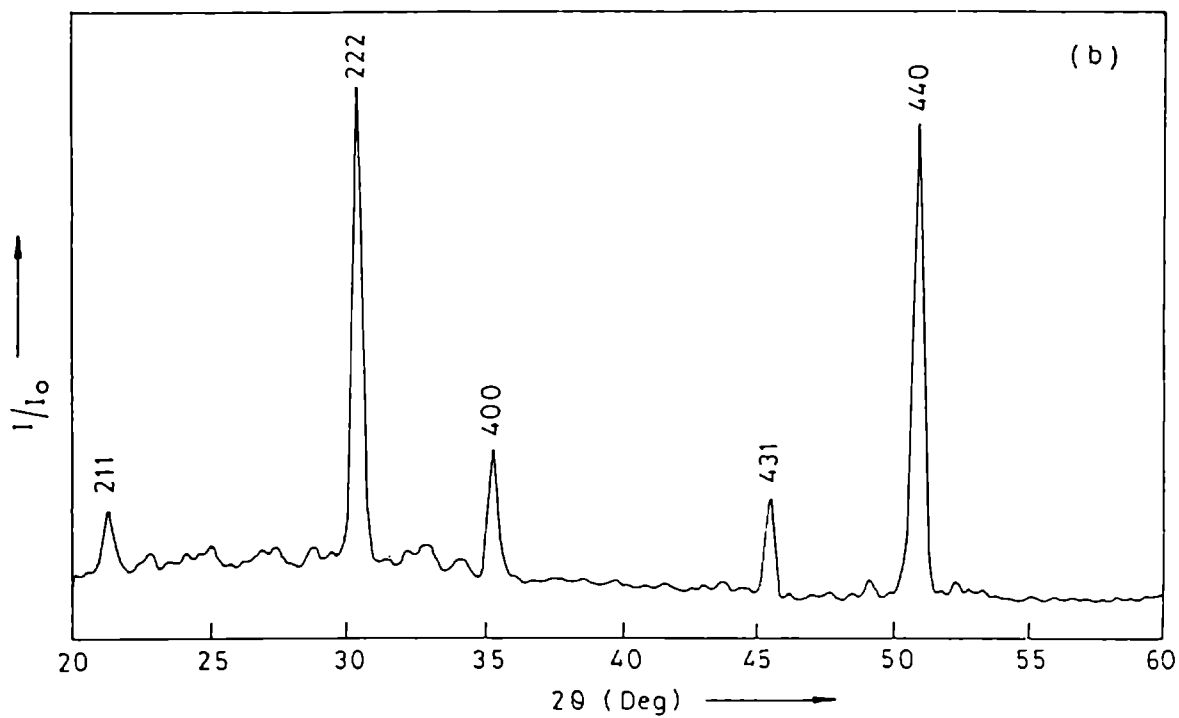
Figure 6.2b X-ray diffraction pattern of ITO thin films prepared at 100°C.
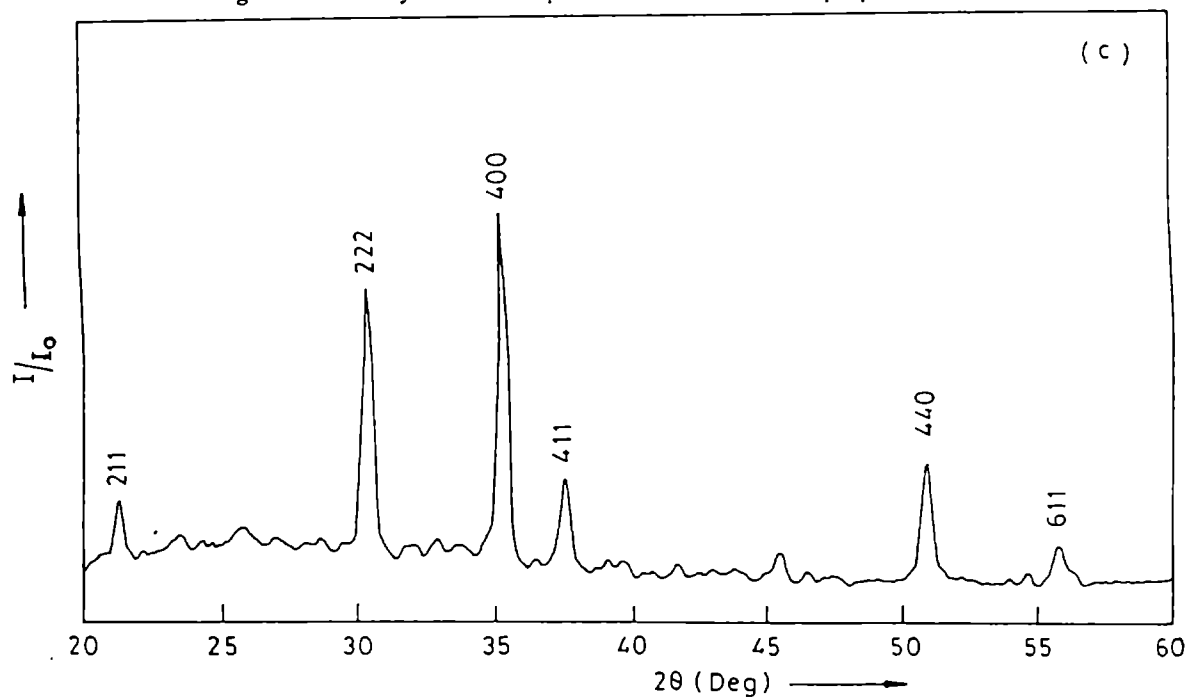
Figure 6.2c X-ray diffraction pattern of ITO thin films prepared at 150°C.
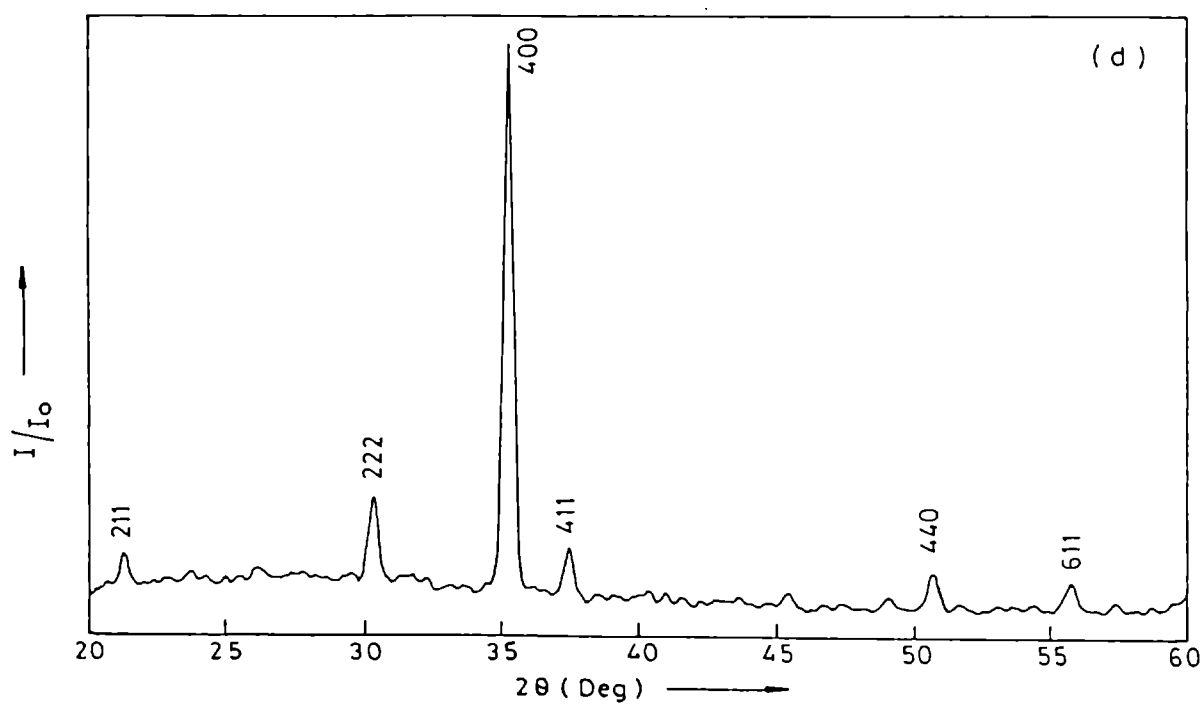
Figure 6.2d X-ray diffraction pattern of ITO thin films prepared at 200°C.
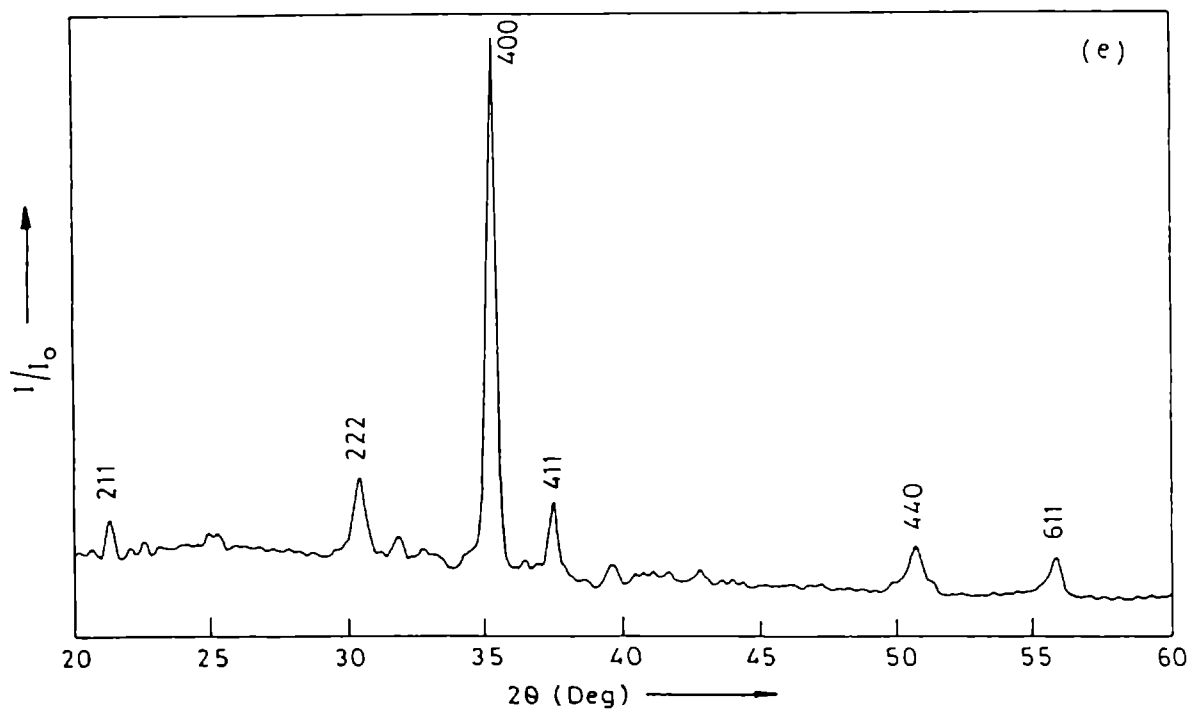
Figure 6.2e X-ray diffraction pattern of ITO thin films prepared at 250°C

Standard data			Substrate Temperature									
JCPDS File No.6-416			Room temperature		100 ^{0}C		150 ^{0}C		200 ^{0}C		250 ^{0}C	
(hkl)	d A^0	I/I$_0$	d A^0	I/I$_0$	d A^0	I/I$_0$	d A^0	I/I$_0$	d A^0	I/I$_0$	d A^0	I/I$_0$
211	4.13	14	4.15	8	4.15	14	4.14	20	4.14	11	4.14	10
222	2.92	100	2.93	100	2.93	100	2.93	75	2.93	24	2.93	20
400	2.53	30	2.54	8	2.54	23	2.54	100	2.54	100	2.54	100
411	2.38	8	---	---	---	---	2.39	23	2.39	14	2.39	12
332	2.16	6	2.17	3	---	---	---	---	---	---	---	---
431	1.98	10	1.98	6	1.99	20	---	---	---	---	---	---
440	1.79	35	1.79	25	1.79	90	1.79	27	1.79	10	1.79	9
611	1.64	6	---	---	---	---	1.64	12	1.65	8	1.65	7

Table 6.1 X-ray diffraction data of ITO films prepared at different substrate temperature.

The lattice parameter 'a' for the ITO film was calculated using the equations

$$2d \sin \theta = n \lambda \text{ and}$$

$$\frac{n^2}{d^2} = \frac{h^2 + k^2 + l^2}{a^2}$$

(6.2)

the calculated 'a' values are given in table 6.3. The lattice parameter of all the ITO films were slightly higher than the value for undoped In$_2$O$_3$, which indicates the occupation of interstitial sites by the dopants [16]

(hkl) →	(222)			(400)			(440)		
T°C	2θ	FWHM	grain size (nm)	2θ	FWHM	grain size (nm)	2θ	FWHM	grain size (nm)
RT	30.35	0.35	23.5	35.3	0.45	18.6	50.8	0.35	25.1
100	30.35	0.35	23.5	35.3	0.35	23.8	50.8	0.35	25.1
150	30.35	0.45	18.4	35.3	0.35	23.8	50.8	0.45	19.6
200	30.3	0.45	18.4	35.2	0.35	23.8	50.7	0.53	16.7
250	30.4	0.53	15.6	35.3	0.35	23.8	50.7	0.53	16.7

Table 6.2 Variation of grain size with substrate temperature of ITO films

(hkl)	Standard value of a in A⁰ JCPDS File No.6-416	Calculated value of 'a' in A⁰				
		Room temperature	100 ⁰C	150 ⁰C	200 ⁰C	250 ⁰C
222	10.118	10.17	10.20	10.17	10.17	11.07
400	10.118	10.18	10.18	10.18	10.18	10.18
440	10.118	10.15	10.15	10.15	10.15	10.15

Table 6.3 'a' values calculated from the XRD pattern for different substrate temperatures

6.4. ELECTRON MICROSCOPIC STUDIES

Figure 6.3(a-e) shows the SEM of the films prepared at different substrate temperature. It shows that all the films were homogeneous and less granular. No measurable change in the grain size was observed, while the substrate temperature was increased from room temperature to 250°C. The grain size calculated from the XRD data shows a slight variation in grain size. The average grain size was found to be ≈ 20nm. That means there was no significant effect of substrate temperature on the grain size. The SEM micrograph shows that the surface of the film is smooth, densely packed with crystallites having very small grain size without any discontinuity.
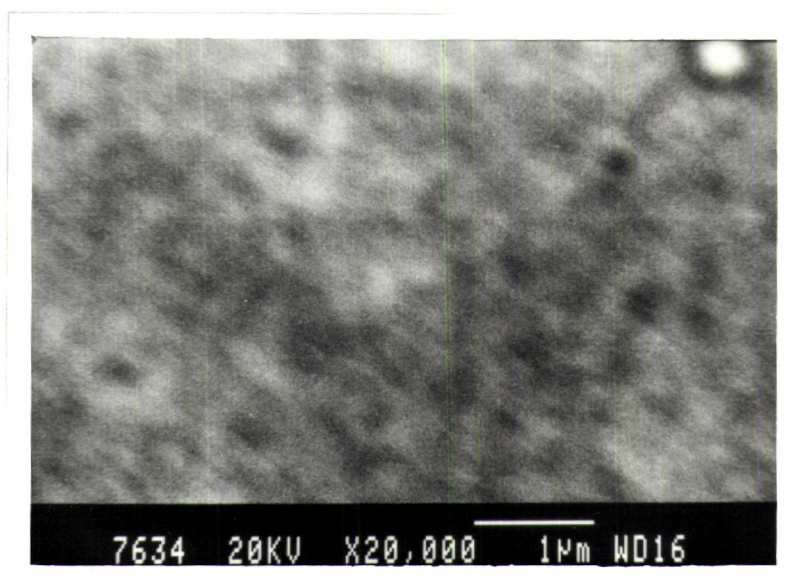
Figure 6.3a SEM of ITO thin films prepared at room temperature,
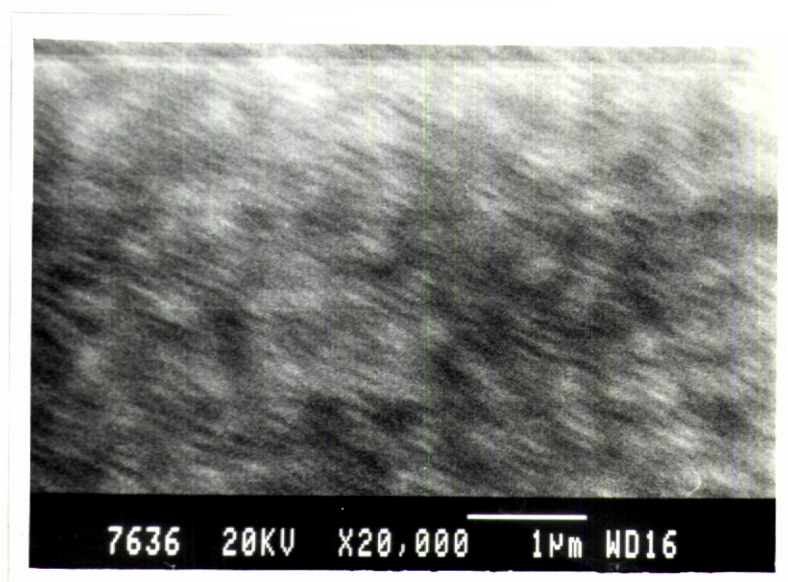
Figure 6.3b SEM of ITO thin films prepared at 100^{0}C
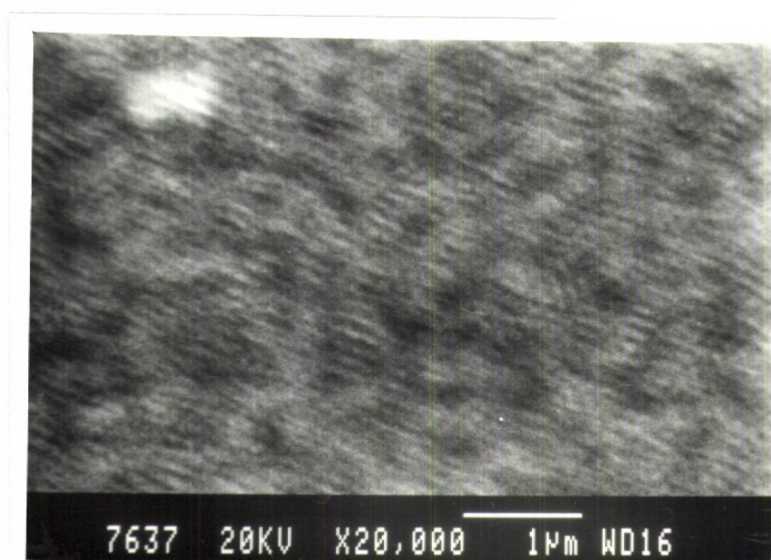
Figure 6.3c SEM of ITO thin films prepared at 150^{0}C
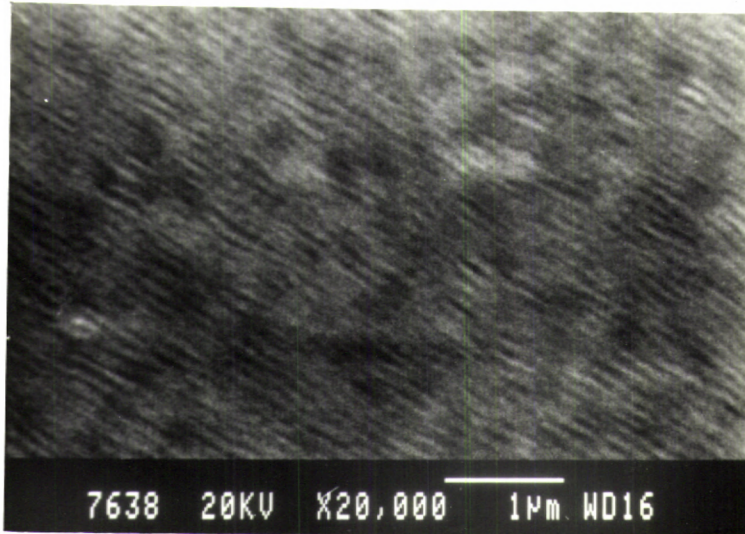
Figure 6.3d SEM of ITO thin films prepared at 200^0C
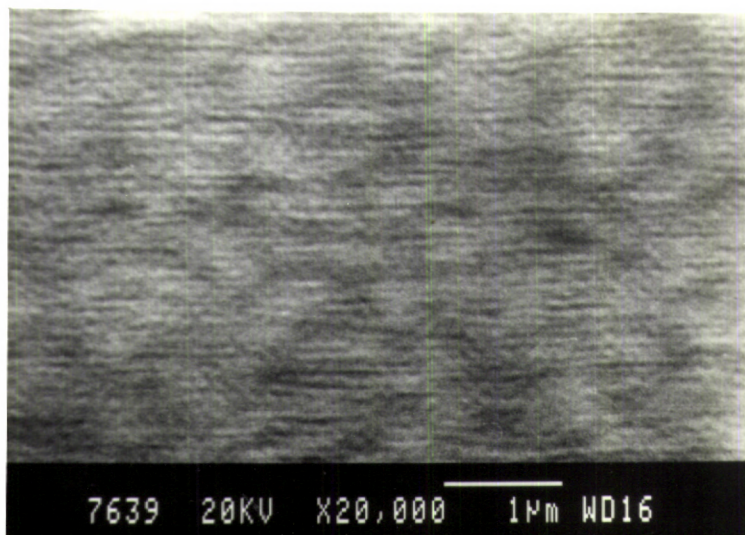
Figure 6.3e SEM of ITO thin films prepared at 250^0C

6.5. ELECTRICAL PROPERTIES

Films used for the electrical studies were prepared by evaporating In+10wt% Sn from a molybdenum boat. The thickness of the films used for the measurements were nearly 350nm. The resistivity, Hall effect and sheet resistance of the samples were measured using van der Pauw technique. Samples used for the measurements were 1cm×1cm in size and thickness ≈ 350nm. The ohmic contacts were made using silver paste. Silver paint was applied at the four corners of the sample, symmetrically, upon which the electrodes were soldered using silver epoxy at the corners A, B, C and D of a square film in the configuration,

A⌐ ⌐D

B└ ┘C
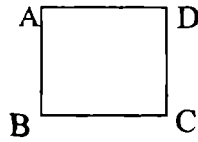
Let R_1 be the potential difference between A and B per unit current through C and D or vice versa. Similarly R_2 is the potential difference between the contacts B and C per unit current through D and A. The sheet resistance R_s can be obtained using the following relation.

$$R_s = \left(\frac{\pi}{\ln 2}\right)\left[\left(\frac{R_1 + R_2}{2}\right)\right] f\left(\frac{R_1}{R_2}\right)$$
(6.3)

where $f\left(\frac{R_1}{R_2}\right)$ the van der Pauw function, given by

$$f\left(\frac{R_1}{R_2}\right) = 1 - 0.3466\left[\left(\frac{R_1 - R_2}{R_1 + R_2}\right)\right]^2$$

The Hall signal was measured between two ends, while passing the current at the other two ends. The thermoelectric and thermomagnetic effect may be eliminated by changing the polarity of the current, which pass through the film and the direction of the magnetic filed. The Hall mobility is given by

$$\mu_H = \left(\frac{\Delta R \times 10^8}{R_s \times B}\right) \quad cm^2\ V^{-1}\ s^{-1}$$
(6.4)

where ΔR is the change in resistance due to the magnetic field (B), which was applied to measure the Hall voltage. The carrier concentration (N) was obtained using the relation.

$$N = \frac{1}{\mu_H \rho \, e} \qquad (6.5)$$

where ρ is the resistivity and e is the electronic charge. The resistivity, mobility, carrier concentration, Hall coefficient and sheet resistance were recorded in the temperature range 300K-400K.

Freshly prepared ITO films with thickness ≈ 350nm, on glass substrates kept at room temperature were used for the measurements. The dependence of conductivity (σ) on temperature (T) is shown in figure 6.4. The activation energy was calculated using Arrehenius relation.

$$\sigma = \sigma_0 \exp\left(\frac{-Q}{kT}\right) \qquad (6.6)$$

where Q is the activation energy, k is the Boltzmann's constant, and T, the absolute temperature. The activation energy was found to be ≈ 2.8 ×10⁻²eV. The activation energy is very small which suggests that the Fermi level is closer to or lie within the conduction band [17,18].
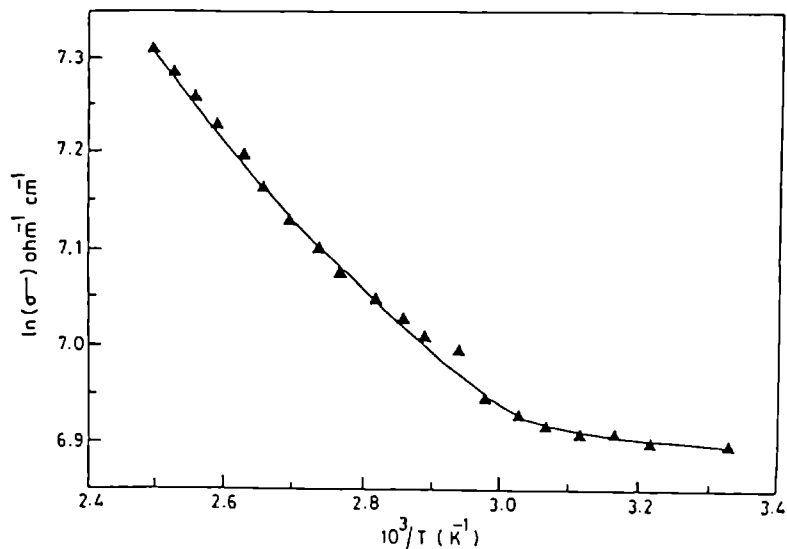
Figure 6.4 Variation of conductivity (σ) with temperature(lnσ Vs 10³/T) of ITO thin film prepared at room temperature.

Figure 6.5. shows the variation of Hall coefficient (R_H) with temperature. It was found that R_H is independent of temperature. Figure 6.6 shows the variation of carrier concentration (N) with temperature. From figure 6.5 and figure 6.6, it can be seen that both R_H and carrier concentration have negligible dependence on

temperature. It suggests that ITO thin film is degenerate [18]. For a highly degenerate semiconductor, the Fermi energy E_F can be evaluated using

$$E_F = \left(\frac{h^2}{8m^*}\right)\left(\frac{3N}{\pi}\right)^{2/3} \qquad (6.7)$$

where m* is the reduced effective mass, h the Planks constant and N the carrier concentration. With m* = $0.3m_0$, for ITO thin films [11,19,20], we obtained E_F = 0.63eV. This is much greater than kT $\approx$ 0.025eV. This again shows that the ITO film is highly degenerate even at room temperature.

Figure 6.7 shows the variation of mobility with temperature. It shows a slight increase in mobility with increase in temperature. As the mobility has a small dependence on temperature, the grain boundary and acoustical phonon scattering have a little role in the scattering mechanism [21]. But the neutral and ionized impurity scattering cannot be neglected in degenerate semiconductors with high carrier concentration [22,23]. Here the measured value of the mobility at room temperature was $\approx$ 16cm^{2}V^{-1}s^{-1}. The observed low value of the mobility may be due to the interaction of the scattering centers and/or the formulation of neutral scattering defects as explained by Gerlach et al [22].
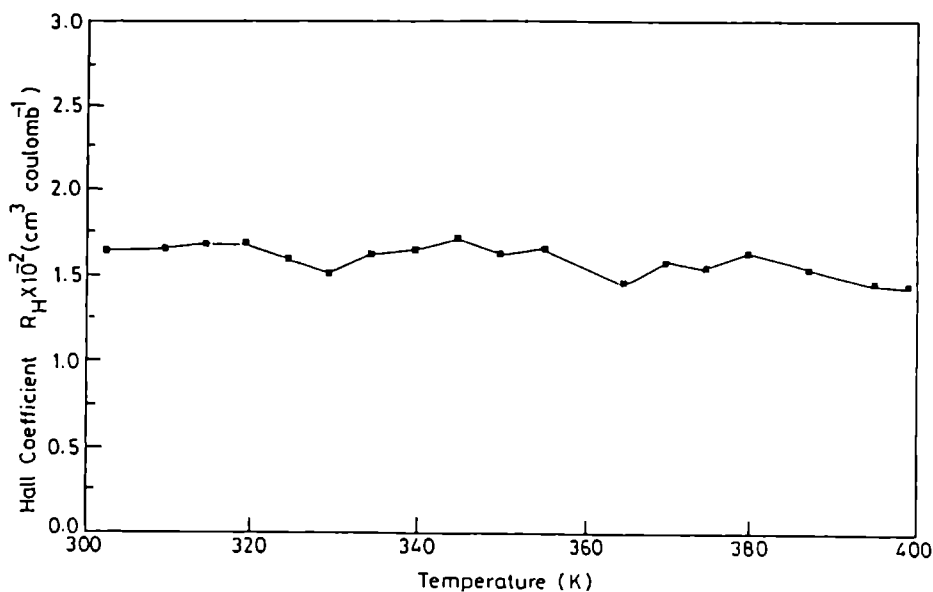
Figure 6.5 Variation of Hall coefficient(R_H) with temperature(T) of ITO thin film prepared at room temperature.
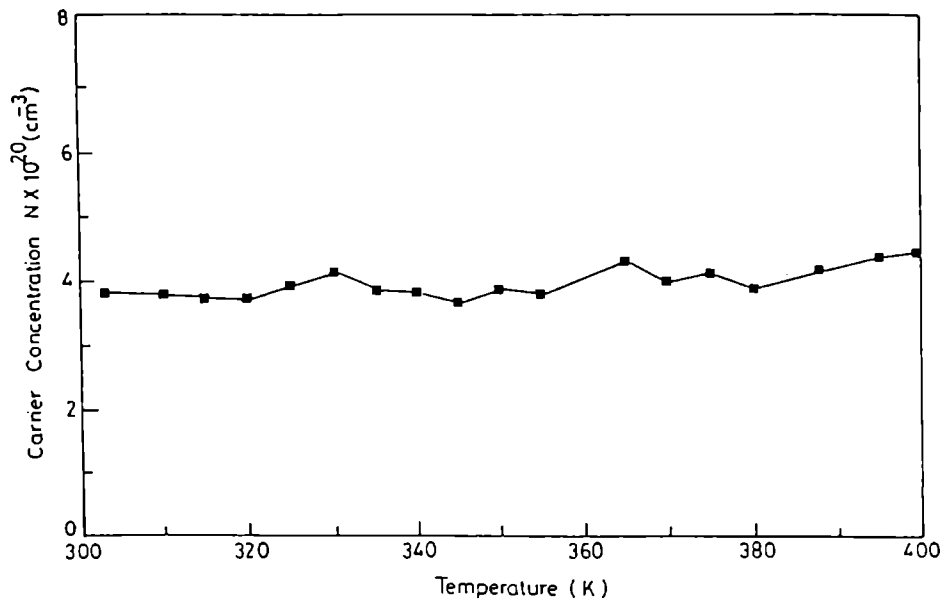
Figure 6.6 Variation of carrier concentration(N) as a function of temperature(T) for ITO thin film prepared at room temperature.
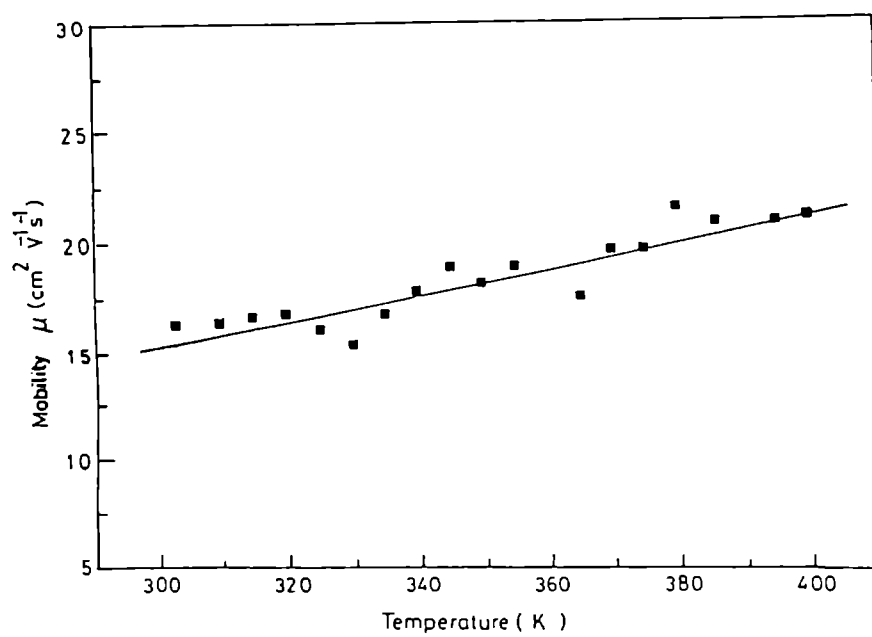
Figure 6.7 Variation of Hall mobility(μ) with temperature(T) of ITO thin film prepared at room temperature.

Figure 6.8 shows the dependence of ln(μ) vs ln(N). The slope of the graph was found to be nearly 0.78, which falls within the limit (0.8±0.2) for ionized impurity scattering, as suggested by Hoffmann et al [17]. The mean free path was calculated using the relation [23].

$$ I = \left(\frac{h}{2e}\right)\left(\frac{3N}{\pi}\right)^{1/3} \mu_H $$

(6.8)

The mean free path was found to be ≈ 2.4nm, which is smaller than the observed grain size. So the scattering at the grain boundary can be ruled out. Therefore in the present case, the ionized impurity scattering seems to be the appropriate scattering mechanism.

Thermoelectric power of ITO film was measured. Samples prepared on glass substrates with thickness ≈ 300nm, length 3cm and breadth 0.3cm were used for the measurements. Silver paint was used as the electrical contact to the specimen. The temperature at each end of the sample and hence the average temperature and the temperature difference (ΔT) were determined by the thermocouples attached to both ends of the sample. Potential difference (ΔV) developed between the two ends of the sample, due to the temperature gradient was measured. The ratio (ΔV/ΔT) gives the thermoelectric power of the specimen.
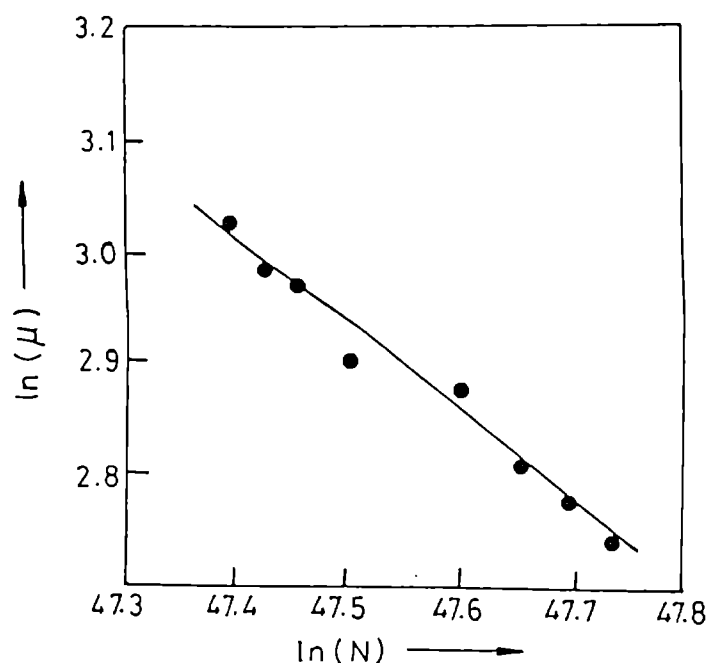
Figure 6.8 Dependence of mobility on carrier concentration (lnμ Vs lnN)

The variation of the thermoelectric power(s) with temperature is shown in figure 6.9. All the samples show a sharp increase in thermoelectric power around 290K. Thereafter it decreases up to 320K, and then it increases gradually up to 390K. Above 390K the thermoelectric power again shows a sharp increase with increase in temperature. The thermoelectric power of the sample measured at room temperature was found to be ≈ 100 μVK^{-1}.

6.5.1. Electrical properties of ITO films with substrate temperature

ITO films with thickness around 350nm were used to study the variation of electrical properties with substrate temperature. The result of the measurements is reported here.

Figure 6.10 shows the variation of sheet resistance (R_s) as a function of temperature, for ITO films prepared at different substrate temperature. The sheet resistance of the films were found to be decreasing gradually with increasing temperature in each case. The variation of Hall coefficient (R_H) with temperature for films prepared at different substrate temperature were shown in figure 6.11. For all the samples R_H value was remaining almost constant throughout the entire range of measurement. Hence we can say that the Hall coefficient is independent of
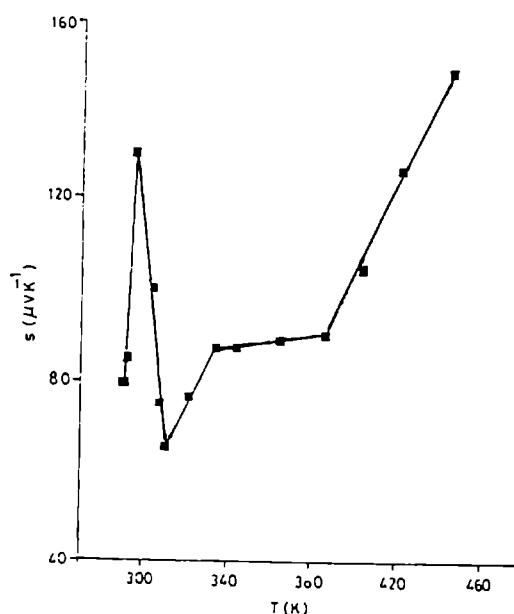
Figure 6.9 Variation of thermoelectric power(S) with temperature(T) of ITO thin film prepared at room temperature.
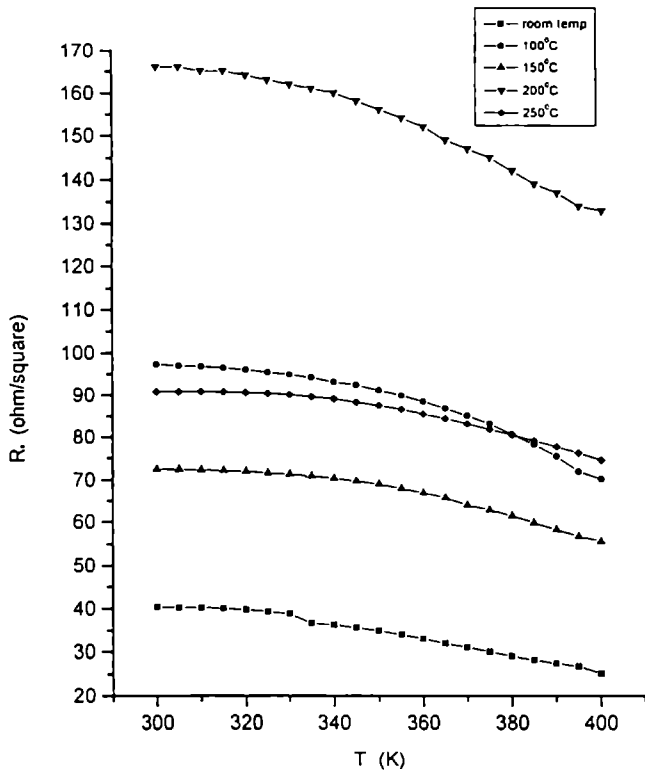
Figure 6.10 Variation of sheet resistance (R_s) with temperature (T) of ITO thin films prepared at different substrate temperature.
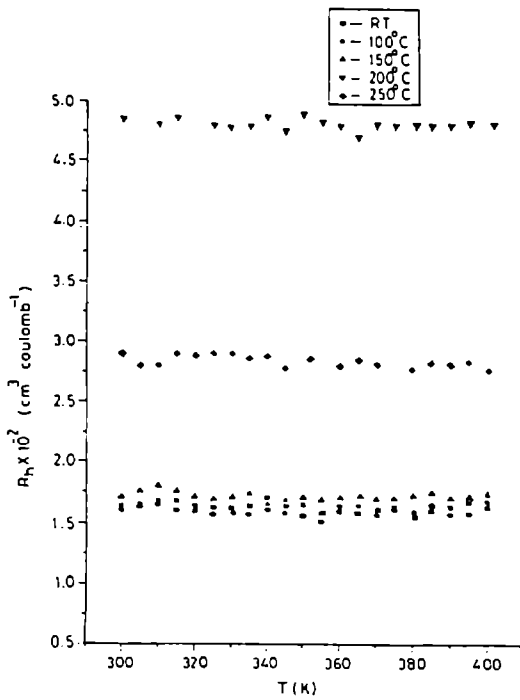

Figure 6.11 Variation of Hall coefficient (R_H) with temperature (T) of ITO thin films prepared at different substrate temperature.
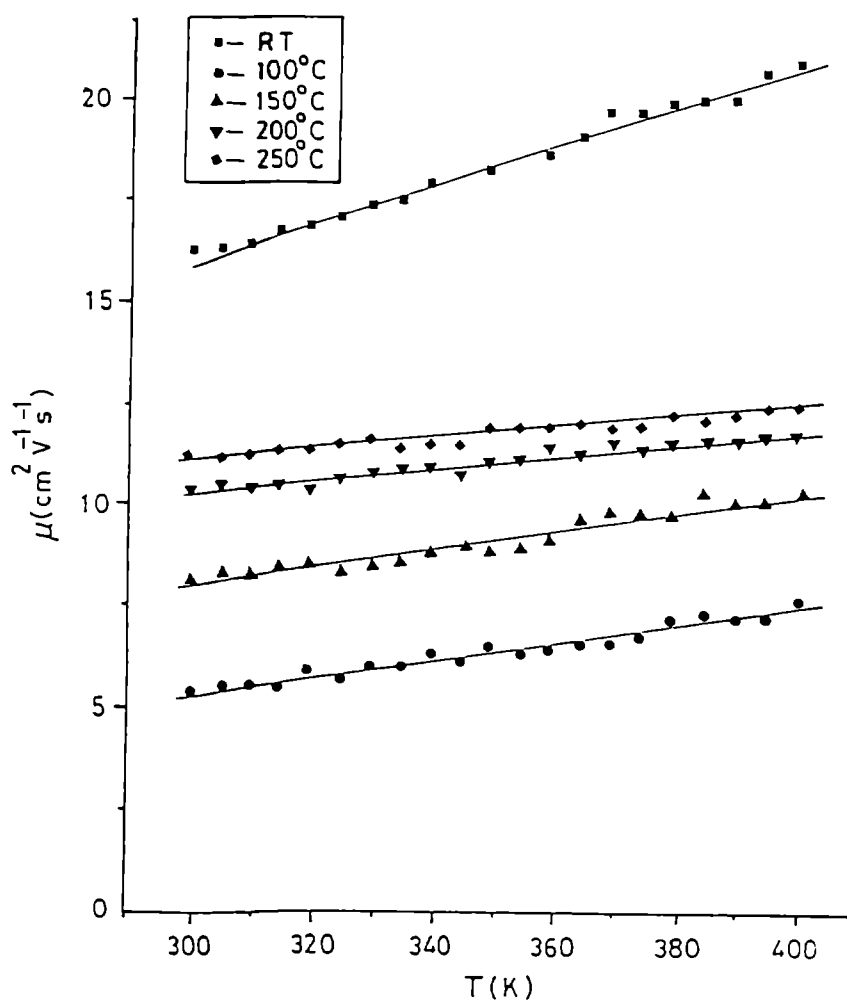
$\mu(cm^2 V^{-1} s^{-1})$

- ■ — RT
- ● — 100°C
- ▲ — 150°C
- ▼ — 200°C
- ◆ — 250°C

T (K)

Figure 6.12 Variation of mobility(μ) with temperature (T) of
ITO thin films prepared at different substrate temperature

temperature for all the samples prepared at different substrate temperatures. This shows the degenerate nature of the samples. Figure 6.12 shows the variation of mobility (μ) as a function of temperature, for films prepared at different substrate temperature. The mobility of the samples remains almost constant throughout the entire range of measurements for all samples except the sample prepared at room temperature. The samples prepared at room temperature were showing a gradual increase in mobility with increase in temperature.
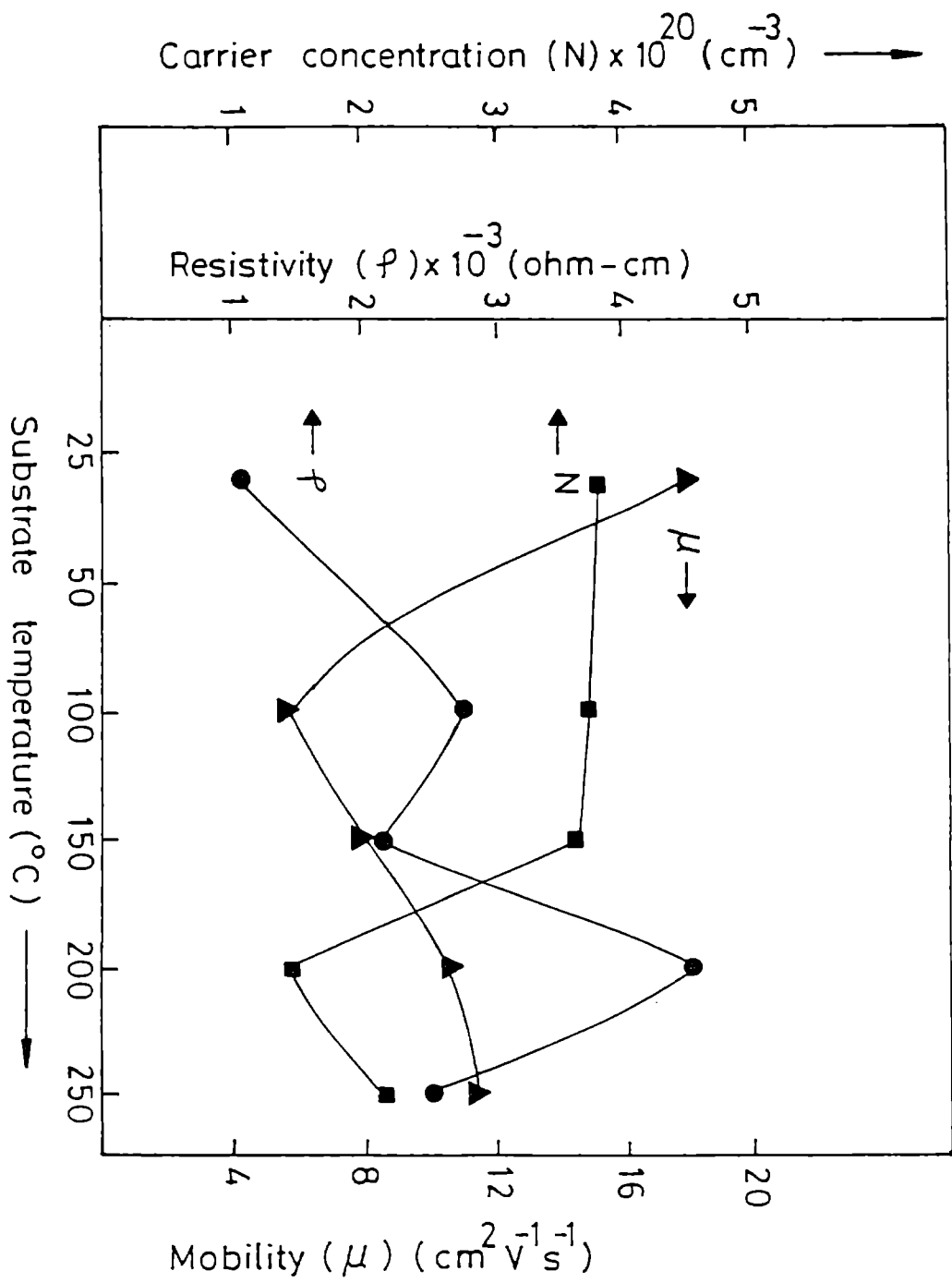
Figure 6.13 Variation of resistivity(ρ), mobility(μ) and carrier concentration(N) as a function of substrate temperature

Figure 6.13 shows the variation of resistivity (ρ), mobility (μ) and carrier concentration (N) as a function of substrate temperature. The resistivity was found to increase with increase in substrate temperature, up to 200°C and then it decreases. The increase in resistivity with substrate may be due to the enhanced oxidation with increase in substrate temperature. It is supported by the variation of carrier concentration with the substrate temperature. The carrier concentration was found decreasing with increase in substrate temperature. It shows that the carrier concentration depends on the oxygen vacancies. A similar behaviour was observed by Noguchi [24] and Kulaszewicz [25] for ITO films prepared by reactive evaporation and spray method. The decrease in resistivity may be due to the enhancement in the crystallinity with increase in substrate temperature beyond 200°C. It was also found that the mobility and carrier concentration increase with substrate temperature in this temperature range.
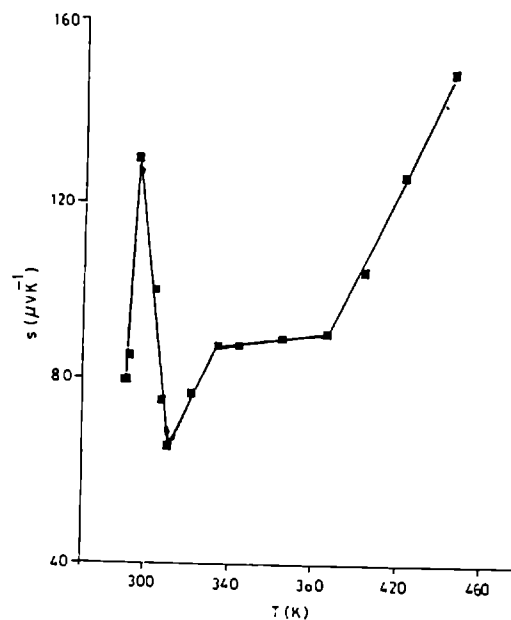

Figure 6.14a Variation of thermoelectric power(S) with temperature(T) of ITO thin films prepared at room temperature,
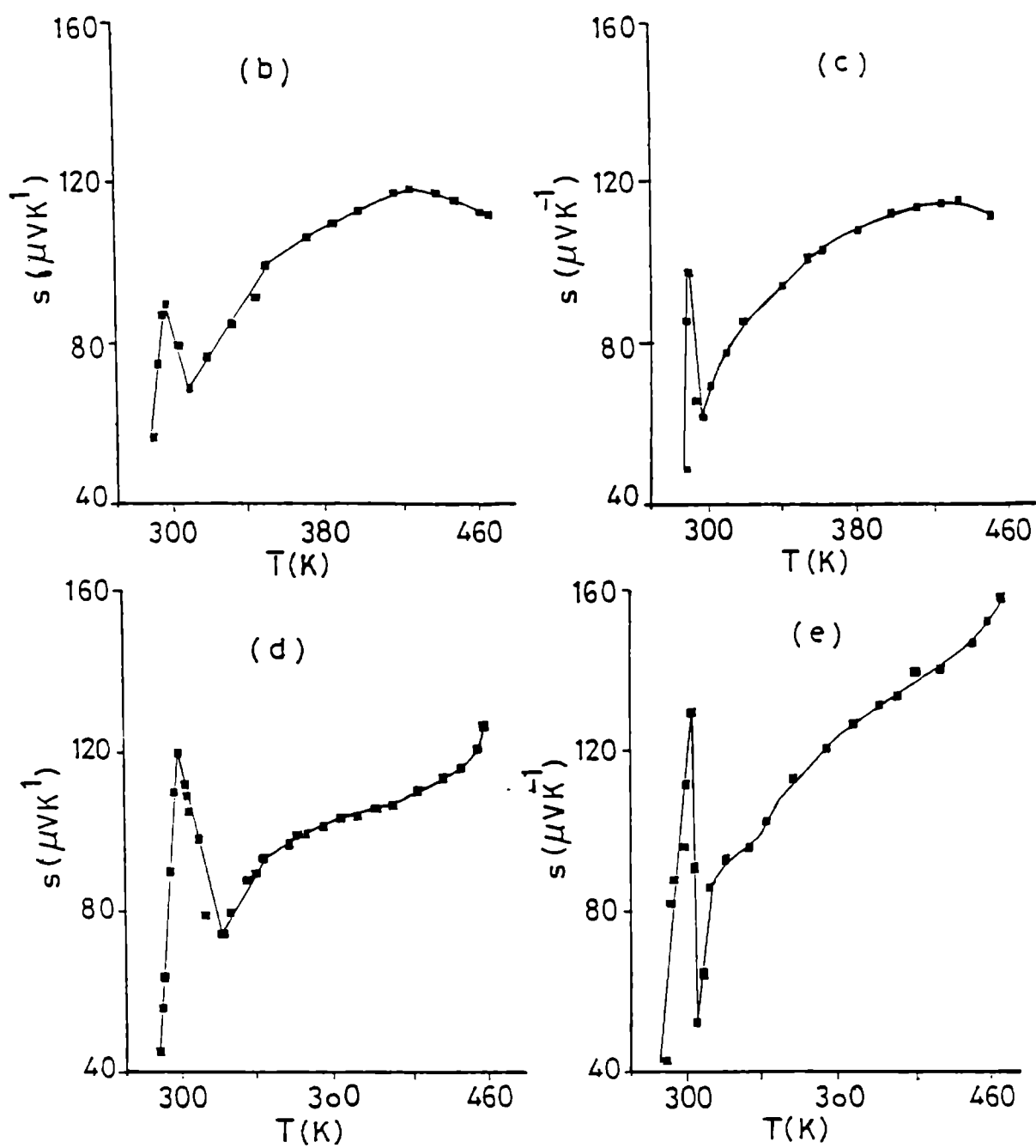
Figure 6.14 Variation of thermoelectric power(S) with temperature(T) of
ITO thin films prepared at different substrate temperature:
(b) 100°C, (c) 150°C, (d) 200°C, (e) 250°C

The mobility is found decreasing up to 100°C and then it increases with increase in substrate temperature. The variation in mobility may be due to the combined effect of various scattering mechanism, say grain boundary scattering, lattice scattering and ionized impurity scattering associated with the structural change, which is related to the substrate temperature. In the present study, the minimum value for the resistivity is associated with the film prepared on substrates at room temperature. The maximum value for carrier concentration and mobility is also obtained for the film prepared at room temperature.

Figure 6.14(a-e) shows the variation of thermoelectric power as a function of temperature for ITO films prepared at different substrate temperature. All the samples show sharp increase in the thermoelectric power around 290K. Then it shows a decrease up to 320K. Above 320K the thermoelectric power was found to be increasing with increase in temperature.

6.6. OPTICAL PROPERTIES

The transmission and reflection spectrum of the films were made using Hitachi U-3410 UV-Vis-NIR spectrophotometer. A typical transmission and reflection spectra of ITO film having thickness 350nm, prepared on glass substrate at room temperature is shown in figure 6.15. The transmittance was found to be decreasing in the lower wavelength region. It is due to the fundamental absorption of the ITO films [26,27]. A decrease in transmittance in the NIR region was also
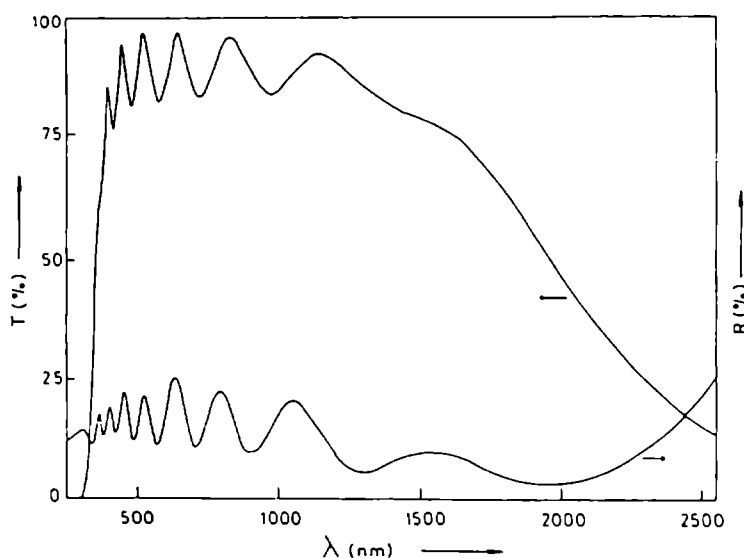

Figure 6.15 Transmission and reflection spectra of a typical
ITO film prepared at room temperature with thickness ≈ 350nm

observed. It may be due to the free carrier absorption, a phenomenon that is common in all transparent conductors having high carrier concentration [28]. It was also supported by the reflection spectrum, being the reflection in the above region is small compared to the decrease in transmittance in the NIR region.

The refractive index (n) of the film was calculated using the interference maxima and minima, using Swanepoels method as explained in section 3.11. Knowing the values of the refractive index, the absorption coefficient (α) in the fundamental absorption region was calculated. Figure 6.16 shows the variation of the refractive index (n) with the wavelength (λ). Refractive index was almost constant in the 500-1000 nm wavelength range, and the average value was found to be 2 ± 0.05. Below 500nm and above 1000nm, the refractive index was found to be increasing.

Figure 6.17 shows the variation of absorption coefficient (α) with the photon energy (hv). The absorption has its minimum value at low energy and increases with increasing optical energy in a similar manner to the absorption edge of the semiconductors.

The optical absorption data were analyzed using the theory of Bardeen et al and found the type of transition involved and the corresponding band gap (Eg). Figure 6.18 shows the variation of $(\alpha hv)^2$ as a function of the photon energy (hv). It is having a linear region and the extrapolation of the linear region to $\alpha = 0$ gives a band gap $\approx$ 3.54eV, which corresponds to the direct allowed transition. Moreover from figure 6.17, it is clear that the value of α, which is of the order of $10^4 cm^{-1}$, is a characteristic of the direct allowed transition in accordance with Smith [29]. Since the measurements were made at room temperature, exciton bands were not likely to be present. Hence the absorption in ITO films was due to the band to band transition. Indirect allowed transition was also found in ITO films. Figure 6.19 shows the variation of $(\alpha hv)^{\frac{1}{2}}$ as a function of photon energy (hv). It is also having a linear region, and the extrapolation of the linear region to $\alpha=0$ gives a band gap of $\approx$ 3eV, which corresponds to the indirect allowed transition. These values were in good agreement with the reported values for ITO [26,27].

The transmission spectra of the ITO films prepared at different substrate temperature are given in figure 6.20. It shows that the average transmittance in the visible region is more or less same for all the films prepared at different substrate
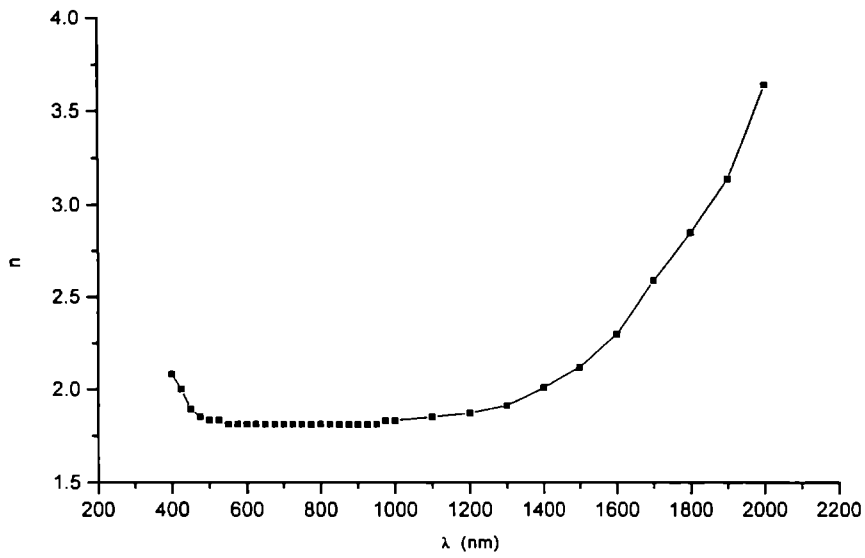
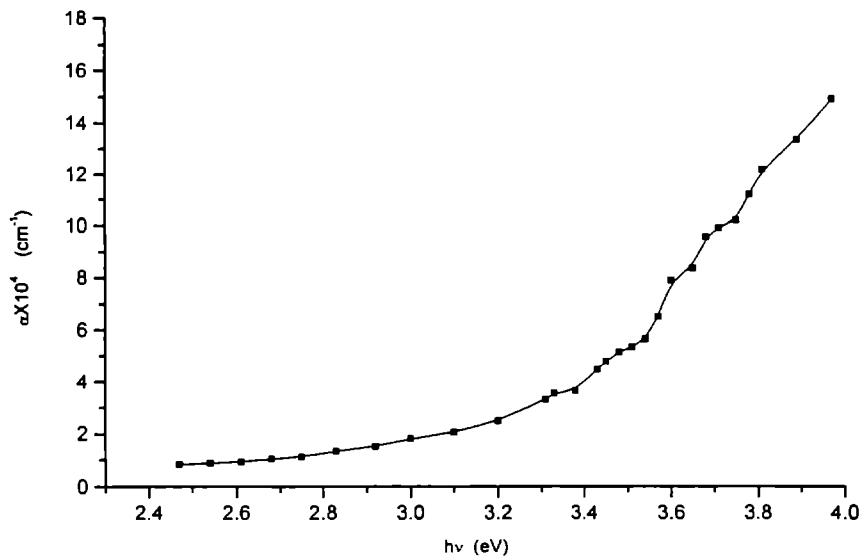**Figure 6.16** Variation of refractive index(n) with wavelength(λ) of ITO thin film prepared at room temperature.

Figure 6.17 Variation of absorption coefficient(α) as a function of photon energy(hv) for ITO thin film prepared at room temperature.
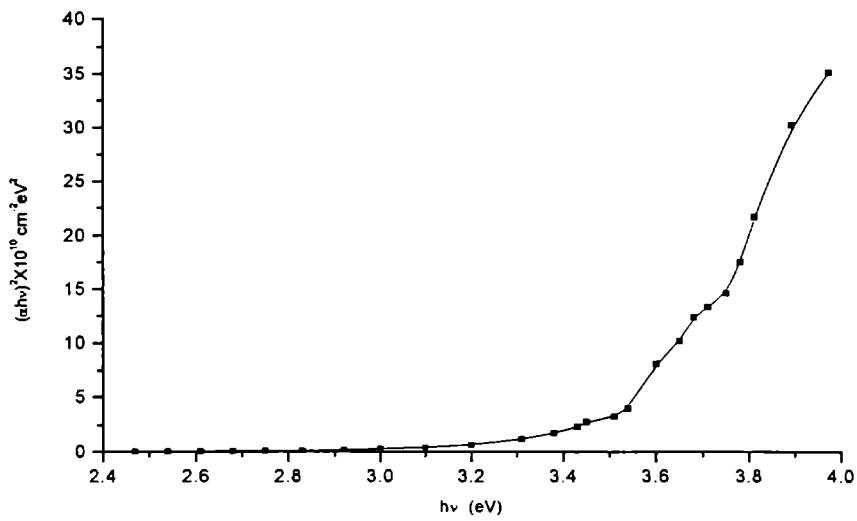
Figure 6.18 Variation of $(\alpha h\nu)^2$ against the photon energy (hν)
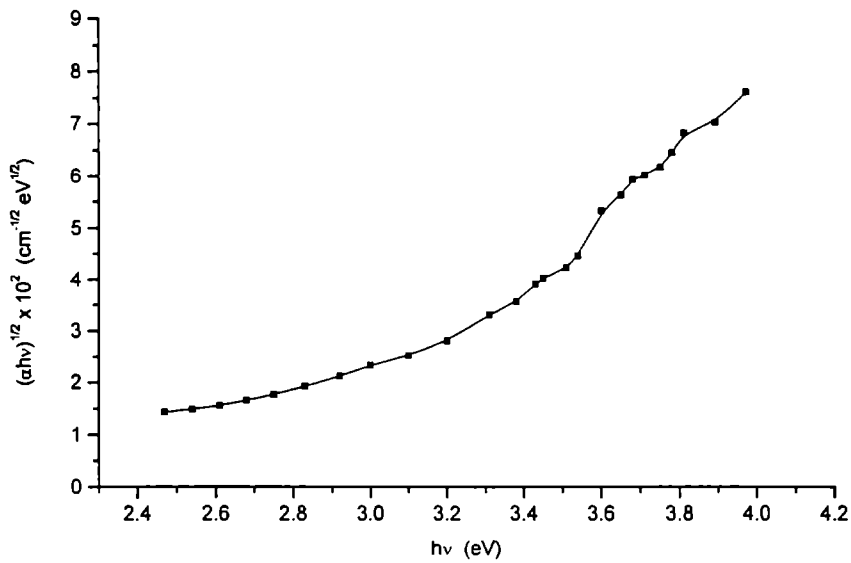for ITO thin film prepared at room temperature.

Figure 6.19 Variation of $(\alpha h\nu)^{1/2}$ against the photon energy (hν)
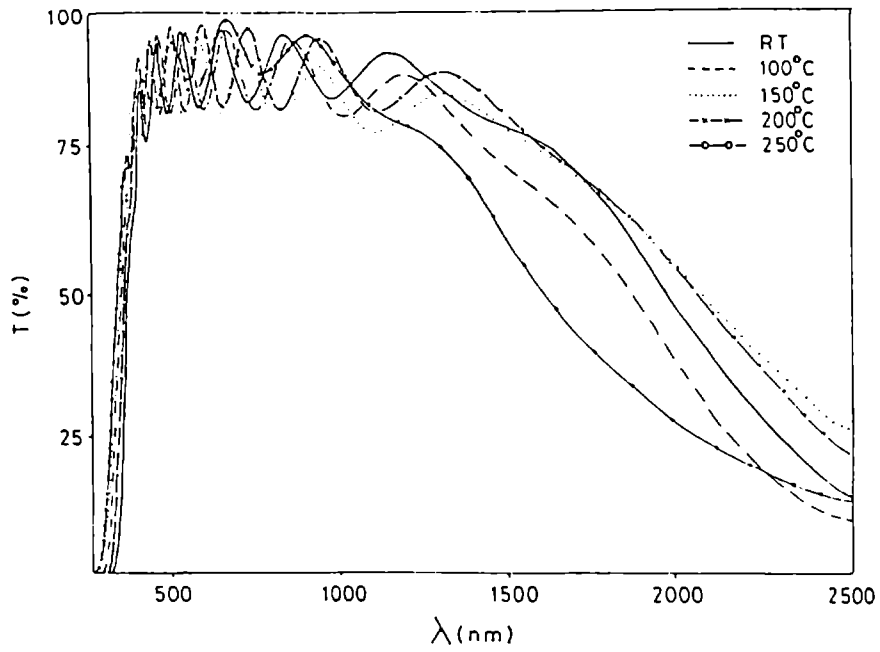for ITO thin film prepared at room temperature.

Figure 6.20 Transmission spectra of ITO film prepared at
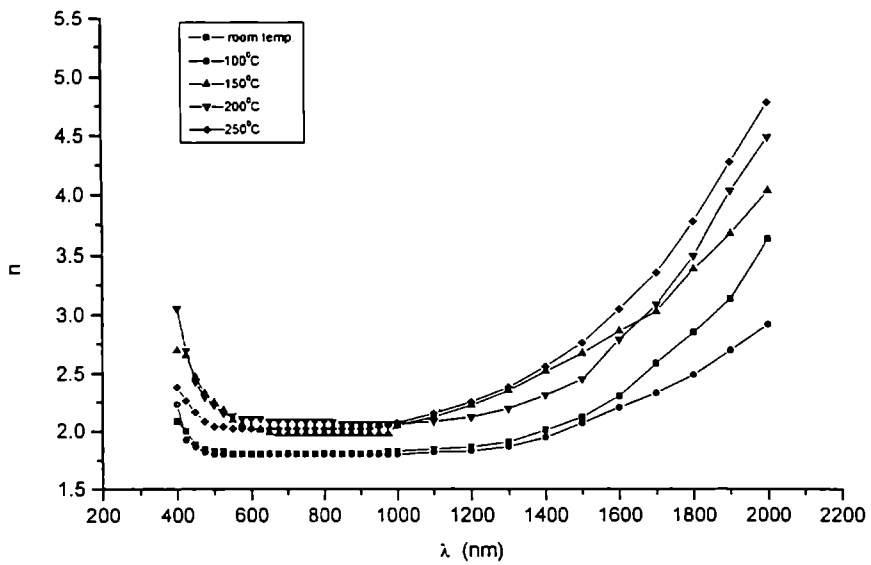different substrate temperature with thickness ≈ 350nm.

Figure 6.21 Variation of refractive index(n) with wavelength(λ) of
ITO thin films prepared at different substrate temperature.

temperature. Variation of refractive index (n) and band gap with substrate temperature was studied. Figure 6.21 shows the variation of refractive index (n) of ITO films prepared at different substrate temperature with wavelength (λ). From the figure it can be seen that n slightly increases with substrate temperature. In all the samples the refractive index remains constant in the wavelength range 500-1000nm. It may be due to the fact that the dispersion effect due to the interband absorption is not dominant in this wavelength region. From the figure it can be seen that the refractive index increases with decrease in λ near the absorption edge and increases with increase in λ in the NIR region. A similar variation in refractive index with wavelength (λ) was observed by Teuwissen et al [30].

Pommier et al [31] have studied the effect of substrate temperature on the refractive index, of spray deposited ITO films. He observed that the refractive index decreases with substrate temperature, possibly because of the increase in carrier density and hence a reduction in resistivity. But in the present study, the refractive index was found to vary with substrate temperature. The variation is analogous to the variation in carrier concentration with substrate temperature as shown in figure 6.13

6.7 VARIATION OF OPTICAL AND ELECTRICAL PROPERTIES WITH THICKNESS

The variation of optical and electrical properties of ITO films with different thickness, prepared on glass substrates at room temperature were studied. The results are reported here.

Figure 6.22 shows the X-ray diffraction pattern of ITO films having various thickness. Figure 6.22a shows the X-ray diffraction pattern of film with thickness 80nm. It gives reflections only from (222) and (440) planes, which are having relative intensity 100 and 35 respectively in the standard XRD data. Figure 6.22b shows the XRD spectrum for a film having thickness 150nm, which gives reflection from (211) planes also, which is having a relative intensity 14 in the standard data, in addition to (222) and (440) planes. Figure 6.22c & figure 6.22d shows the XRD pattern of films having thickness 270nm and 350nm respectively. Here two more planes with relative intensity 6 and 10, get resolved. It shows that as the film thickness increases, the XRD pattern agrees very well with the standard data. In the case of film with lower thickness, only those planes having higher relative intensity is resolved.
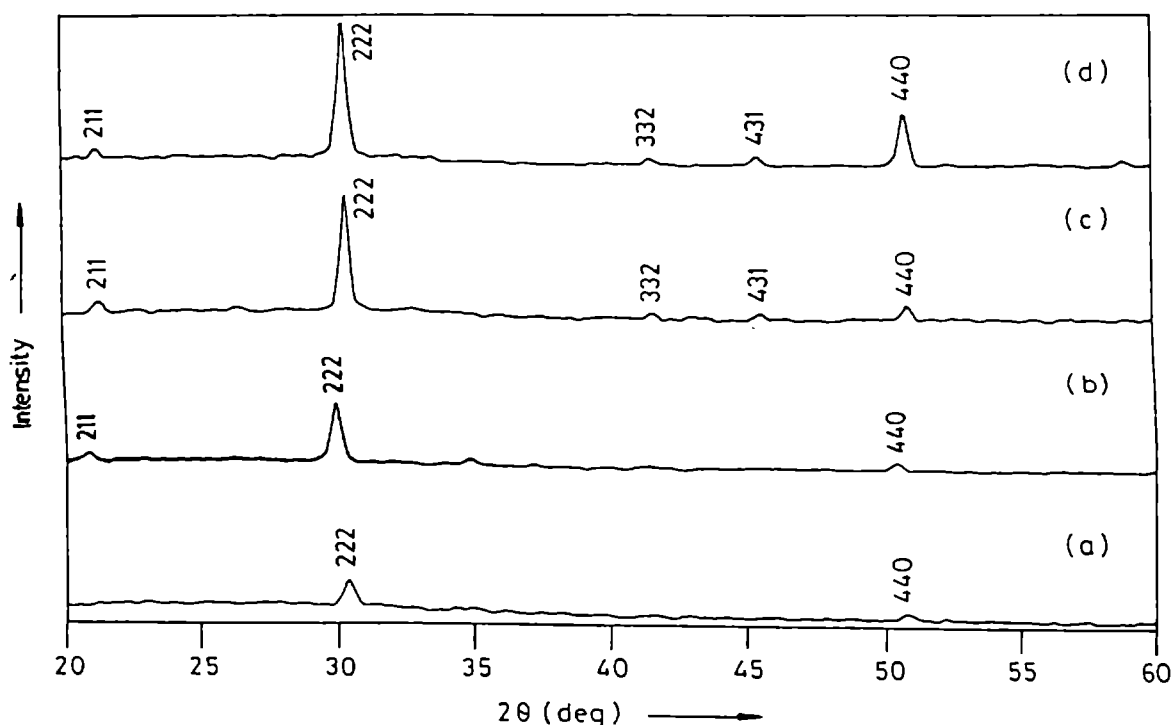
Figure 6.22 X-ray diffraction pattern of ITO thin films prepared
at room temperature with different thickness: (a) 80nm,
(b) 150nm, (c) 270nm, (d) 350nm.

The grain size was calculated from the XRD pattern using Debye-Scherrer formula. Figure 6.23 shows the variation of grain size with film thickness. It can be seen that the grain size remains same for films with thickness greater than 150nm. Here the average grain size is 16nm. Figure 6.24 shows the variation of sheet resistance with film thickness. It was observed that the decrease in sheet resistance is rapid when the film thickness increases from 80nm to 150nm, whereas this decrease is very slow when the thickness is greater than 150nm. A similar variation in sheet resistance with thickness has been reported for ITO and SnO_2 films [32,33]. The observed increase in sheet resistance for films having thickness less than 150nm was probably due to the discontinuous nature of the film.The observed dependence of sheet resistance on thickness is in good agreement with that reported in literature [34].
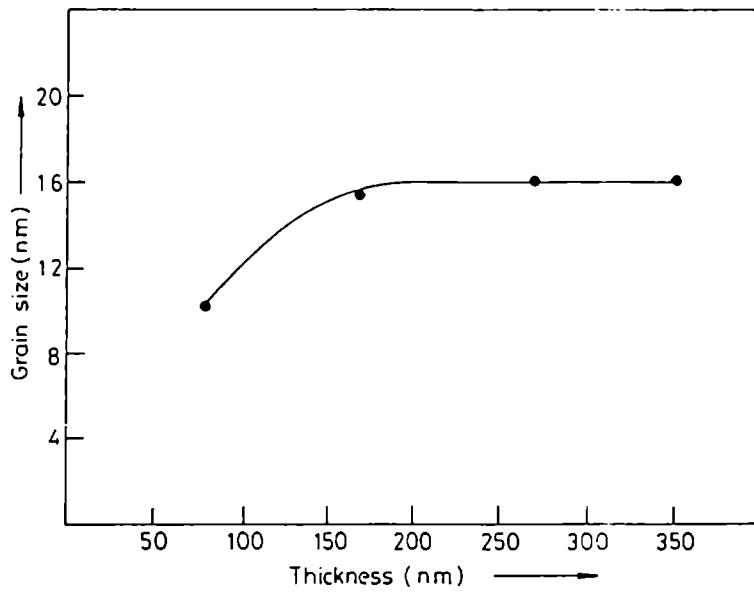
Figure 6.23 Variation of grain size with thickness of the
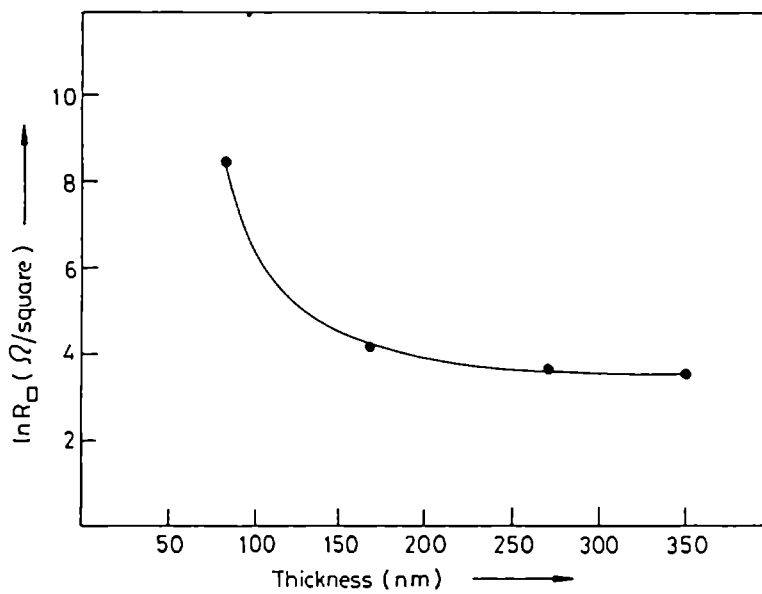films prepared at room temperature.

Figure 6.24 Variation of sheet resistance with thickness of the
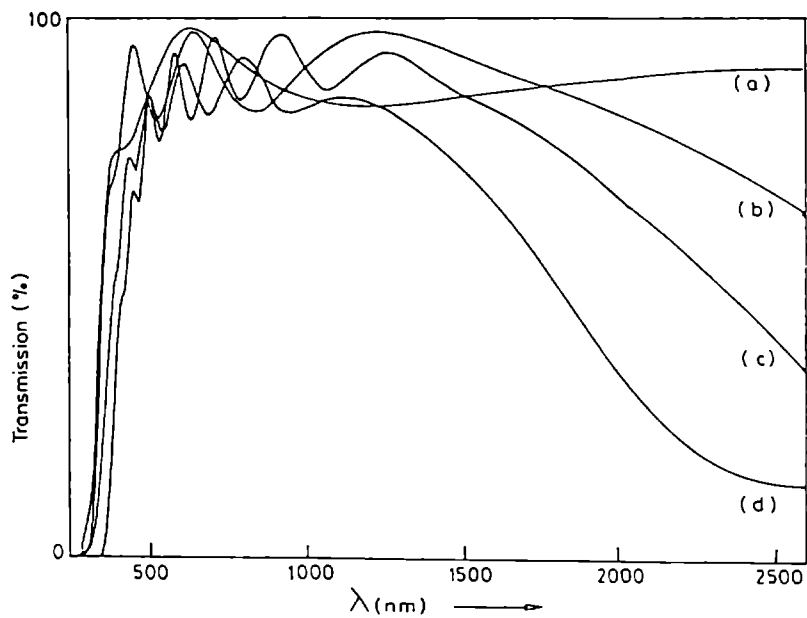films prepared at room temperature.

Figure 6.25 Transmission spectra of ITO thin films prepared
at room temperature with different thickness: (a) 80nm,
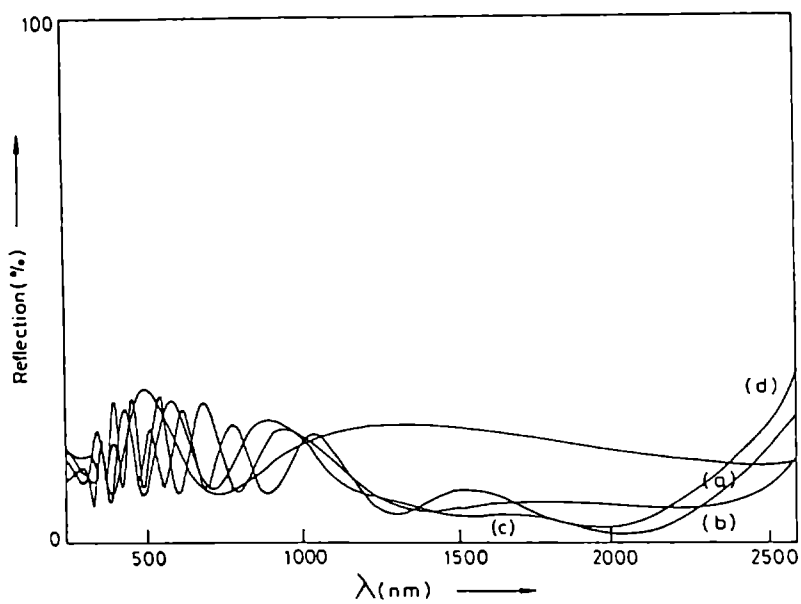(b) 150nm, (c) 270nm, (d) 350nm.

Figure 6.26 Reflection spectra of ITO thin films prepared
at room temperature with different thickness:
(a) 80nm, (b) 150nm, (c) 270nm, (d) 350nm.

Figure 6.25 shows the transmission spectra of ITO films with different thickness. The transmittance in the visible region was found to be almost independent of film thickness. But the transmission in the NIR region decreases with increase in film thickness. Figure 6.26 shows the reflection spectra of the same set of samples. It shows that there is no appreciable reflection in the NIR region for all the samples. But in the case of samples having higher thickness, the reflectance increases slightly for wavelength above 2000nm. But this increase in reflectance is not comparable with the decrease in transmittance in the same region. So the decrease in transmittance with increase in thickness, in the NIR region, is due to the free carrier absorption, a phenomenon that is common in all transparent conductors having high carrier concentration [28]. It is also supported by the Hall effect studies. Table 6.4 summarizes the results obtained from the Hall effect measurements. It shows that the carrier concentration increases with increase in film thickness. A similar variation in carrier density with film thickness has been reported in the case of Sb doped SnO_2 films by Kaneko et al [35]. The decrease in transmittance in the NIR region with increase in thickness for ITO films has been observed by other authors also [32, 36, 37].

d (nm)	n (cm^{-3})	ρ (Ω-cm)	μ (cm^2 V^{-1}s^{-1})
80	3.87×10^{18}	3.3×10^{-2}	48
150	1.12×10^{20}	1.4×10^{-3}	34
270	3.8×10^{20}	1.05×10^{-3}	28
350	6.3×10^{20}	1.01×10^{-3}	16

Table 6.4 variation of refractive index(n), resistivity(ρ) and mobility(μ) with thickness

6.8 FIGURE OF MERIT

Usually the performance of transparent conductors is compared using the figure of merit. According to Hacke [38], the figure of merit is defined as

$$\phi_{TC} = \frac{T^{10}}{R_s} \tag{6.9}$$

where T is the average transmittance and R_s is the sheet resistance. The sheet resistance of the film was measured using van der Pauw method. It was found to be 40Ω/square. The average transmittance in the 500-1000nm wavelength range was ≈ 90%. Using these data, the figure of merit of ITO film prepared on glass substrate at room temperature with thickness ≈ 350nm was calculated, and found to be 8.7 x 10^{-3}. A comparison of the performance of transparent conducting oxide films prepared by various authors is given in table 6.5.

Material	Technique	Sheet resistance Ω / square	T%	Figure of merit ϕ_{TC}	Mobility $cm^2V^{-1}s^{-1}$	N cm^{-3}	Reference
ITO	ARE	40	90	$8.7x10^{-3}$	16	$3.8x10^{20}$	Present work
In_2O_3	ARE	38.6	80	$2.8x10^{-3}$	15	$2.97x10^{20}$	40
ITO	ARE	20	90	$1.7x10^{-3}$	20-30	$1x10^{21}$	41
In_2O_3:F	Ion Plating	40	80	$2.7x10^{-3}$	13	$7x10^{20}$	42
ITO	Magnetron sputtering	40	90	$8.7x10^{-3}$	----	---	43
ITO	CVD	3	75	$1.8x10^{-3}$	---	---	44
ITO	Spray	4	90	$8.7x10^{-3}$	50	$6x10^{20}$	32

Table 6.5 comparison of properties of transparent conducting oxides

6.9. CONCLUSION

Polycrystalline ITO films were prepared on glass substrates kept at room temperature by activated reactive evaporation. The films were found to be n-type. The films show a low resistivity ≈ $1.01x10^{-3}$ohm-cm, high carrier concentration ≈ $3.81x10^{20}cm^{-3}$ and mobility ≈ $16cm^2V^{-1}s^{-1}$ at room temperature. The average transmittance in the visible region was found to be 90%. The films show both direct and indirect allowed transition with band gap ≈ 3.54eV and 3eV respectively.

REFERENCES

1. K. Badeker, Ann. Phys. (Leipzig) **22** (1907) 749.

2. K.L. Chopra, S. Major and D.K. Pandya, Thin Solid Films **102** (1983) 1.

3. A.L. Dawar and J.C. Joshi, J. Mater. Sci. **19** (1984) 1.

4. S.A. Bashar, A.A. Rezazedeh,
    IEEE Trans. Microwave Theory and Tech. **43** (1995) 2299.

5. C.H. Lee, C.S. Huang, Mater. Sci. and Eng. B. **22** (1994) 223.

6. Z. Crujak, B. Orel, and M.K. Qunde, Solar Energy Cells **26** (1992) 105.

7. A. Vasu and A. Subrahmanyan, Thin Solid Films **189** (1990) 217.

8. G. Rupprecht, Z. Phys. **139** (1954) 504.

9. T.J. Vink, M.H.F. Ovenwijk and W. Walrave, J. Appl. Phys. **80** (1996) 3734.

10. G. Frank and H. Kostlin, Appl. Phys. A **27** (1982) 197.

11. I. Hamberg and C.G. Granqvist, J. Appl. Phys. **60** (1986) 123.

12. P. Nath, R.F. Bunshah, Thin Solid Films **69** (1980) 63.

13. M. Rottmann, H. Hennig, B. Ziemer, R. Kalahne and K.A. Heekner
    J. Mater. Sci. **31** (1996) 6495.

14. H.L. Hartnagel, A.L. Dawar, A.K. Jain, C. Jagadish,
    Semiconducting Transparent Thin Films, (IOP Publishing, London, 1995).

15. P.J. Martin and R.P. Netterfield, Thin Solid Films **207** (1986) 137.

16. Y. Shigesato, S. Takaki, T. Haranon, Appl. Surf. Sci. **48/49** (1991) 269.

17. H. Hoffmann, A.D. Dietrich, J. Pickal and D. Kreuse,
    Appl. Phys. **16** (1978) 239.

18. N.B. Hannay, *Seconductors,* (Chapman and Hall, London, 1960).

19. Bel Hadj Tahar R, Tahayuki Ban, Yutaha Ohya and Yasutaha Takahashi,
    J. Appl. Phys. **83** (1998) 2631.

20. R. Clanget, Appl. Phys. **2** (1973) 247.

21. V.F. Korzo and V.N. Chernyaev, Sov. Phys. Solid State **8** (1967) 2769.

22. E. Gerlach and M. Routenberg, Phys. Stat. Sol. (b) **86** (1978) 479.

23. M. Bender, J. Trube and J. Stollenwerk, Thin Solid Films **354** (1999) 100.

24. S. Noguchi and H. Sakata, J. Phys. D; Appl. Phys. **13** (1980) 1129.

25. S. Kulaszewicz, W. Jarmoc and K. Turowska,
    Thin Solid Films **112** (1984) 313.

26. J. Szezyrbowski, A. Dietrich and H. Hoffmann,

   Phys. Stat. Sol.(a) **78** (1983) 243.

27. N. Balasubramanian, A. Subramanyam, J. Phys. D; Appl. Phys. **22** (1989) 206.

28. M. Mizuhashi, Thin Solid Films **70** (1980) 91.

29. R.A. Smith, *Semiconductors,* 2nd Edn.

   (Cambridge University Press, 1978). **p.** 314.

30. A.P. Teuwissen and G.J. Declerk, Thin Solid Films **121** (1984) 109.

31. R. Pommier, C.Gril and J. Marucchi, Thin Solid Films 77 (1981) 91.

32. R. Banerjee, S. Ray and A. K. Barua, J. Mater. Sci. Lett. **6** (1987) 1203.

33. O. A. Omar, H.F. Rigaie and W. Fikry,

   J. Mater. Sci. Mater. Electron. **3** (1990) 79.

34. M. S. Ali, K. A. Khan and M.S.R. Khan,

   Phys. Stat. Sol (a) **149** (1995) 611.

35. H. Kaneko and K. Miyake, J. Appl. Phys. **53** (1982) 362.

36. F.O. Adurodija, H. Izumi, T. Ishihara, H. Yoshioka, K. Yamada,

   H. Matsui and M. Motoyama, Thin Solid Films **350** (1999) 79.

37. Li-Jian Meng and M.P. dos Santos, Thin Solid Films **303** (1997) 151.

38. G. Hacke, J. Appl. Phys. **47**, (1976) 4086.

39. M. D. Benoy and B. Pradeep, Bull. Mater. Sci. **20** (1997) 1029

40. P. Nath, R.F. Bunshah, B.M. Bosol and O.M. Staffsud,

   Thin Solid Films **72** (1980) 463

41. J. N. Avaritsiotis and R. P. Howson, Thin Solid Films **80** (1981) 63

42. J. F. Smith, A. J. Aronson, D. Chen and W.H. Class,

   Thin Solid Films **29** (1975) 155

43 J. Kane and H. P. Sweitzer, Thin Solid Films **77** (1981) 91

CHAPTER 7

PREPARATION AND CHARACTERISATION OF

LEAD SELENIDE (PbSe) THIN FILMS

7.1 INTRODUCTION

Lead selenide, like other lead salts, crystallises into the FCC, NaCl type structure (O_h^5) at ambient conditions. It is reported to undergo a high-pressure induced structural phase transition to the orthorhombic T II - type phase (D_{2h}^{16}) at pressure of about 4.5GPa and another one to the CsCl- type (O_h^1) phase at about 16 G Pa [1]. So PbSe is a material that possesses two high pressure metastable crystal modifications.

It is an indirect band gap semiconductor [2-4]. In recent years there has been considerable interest in the potential application of polycrystalline PbSe thin films in photoluminescence and photoconductive devices [5,6]. There has also been industrial and commercial use of this material by adopting the photochemical technique to make patterns in porous glass such as chemical wave guides, gratings, and lenses [7].

Literature reports indicate that the thin films of PbSe have been produced by a number of techniques. This includes the epitaxial growth of single crystals on alkali halide substrates [8-10], thermal evaporation from bulk [11,12], chemical method[13,14], successive ionic layer adsorption and reaction technique[15], electrochemical method[16] and laser assisted deposition[17].

Polycrystalline thin films of lead chalcogenide and their alloys are efficient in IR detection and IR photography [16,17]. Recently it has been shown that PbSe films are widely used for photodiode and photodetectors also.

Although there have been a number of investigations on the preparation of this material by different techniques, both physical and chemical, nobody has yet reported the preparation of PbSe thin films by three-temperature method. The present chapter reports the preparation of polycrystalline lead selenide thin films by reactive evaporation. Structural characterisation of the film was done by taking X-ray diffraction. Variation of conductivity with temperature was studied. Using the transmission spectra, the refractive index, absorption coefficient and band gap of the films were studied.

7.2 EXPERIMENTAL

Lead selenide thin films were prepared by reactive evaporation, a variant of three-temperature method, in which the individual elements were evaporated from separate sources. The films were deposited on glass substrates, kept at an elevated temperature. It has been found that for many binary system, a stoichiometric interval exists with a limited degree of freedom in selecting the individual components and substrate temperature for obtaining a particular compound of the system [18,19]. The details of the preparation techniques are given in chapter 3

Lead and selenium (99.999% pure) were used as the source materials. Lead was evaporated from a molybdenum boat and selenium from a quarts crucible. The deposition was performed in a vacuum chamber at a pressure $\approx 10^{-5}$m.bar. Optically flat glass slides were used as substrates. They were cleaned using an industrial detergent and then ultrasonically agitated in distilled water for 15 to 20 minutes. The slides were dried with hot air. These glass substrates were fixed on a heater, whose temperature could be controlled with an accuracy of ± 10K. Chromel-alumel thermocouple placed in contact with the substrate was used for measuring the temperature.

After stabilising the required substrate temperature, the current through the selenium source was switched on and was allowed to melt in the crucible with a shutter placed over the selenium and lead sources. The lead source current was then switched on and was increased to the pre-determined value. Then the shutter was removed and the deposition of the compound film was allowed to take place.

When the lead and selenium atoms impinge on the substrate surface, they were adsorbed and begin to react by acquiring sufficient activation energy from it to form the compound. This is an ordering process in which the atoms diffuse across the surface until they fall into potential wells, represented by regular lattice sites. The unreacted atoms were unable to stick on the substrate independently at the given elevated temperature and they were adsorbed after a finite interval of time.

The rate at which the metal atoms arrive at the unit area of a substrate was calculated using equation 3.2.

PbSe films were prepared on glass substrates at room temperature and 373K. The films prepared at room temperature were found to be amorphous or partially crystalline. But the films prepared at 373K were polycrystalline in nature. It was

found that polycrystalline films of lead selenide were obtained using the following deposition parameters,

Lead flux $\approx 2.02 \times 10^{15}$ atoms cm^{-2} s^{-1}

Selenium flux $\approx 3.01 \times 10^{15}$ atoms cm^{-2} s^{-1}

Substrate temperature = 373 ± 10K.

The deposition rate of PbSe films was ≈ 70 nm/minute. Highly reproducible PbSe films were obtained under these conditions.

7.3 X-RAY DIFFRACTION STUDIES

The structural characterisation of the films was carried out by X-ray diffraction. The thickness of the films used for the XRD studies were of the order of 250nm. Diffraction pattern of the films were taken using monochromatic Cu k_{α} radiation.

Figure 7.1(a) shows the X-ray diffraction pattern of a typical PbSe thin film prepared at room temperature. It shows a broad peak at $2\theta = 29°$, which corresponds to the (200) peak of PbSe. It was noted that this is the only peak observed in the XRD pattern of films prepared at room temperature. It may be due to the fact that the films prepared at room temperature were amorphous or partially crystalline in nature.

Figure 7.1(b) shows the XRD pattern of a typical PbSe thin film prepared on glass substrate at 373K and having thickness around 250nm. It shows reflections from (111), (200), (220) and (222) planes. All the peaks correspond to the cubic structure of PbSe, indicating that the films prepared at 373K were polycrystalline in nature.

The d values were calculated from the XRD pattern .The calculated d values and the relative intensities are given in table 7.1 along with the standard data given in the JCPDS file No. 6-354. The lattice parameter was also calculated. It was found to be 6.13A°, which corresponds to the cubic structure of PbSe and is in good agreement with the standard value. The grain size of the film was calculated using the Scherrer formula

$$\frac{0.9\lambda}{\beta \cos\theta} \qquad\qquad (7.1)$$

where

λ - wavelength of the X-ray used

β - full width half maximum

θ - angle of diffraction

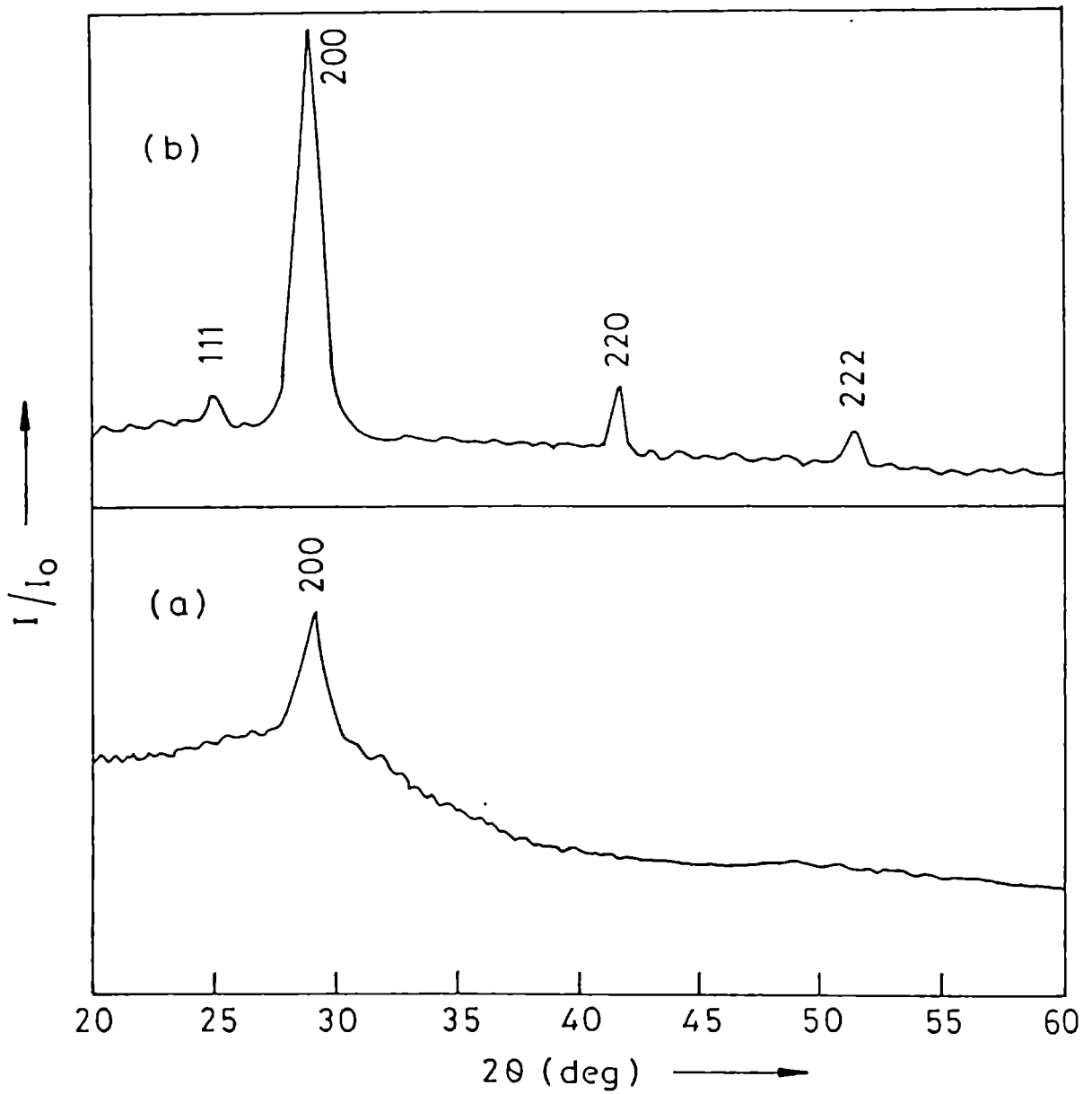The average grain size of the film was found to be 36nm.

Figure 7.1 X-ray diffraction pattern of PbSe thin film prepared at different substrate temperatures: (a) room temperature and (b) 373K

Substrate temperature	(hkl)	Calculated values		Standard data (JCPDS File No. 6-354)	
		d A°	I/I₀	d A°	I/I₀
300 K	200	3.069	100	3.062	100
373 K	111	3.531	29	3.536	30
	200	3.069	100	3.062	100
	220	2.168	25	2.165	70
	222	1.771	13	1.768	20

Table 7.1 X-ray diffraction data for PbSe thin films prepared at 300K and 373K

7.4 ELECTRICAL PROPERTIES

The films prepared for electrical measurements were of thickness nearly 250nm. The thickness of the films were measured using Tolansky's multiple beam interferometric method as described in section 3.7. The details of the conductivity measurement set up are given in section 3.7. The samples used for the measurements were having length 3cm and breadth 0.25cm. Ohmic contacts to the samples were made using silver paste. The ohmic nature of the contacts was verified by the linear current-voltage characteristics through out the temperature range studied (300-420K). The current and voltage were measured using Keithley 195 DMM. All these measurements were done under a vacuum of the order of 10^{-2}m.bar. Freshly prepared samples were used for the measurements. The conductivity type was identified by hot-probe method [20]. It showed that the films were of p-type. According to Maier and Daniel [21], an excess chalcogen is responsible for the p-type conduction. Hence the p-type conduction in PbSe was due to the presence of excess selenium, which will not leave any unreacted lead inside the crystallite.

Figure 7.2 shows the variation of the current with the reciprocal of temperature (ln I Vs 10^3/T) for lead selenide thin film prepared at room temperature with thickness ≈ 250nm. During the heating cycle, the current through the film increases with temperature up to 363K. Then it shows a sudden decrease and then increases. During the cooling cycle, the current through the sample was found to be decreasing. The activation energy was calculated and was ≈ 0.04eV. Figure 7.3 shows the variation of current against the reciprocal of the temperature, for PbSe films prepared at 373K with thickness ≈ 250nm. In the heating cycle, the current

through the sample increased with increase in temperature. During the cooling cycle, the current through the samples were found to be decreasing very slowly.

From figure 7.2, it can be seen that the current through the sample decreases sharply around 363K and then increases. But no such change in current through the sample is observed for films prepared at 373K. The sharp decrease in current around 363K for films prepared at room temperature may be due to a transition from amorphous to polycrystalline state.

From figure 7.2 and figure7.3 it can be seen that the resistance of the film prepared at 373K is higher than that prepared on substrates at room temperature. The high resistance of the films prepared at 373K may be due to the creation of thermally
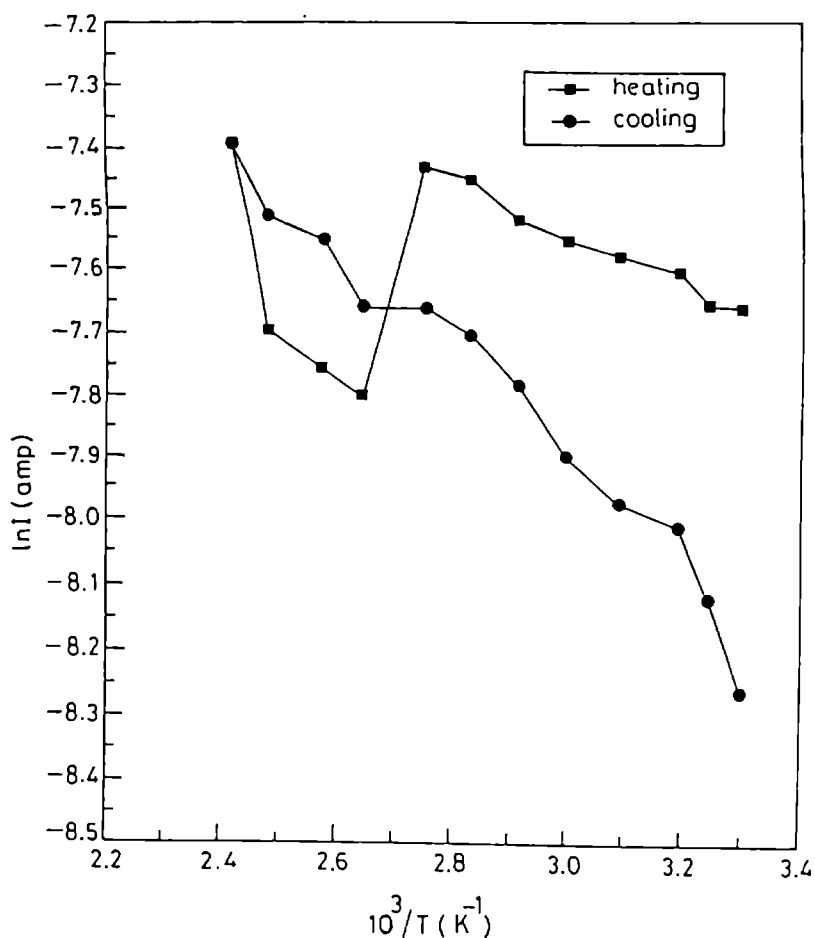
Figure 7.2 Variation of current with temperature ($\ln I$ Vs $10^3/T$)
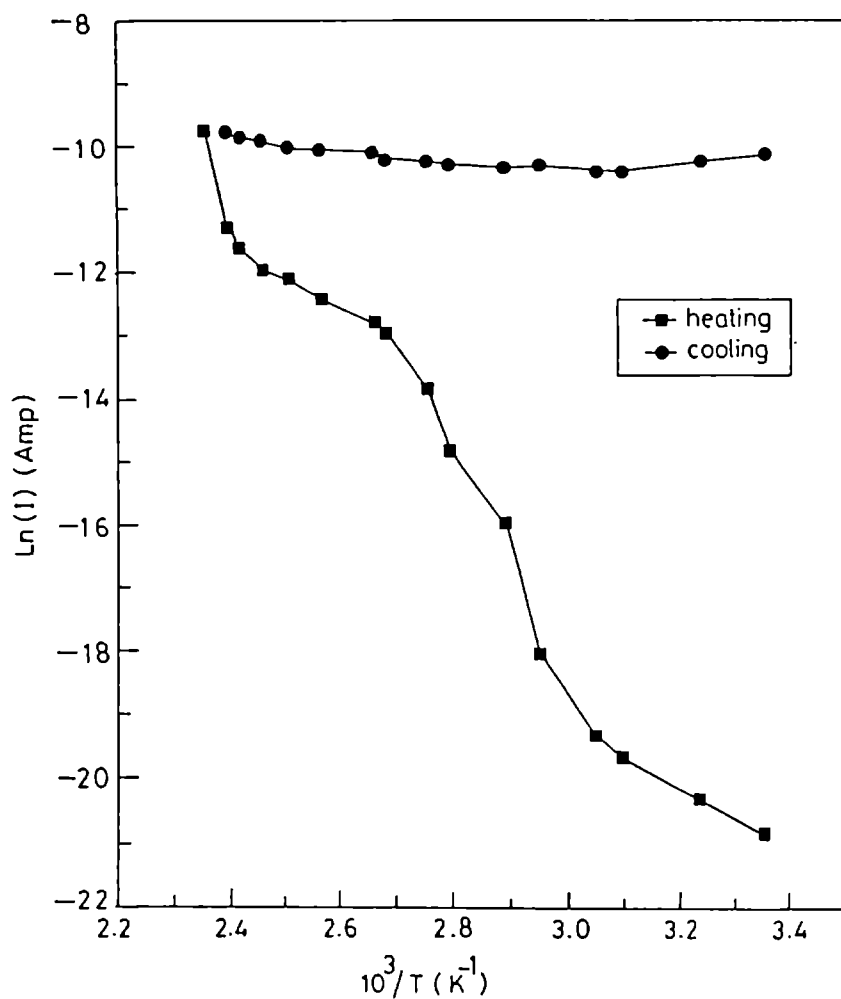for PbSe thin film prepared at room temperature.

Figure 7.3 Variation of current with temperature (lnl Vs 10^3/T)
for PbSe thin film prepared at 373K

generated defects, proposed by Smith [22] and later confirmed by Newman [23] and Miller et al [24]. It is argued that in chalcogenides, defect will be created at high temperatures. These defect can act as scattering centres, thereby appreciably bring down the mobility of the carriers. This results in an increase in resistance of the film. During the heating cycle, the resistance of the film decreases with increase in temperature. But in the cooling cycle, the resistance increases very slowly with decrease in temperature. The activation energy was calculated and was found to be 0.33eV

7.5 OPTICAL PROPERTIES

The optical measurements of the films were made using Hitachi U 3410 UV-Vis- NIR spectrophotometer. Transmission spectrum of PbSe thin films prepared at room temperature and 373K, with thickness ≈ 250nm were shown in figure 7.4. The refractive index, absorption coefficient and hence the band gap were calculated from the interference maxima and minima using Swanepoels method as explained in section 3.11.

Figure 7.5 shows the variation of refractive index with the wavelength, for the film prepared at room temperature. It shows that the refractive index increases with increase in wavelength, reaches a maximum value, then it decreases and remains almost constant around 2.75. Figure 7.6 shows the variation of refractive index with wavelength for the film prepared at 373K. In this case also the average value of refractive index is found to be around 2.75.
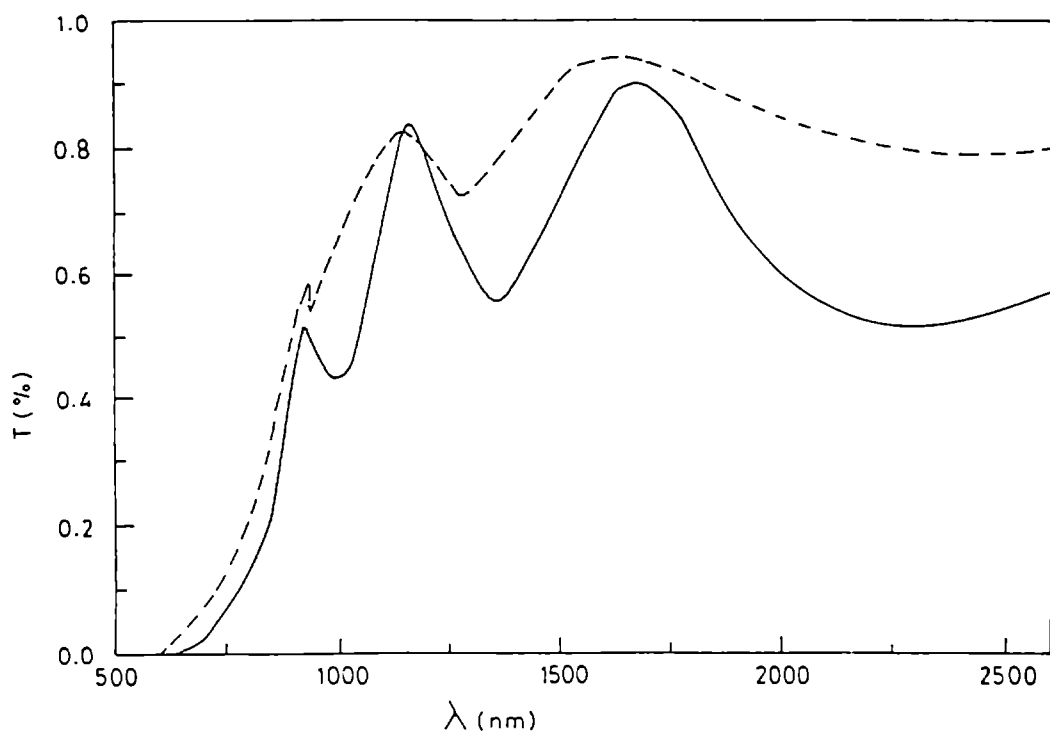

Figure 7.4 Transmission spectra of PbSe thin films prepared on
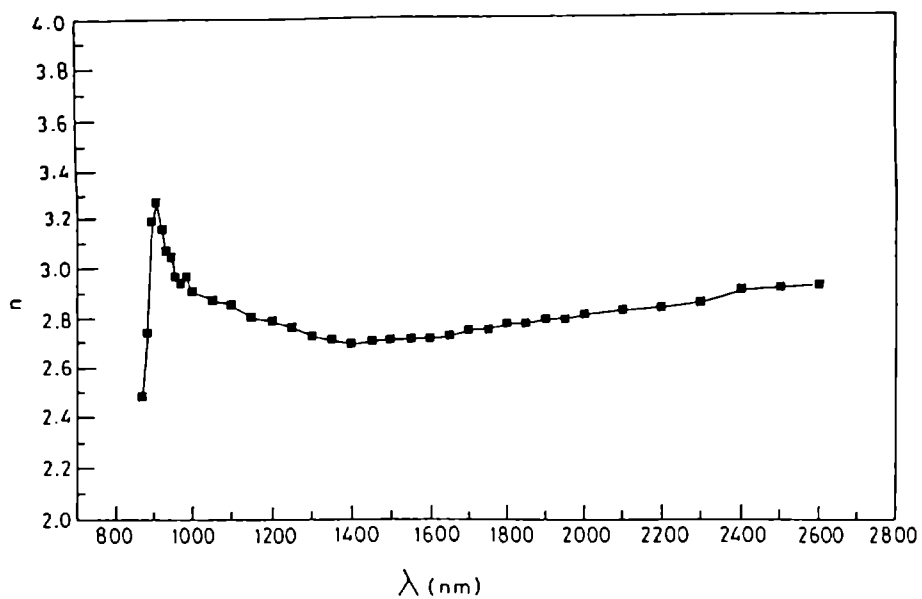substrates at room temperature(- - - -) and 373K (_____)

Figure 7.5 Variation of refractive index(n) with wavelength(λ) for PbSe thin film prepared at room temperature.
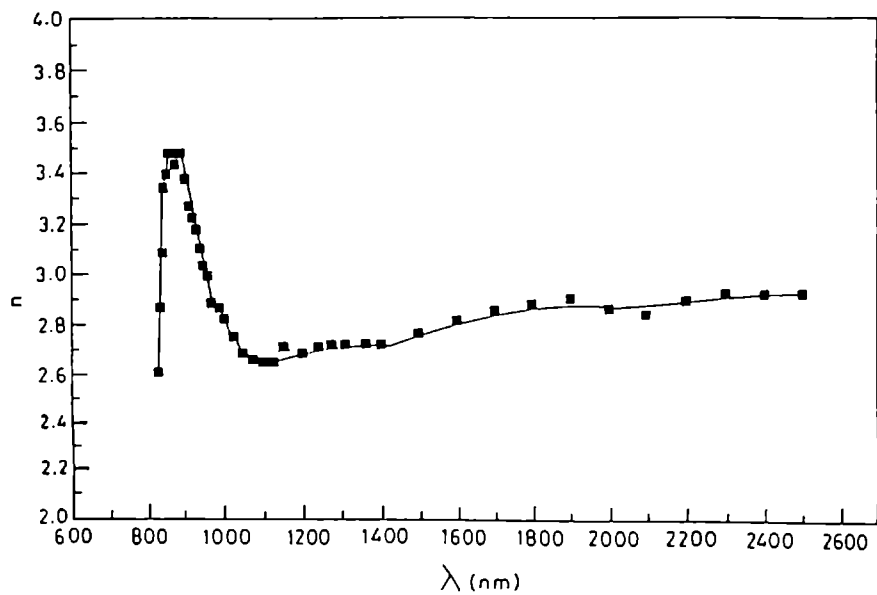

Figure 7.6 Variation of refractive index(n) with wavelength(λ) for PbSe thin film prepared at 373K.

Figure 7.7 and figure 7.8 shows the variation of absorption coefficient (α) as a function of photon energy (hv) of PbSe thin films prepared at room temperature and 373K respectively. The absorption has its minimum value at its low energy and increases with increasing optical energy in a similar manner to the absorption edge of the semiconductor.

The optical absorption data of PbSe films were analysed in accordance with the theory of Bardeen [25] and Smith [26]. The theory predicts that the absorption coefficient (α) due to the direct transition between the valence and conduction band is given by

$$(\alpha h v) = A (h v - E_g)^x, \qquad (7.2)$$

where x takes values of 1/2 for the allowed direct transition and 3/2 for the direct forbidden transition .For absorption due to indirect transition, absorption and
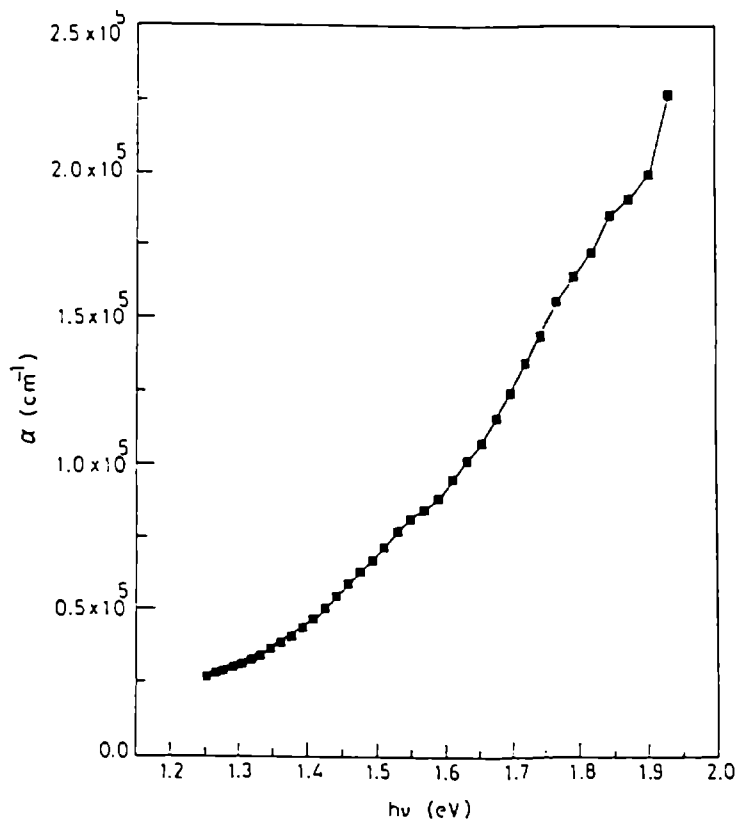
Figure 7.7 Variation of absorption coefficient(α) as a function of
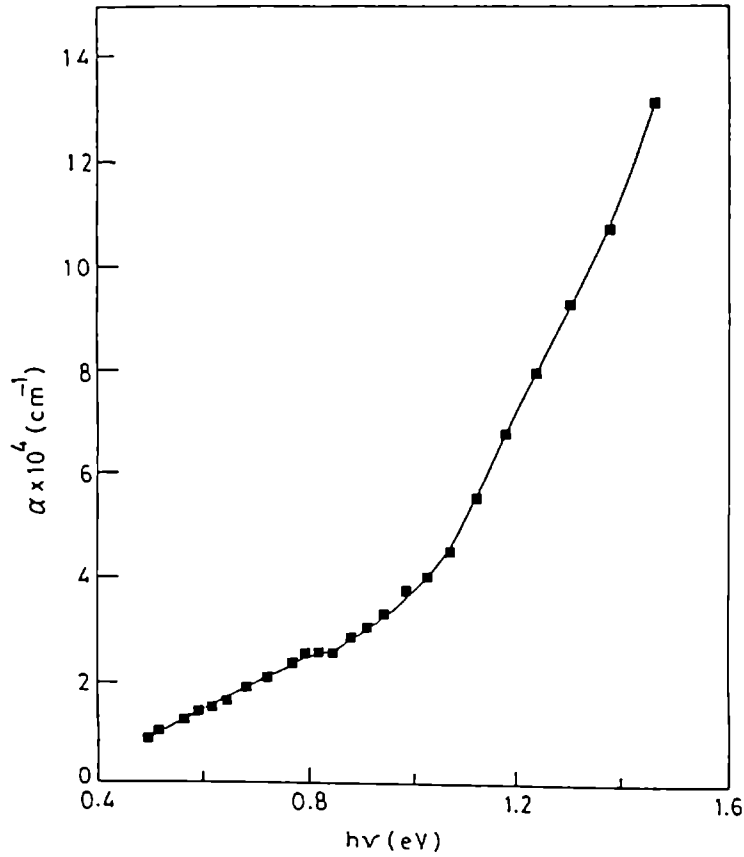photon energy(hv) for PbSe thin film prepared at room temperature

Figure 7.8 Variation of absorption coefficient(α) as a function of
photon energy(hv) for PbSe thin film prepared at 373K

emission due to phonon are also involved and the expression for α is as follows:

$$(\alpha h v) = B \, (h v - E_g \pm E_p \,)^x, \qquad (7.3)$$

here E_g is the indirect energy gap and E_p is the absorbed(+) or emitted(-) phonon energy. In this case $x = 2$, for indirect allowed and $x = 3$ for indirect forbidden transition.

Figure 7.9 shows the variation of $(\alpha h v)^{1/2}$ as a function of photon energy (hv), for a typical film prepared at room temperature. Due to the appreciable linearity of the curve, it is confirmed that the absorption near the fundamental edge was due to the indirect allowed transition. Moreover from figure 7.8 it can be seen that the

absorption coefficient is of the order of $10^5 cm^{-1}$, and it is a characteristic of allowed transition[26]. Because the measurements were made at room temperature, exciton bands were not likely to be present. Hence it is reasonable to believe that the absorption in the films were due to band to band transition. The extrapolation of the linear part of the graph to $\alpha = 0$ gives a band gap of (1.15 ± 0.01) eV. Figure 7.10 shows the variation of $(\alpha h\nu)^{1/2}$ against the photon energy (hν), for the film prepared at 373K. The extrapolation of the linear part of the curve to $\alpha = 0$ gives an energy gap of (1.02 ± 0.01) eV, which corresponds to the indirect allowed energy gap.
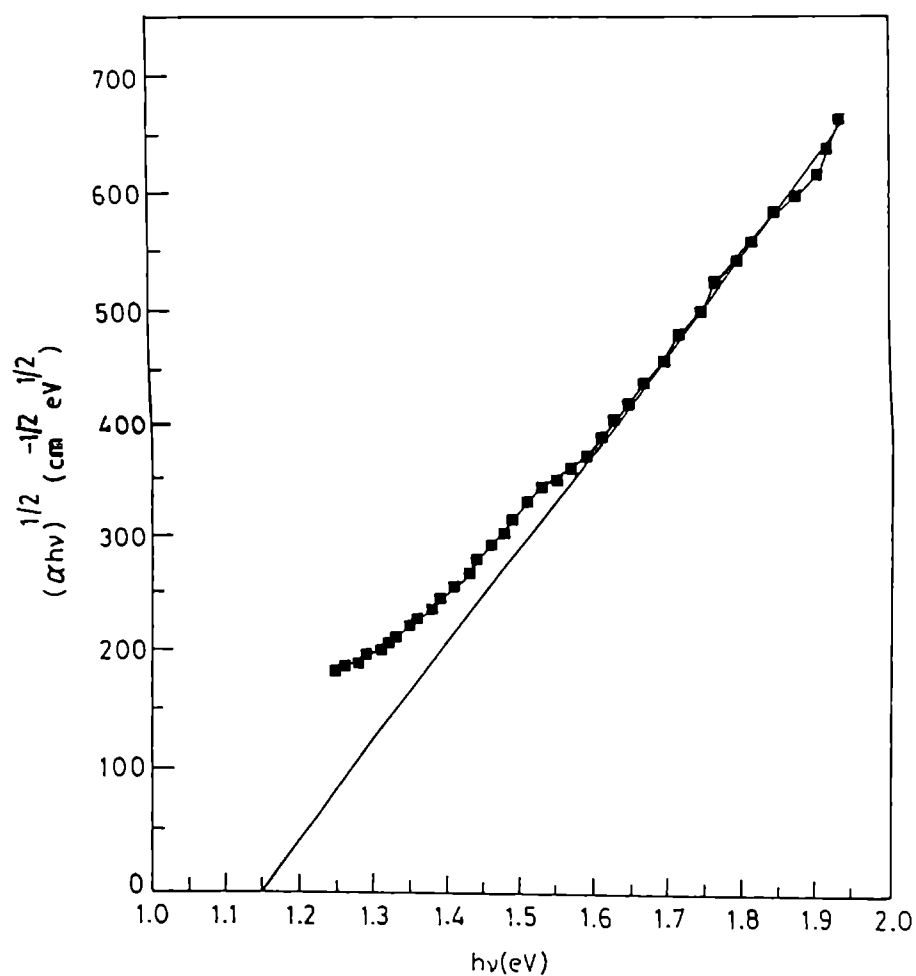

Figure 7.9 Variation of $(\alpha h\nu)^{1/2}$ against the photon energy (hν) for PbSe thin film prepared at room temperature.
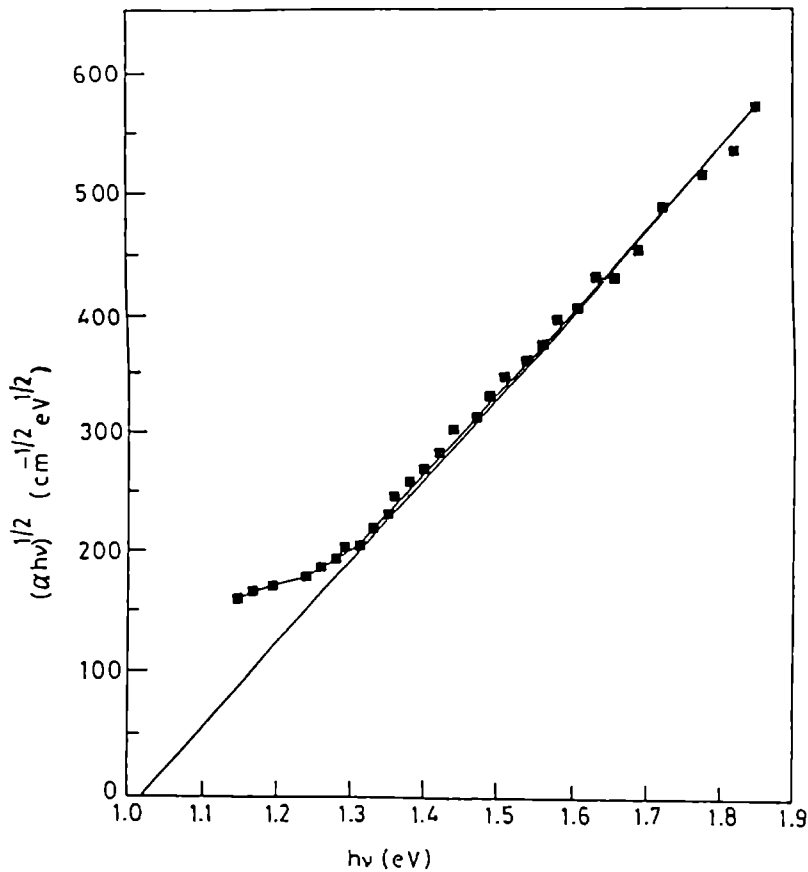
169

Figure 7.10 Variation of $(\alpha h\nu)^{1/2}$ against the photon energy (hv)
for PbSe thin film prepared at 373K

7.6 CONCLUSION

Lead Selenide thin films were prepared on glass substrates by reactive evaporation. Hot probe studies show that the films were p- type. The films prepared at room temperature were amorphous and the films prepared at 373K were polycrystalline. The activation energy for conduction was calculated. It was found to be nearly 0.04eV for films prepared at room temperature and 0.33eV for films prepared at 373K. The average value of refractive index for both the films were found to be 2.75. Analysis of the absorption coefficient data shows that the transition was indirect allowed one. The corresponding band gap was calculated and was found to be 1.15eV for the films prepared at room temperature and 1.02eV for the films prepared at 373K.

REFERENCES

1. M. Baleva and E. Mateeva, J. Phys. Condens. Matter 5 (1993) 7959

2. D. E. Bode, Phys. Thin Films 3 (1966)

3. Y. I. Ravich, B. A. Efimova and I. A. Smirnov, *Semiconducting Lead Chalcogenide* (Plenum press, New York, 1970)

4. Y. Yasokaand M. Wada, Japan J. Appl. Phys. 9 (1970) 452

5. N. P. Anisemeva, T.R. Globus, L.K. Dikov, V. Kalinin,
   T. G. Nikolaeva and S.A. Olesck, Sov. Phys. Semicond. 17 (1983) 336

6. N. P. Auiscmiva, T. R. Globus and S.A. Olesck,
   Sov. Phys. Semicond. 22 (1988) 1005

7. N. F. Borrelli and J. c. Loung, Proc. SPIE 886 (1988) 104

8. I. N. Jemel, J. D. Jensen,and R. B. Schoolar, Phys. Rev. 140 (1965) 330

9. C. E. Blomquist and P. O. Nilsson, Phys. Rev.174 (1968) 849

10. V. Damodara Das and S. Bhatt, Thin Solid Films 116 (1984) 201

11. V. Damodara Das and Seetharama Bhatt., Phys. Rev. B 40 (1989) 7696

12. M. S. Ali, K. A. Khan and M. S. R. Khan,
    Phys. Stat. Sol. A 149 (1995) 611

13. P. Pramanik, S. biswas, P. K. Basu and A. Mondal,
    J. Mater. Sci. Lett. 9 (1990) 1120

14. V.V. Tetyorkin, V.b. Orletski, F. F. Sizov, N. O. Tashtanbajev,
    and A. G. Stepanushkin, Optical Engineering 33 (1994)1450

15. T. Kanniainen, S. Lindross, J. Ihanus and M. Leskela
    J. Mater. Chen. 6 (1996) 983

16. A. N. Molin and A. I. Dikusar, Thin Solid Films 265 (1995) 3

17. M. Baleva, T. Georgiev and G. Lashkarev,
    J. Phys. Condens. Matter 1 (1990) 2935

18. J. George, *Preparation Of Thin Films,* (Marcel Dekker, New york, 1992)

19. K. G. Gunther, *The Use Of Thin Films in Physical Investigation,*
    (J. C. Anderson, Ed., Academic Press, New York,1966) p.213

20. R. B. Adler, A. C. Smith and R. L. Longini, *Introduction to Semiconductor Physics,* (John Wiley and Sons, New York, 1964) p.197

21. H. Maier and D. R. Daniel, J. Elect. Mater. **6** (1977) 693

22. R. A. Smith, Physics **20** (1954) 910

23. P. C. Newman, Proc. Phys. Soc. London **79** (1962) 1299

24. E. Miller, K. Komarck and I. Cadoft, J. Appl. Phys. **32** (1961) 2457

25. J. Bardeen, F. J. Blatt and l. H. Hall, *Proc. of Photoconductivity Conference*,
     Atlanta City (Wiley, New York)

26. R. A. Smith, *Semiconductors,*
     (Cambridge University Press, London, 1956) **p.** 314